Determination of Local Pin Powers in the Framework of Nodal Coarse-Mesh Solutions

Nissen, F

Publication date:
1982

Document Version
Publisher's PDF, also known as Version of record

Risø-R- 474

RISØ

Risø-R- 474

Determination of Local Pin Powers in the Framework of NODAL Coarse-Mesh Solutions

Flemming Nissen

Risø National Laboratory, DK-4000 Roskilde, Denmark
August 1982

Risø-R-474

DETERMINATION OF LOCAL PIN POWERS IN THE FRAMEWORK OF NODAL COARSE-MESH SOLUTIONS

Flemming Nissen
Department of Energy Technology

Abstract. Several methods are described of regaining the information on local properties of single heterogeneous subassemblies after the three-dimensional coarse-mesh solution has been found.

The efficiency and accuracy of these methods are determined by testing them on three benchmark problems. Finally, new homogenization methods are described that are capable of accurately predicting average values of boundary fluxes and currents.

INIS-descriptors: BWR TYPE REACTORS; COMPUTERIZED SIMULATION; FUEL PINS; HETEROGENEOUS REACTOR CORES; HOMOGENIZATION METHODS; NEUTRON DENSITY; POWER DENSITY; POWER DISTRIBUTION

UDC 621.039.51 : 621.039.524.44

August 1982
Risø National Laboratory, DK-4000, Roskilde, Denmark

ISBN 87-550-0904-2
ISSN 0106-2840

Risø repro 1983

CONTENTS

Page

Page

NOMENCLATURE

Symbol	Dimension	Meaning
ϕ	$cm^{-2} \cdot s^{-1}$	Neutron flux
ϕ^{HET}	$cm^{-2} \cdot s^{-1}$	Heterogeneous neutron flux
ϕ^{HOM}, $\bar{\phi}$	$cm^{-2} \cdot s^{-1}$	Homogeneous neutron flux
J, J^{NET}	$cm^{-2} \cdot s^{-1}$	Net neutron current
J^{HET}	$cm^{-2} \cdot s^{-1}$	Heterogeneous net neutron current
J^{HOM}	$cm^{-2} \cdot s^{-1}$	Homogeneous net neutron current
J^{+}	$cm^{-2} \cdot s^{-1}$	Partial current into the region
J^{-}	$cm^{-2} \cdot s^{-1}$	Partial current out of the region
$\frac{J}{\phi}$	-	Extrapolation distance
$\frac{J}{\phi}(\lambda)$	-	Extrapolation distance as a function of the eigenvalue
S_G	$cm^{-3} \cdot s^{-1}$	Source term in group G
p^{HET}	-	Heterogeneity factor
P	$W \cdot cm^{-1}$/pin	Pin power
p^{HET}	$W \cdot cm^{-1}$/pin	Heterogeneous pin power
p^{HOM}	$W \cdot cm^{-1}$/pin	Homogeneous pin power
$\nu\Sigma_{fG}$	cm^{-1}	Fission yield multiplied by the macroscopic fission cross section
$\Sigma_{n \to m}$	cm^{-1}	Scattering cross section
Σ_{aG}	cm^{-1}	Absorption cross section in group G
D_G	cm	Diffusion coefficient in group G

1. INTRODUCTION

1.1 Overview and motivations for a local pin power determination

The design and analysis of modern light water reactors require an extensive knowledge of spatial power distributions, control rod worths, and neutron absorption rates. The determination of these quantities requires a knowledge of the free neutron density in space, direction, and energy. Transport theory tools such as continuous-energy Monte Carlo or multigroup discrete ordinates methods are capable of performing the required analysis (Ref. 1). Unfortunately, the complexity which is inherent in explicit transport theory modeling of heterogeneous reactor details (such as control rods, burnable poisons, and water rods) results in mathematical problems of such a complexity as to be intractable for even the most advanced digital computers.

The most commonly employed alternative to solving the global transport equation is to approximate the solution of the transport equation by solving the multigroup diffusion equation. However, the diffusion theory approximation implicitly assumes that the angular distribution of neutrons be at most linearly anisotropic, and this restricted representation does not approximate accurately the actual angular distribution which occurs near regions of high neutron absorption (such as control rods or burnable poison pins) or highly scattering regions with little absorption (such as water rods, water gaps, or reflectors). Nevertheless, even the diffusion theory problem may remain quite intractable. The reason for this is simply that there exists a very large number of spatial regions in a reactor core. Typically, a reactor may contain several hundred fuel assemblies, and each fuel assembly may contain several hundred fuel pins. Hence, an explicit representation of heterogeneous assemblies requires tens of thousands of distinct regions for each axial plane in the reactor core that is to be analyzed. Since many core calculations are required in the design and analysis of a

nuclear reactor, there are considerable economic incentives to develop methods of analysis that avoid the explicit modeling of full heterogeneous details. The usual approach to this problem is to treat large "nodes" (usually entire assemblies in a radial plane) as homogenized regions. If homogenized diffusion theory parameters (usually spatially constant within each node) can be determined, the reactor core calculation can be reduced to a problem involving only several hundred homogeneous regions in each axial plane of the reactor core.

Once the homogenized parameters have been calculated, the resulting diffusion theory calculation can be performed by nodal or finite element methods (Ref. 1). These methods for solving the neutron diffusion equation are capable of employing very large mesh spacings within each of the homogenized regions; hence, they are computationally very efficient.

The use of homogenized parameters to predict reactor properties results in an inevitable loss of certain information which is otherwise available if the reactor is analyzed by methods which do not involve homogenization. If one is satisfied, knowing the average values of spatial power distributions, the three-dimensional nodal coarse-mesh solution will constitute the final solution. On the other hand, in reactor design practice one often needs direct information about the local pin power distribution for the actual heterogeneous assemblies. However, one usually is interested in such local details only at specific points or in certain regions of the reactor as, for instance, the positions and values of local pin power peaks in regions of high power density or the detailed pin power distribution for some assemblies that are of particular interest from a fuel performance point of view. Another example is the capability of making accurate predictions of local detector response, such as the activations at the position of aeroball channels or the signals of fixed incore flux detectors. Last but not least, the local pin power determination makes it possible to examine the correctness of the approximations that have been made on the different stages of reactor calculation.

For all these reasons, after having solved the global reactor problem, we have to look into the possibilities of regaining in a second step the information on the local properties of single heterogeneous subassemblies. The practical advantage of such a two-step approach for multidimensional reactor calculations are quite obvious. If it can be shown to be feasible and sufficiently accurate, it means that in solving the global problem one can temporarily forget most of the details and complications of the heterogeneous reactor core, which may, however, be re-introduced in the second step where and when needed. Such a procedure requires, of course, that the coarse-mesh global reactor solution is sufficiently accurate.

The solution to the problem of deriving fluxes and currents from the converged coarse-mesh solution, to be used in the local pin power model lies outside the scope of this work and it will be referred to only superficially in Chapter 7 and Chapter 8.

The objective of this thesis is to develop accurate and efficient ways of regaining the information on local properties of single heterogeneous subassemblies after the three-dimensional coarse-mesh solution has been found.

Four different ways of calculating local pin power distributions will be examined:

1. The Normalization Method, where the net currents on the boundaries of the nodes are neglected.

2. The Flux-lupe Method where the boundary parameters from the converged coarse-mesh solution are used as boundary conditions in a new assembly calculation.

3. The Superposition Method where the diffusion theory equation is solved by dividing the problem into a number of subproblems. First, these subproblems are solved; next, the final solution is obtained by combining the solutions to the subproblems.

4. The Modulation Method where the smooth power distribution from the converged coarse-mesh solution is multiplied on some precalculated form factors.

The efficiency and accuracy of these methods will be determined by testing them on three benchmark problems defined in Chapter Two.

2. BENCHMARK PROBLEMS AND REFERENCE SOLUTIONS

2.1. Introduction

As local pin power problems define a new reactor physical area, pin power benchmark problems have not yet been described.

If the purpose of a local pin power investigation is to examine the accuracy and efficiency of different ways of calculating local pin power distributions in the framework of coarse-mesh solutions, the benchmark problem is to be defined in a way that excludes other errors than those belonging to the pin power models. This means that the dimensions and complexity must not exceed levels that would make it impossible to solve the whole problem in the same detail as that of the assembly calculation. This restrains the complexity and the size of the core or subregion of the core to be used as benchmark problem. The benchmark problems defined here are realistic with respect to the complexity of modern LWR. As mentioned previously limitations in computer capacity makes it impossible to perform a detailed calculation on the entire reactor core. We therefore select three representative regions of the core and perform the calculations separately on each of them.

Each subregion is imbedded in its "natural" environment of adding a buffer zone around the region. The cross sections in this buffer zone are found by means of an iterative procedure deter-

mined in a way that makes the subregion plus buffer zone critical.

The application of the Modulation Method (to be described later in a subsequent chapter) to determine the local pin powers in PWR's during the last four years at KWU in Germany, makes it more interesting to examine Pin Power Benchmarks based on BWR layouts. The major difference between BWR- and PWR-problems can be summarized as follows: In BWR the heterogeneous thermal flux distribution is, on the one hand, a strongly varying function in each assembly and depends on the local moderator density as well. Furthermore, the influence on the larger water gap of the heterogeneous structure of adjacent areas is, on the other hand, smaller than in the case of PWR.

2.2. Two-dimensional BWR benchmark problem

In this thesis three BWR benchmark problems are chosen to test the accuracy and efficiency of the local pin power models to be developed. Because the flux distribution is rather smooth in the axial direction, our principal concern is with pin power distributions in the radial plane. Thus, all three benchmark problems represent a two-dimensional reactor core. As mentioned earlier the benchmark problems consist of subregions of the core.

A plane view of the BWR used as benchmark is shown in Fig. 2.1. The plane view is taken from the bottom of the core, e.g. there is no void. The calculations have been simplified by assuming that the assemblies are of the same type throughout the core. The assemblies are composed of 63 fuel pins and a waterhole. As shown in Fig. 2.2 the fuel pins have four different enrichment values: 0.97, 1.40, 1.88, and 2.47 w/o U-235. Two of the pins contain Gadolinia. In the present application we shall concentrate on the three subregions shown in detail in Fig. 2.1. The first subregion (Test One) is composed of 3 × 3 assemblies and 1 control rod blade. The second subregion (Test Two) is composed of 3×3 assemblies and $\frac{1}{2} + \frac{1}{2}$ control rod blades. The third subregion (Test Three) is composed of 6 assemblies of which three

lie next to the reflector region. Also shown in Fig. 2.1 is the numeration of the assemblies constituting the test cases.

The three reference solutions to these problems have been generated from diffusion theory calculations with the code "CDB" (Ref. 7). The calculations are performed in five energy groups, and each assembly is divided into 100 subregions (shown in Fig. 2.3). The size and layout of the assemblies defining the buffer zone are shown in Fig. 2.4. The mesh division of the buffer zone is the same as in case of the heterogeneous assembly (Fig. 2.3). Appendix A summarizes the five group cross sections.

The reference solutions to the three test problems are displayed in Figs. 2.5-2.7. Based on these solutions the average power in each assembly has been calculated. These results are shown in Fig. 2.8.

3. THE NORMALIZATION METHOD

3.1 Introduction

As mentioned in the introduction, the large number of spatial regions in a reactor core encourage the development of methods which avoid the explicit modeling of full heterogeneous details. This is done by treating large "nodes" as homogenized regions. The most commonly employed procedure is to flux-volumen weight the heterogeneous cross sections. In order to do that a high-order calculation is performed (which either directly or indirectly represents all heterogeneous details) for each assembly type, with a zero net neutron current condition imposed across each assembly surface. The assumption that homogenized parameters can be computed from an assembly calculation with zero current boundary conditions is usually rationalized by noting that most assemblies in a reactor are surrounded by other assemblies of a similar composition. Also, global flux shapes

are such that only a slight amount of curvature exists across each assembly; consequently, net surface currents should be small in magnitude.

After the global solution has been found, the simplest procedure to determine the local pin powers would be to use the already known power distribution and renormalize the average power to the actual nodal power from the overall solution. Consequently, we assume that the power distribution in each assembly is not affected by the power distribution in neighbouring assemblies. If this approach were adopted we have only to store the power distribution for each burnup step and for each assembly type during the assembly-homogenization process. When the overall three-dimensional calculation has been performed and one knows the average power in each assembly, we pick out the most interesting assemblies and renormalise the heterogeneous power distribution to the known average nodal powers.

The purpose of this investigation is to ascertain if the assumption of zero net current boundary conditions is plausible, and to identify the influence on the local power distribution caused by net currents differing from zero.

3.2 The use of the Normalization Method on the two-dimensional BWR benchmark

When applied to the two-dimensional BWR benchmark problem defined in Chapter 2, the Normalization Method requires two assembly calculations, one for a rodded assembly and one for an unrodded one. For reasons of consistency with the reference solution, these calculations are also performed in five energy groups. For each of the assemblies in the three test cases the average power distribution is renormalized to the average value of the power distribution in the rodded and unrodded assembly solution. This is done in order to obtain a standard of reference for all 24 assemblies. This is, of course, the opposite of the real use of the Normalization Method, where the assembly-solutions are normalized to the average nodal powers from the three-dimensional coarse-mesh solution.

In Figs. 3.1-3.3 the differences between the normalized reference solutions and the assembly solutions are summarized. From these figures it appears that the predicted form factors may be in error by as much as 49% if the Normalization Method is used as pin power model.

If one wants to calculate the absolute values of the errors shown in Figs. 3.1-3.3, the following equation can be used:

$$P_{ERROR} = F_{OVERALL} \cdot F_{SUB} \cdot E_{ER} \cdot P_{AV} \qquad (3.1)$$

where

P_{ERROR} : Absolute value of the error in the local pin power determination.
$F_{OVERALL}$: The average form factor for the subregion.
F_{SUB} : The form factor for each assembly inside the subregion (Fig. 2.6).
E_{ER} : The error in per cent divided by one hundred.
P_{AV} : Average pin power in the core.

The absolute value of the maximum error in the pin powers in the 24 assemblies under examination are determined using Equation 3.1. The following assumptions are made:

$F_{OVERALL}$ (TEST 1) = $F_{OVERALL}$ (TEST 2) = 1.2
$F_{OVERALL}$ (TEST 3) = 0.8

P_{AV} = 160 W/cm/pin

Figure 3.4 summarizes the results of this calculation. It appears that the maximum error of 66 W/cm occurs in box No. 6 in Testcase 1.

Although the Normalization Method is clearly in error in nearly all 24 assemblies, there exist many assemblies in a reactor core for which the method is quite accurate. For instance, assemblies lying in the center of the core away from control rods and adjacent to assemblies of the same type have net surface currents which are close to zero.

The problem consists in determining whether or not it is possible to point out the assemblies where the Normalization Method can be used without causing large errors in the local pin power determination. An obvious guess would be to assume that the nodes which have large flux gradients across them are those in which the difference between the normalized assembly solution and the reference solution tends to be most significant. The question of whether or not there exists a relation between the flux gradients across the assembly and the maximum error in the local pin power caused by the Normalization Method has been examined and it has been shown that the aforementioned assumption is quite valid for the greater part of the 24 assemblies. There do exist assemblies for which it is quite invalid, as for instance, box 6 and box 8 in test case two.

Figure 3.5 shows the condensed two-group average fluxes in the adjoining nodes to box 6 and box 8. It appears that the maximum error in the form factor is larger in box 8 although the flux gradients across box 8 are smaller than in the case of box 6. Figure 3.5 also shows the average currents on the four faces together with the corner currents. Only when these net neutron currents are taken into account can one explain why the Normalization Method has a greater error when used on box 6 than box 8. The reason is that in the case of box 8 the net currents into the node are concentrated in the upper right corner, whereas the currents into and out of box 6 are more commonly distributed. Hence, one cannot in general claim the existence of a unique relation between flux gradients and the accuracy of the Normalization Method. But as a rule one can say that the Normalization Method cannot be used on nodes where the net currents are large and unsymmetrical.

3.3 Summary

The Normalization Method proves to be a very efficient way of regaining the heterogeneous structures in the assemblies after the global coarse-mesh solution has been found. It requires no storing of large numbers of data, and the process-time is lim-

ited. The only problem that arises is that many assemblies are present in a reactor for which the assumption of zero net neutron currents on the boundaries of the nodes is quite invalid. For instance, assemblies that contain control rods, those adjacent to rodded assemblies, and those near the reflector have surface currents that are quite large. Consequently, the zero net current assumption may be grossly in error. In many cases these assemblies constitute those for which the knowledge of local pin powers are most important from a reactor design or fuel performance point of view.

The practical use of the Normalization Method is therefore limited. One has to take into account the net surface currents, if it is necessary to determine the local pin power distribution accurately throughout the reactor core.

4. THE FLUX-"LUPE" METHOD

4.1 Introduction

In this chapter we will examine the most direct way to determine heterogeneous pin power distributions, in the framework of, and as an extension of the coarse mesh nodal methods: The Flux-"LUPE" Method (Ref. 2).

Lupe is the German word for magnifying glass that one uses for viewing local details in an overall environment. The basic approach to this method is to derive inner boundary conditions directly from the converged global coarse-mesh solution, to be used in a number of new assembly calculations. In contrast to the assembly calculations performed in order to determine homogenized cross sections, where we assume zero net current boundary conditions, this second assembly calculation is performed with the fuel boxes imbedded in their natural environment. A further difference between the homogenization and pin power steps is the

insufficiency of still performing one assembly calculation per fuel box type. We have to perform one assembly calculation for each fuel box that we wish to examine in more detail. Hence, if we want to determine the local pin powers throughout the reactor core, we have to perform a great deal of assembly calculations. On the other hand, if we wish merely to determine local pin powers in the most interesting assemblies from a fuel performance point of view, the Flux-lupe Method makes it possible to concentrate the computational effort on those areas where further investigations are needed, without wasting computing time for areas which turn out to be of no particular interest.

4.2 Errors in the local pin power determination in relation to the method of approximation of the boundary parameters

The accuracy of the Flux-lupe Method depend on how precisely the inner boundary conditions can be derived from the converged coarse-mesh solution. Only if the "homogenized" fluxes and currents on the node interfaces equal the actual heterogeneous boundary values, will the Flux-lupe Method determine the local pin powers exactly. The question of how the boundary fluxes and currents can be accurately determined based on a three-dimensional coarse-mesh nodal solution is examined in Chapter 8 and Ref. 3. Here we will examine the relations between the way the boundary parameters are approximated and the degree of accuracy with which the local pin powers can be calculated using the Flux-lupe Method.

In order to determine this relation we use a slightly modified version of the benchmark problems defined in Chapter 2. For simplicity, the leakage rates out of or into the subregions are defined so that there exists a symmetry line from the upper left to the lower right corner.

This simplification means that we have merely to calculate the boundary parameters on two of the four faces of the nodes.

For each of the three test examples the Flux-lupe Method is tested on "fuel box number five". Based on the reference solution to the simplified benchmark problems, the real values of the boundary parameters $J(s)$, $J^+(s)$, $J^-(s)$, $\emptyset(s)$, $J/\emptyset(s)$ are calculated in five energy groups.

The angular distribution is assumed to be such that the heterogeneous surface net currents and surface fluxes can be expressed in terms of the partial currents on that surface by:

$$\emptyset(s) = 2(J^+(s) + J^-(s))$$
$$J(s) = J^+(s) - J^-(s)$$

With respect to the spatial shape of the boundary parameters, three approximations are assumed:

1) Flat : based on the average value on each of the four faces.

2) Tilt : based on the corner values.

3) Parabolic: based on both the corner and average values.

In order to be consistent with our reference solutions, assembly calculations will always be performed throughout this investigation with "CDB" using five energy groups in the "overall" solution. The details of how to use this code to solve problems with incoming partial currents (J^+), outgoing partial currents (J^-), net currents (J), boundary fluxes ($\emptyset$), and problems where the eigenvalue is multiplied by the $J/\emptyset$-ratio as boundary conditions are given in Appendix B.

The calculational procedure is identical for each type of boundary parameter used on each of the three test examples. In the following the calculational procedure for the net currents $J(s)$, used on the first test example is described in details.

At first, the "real" net currents from the reference solution are used as boundary values in a rodded assembly calculation.

The power distribution determined in this way (shown in figure 4.1) is equal to the power distribution for box number five in test example one, which means that the net currents we use are correctly determined.

In the second step, the average values of the net currents on each of the four faces are calculated and a new assembly calculation is performed with the average values as boundary conditions. The resulting power distribution is compared with the reference solution. The difference between the two of them is shown in Fig. 4.2 A. Table 4.1 contains the results of a more detailed investigation of the errors in the local pin power distribution when the flat-approximation of the net currents is used as boundary condition. Also shown in Table 4.1 is the average value of the difference between the actual boundary-current shape and the approximated shape.

The third step is a reiteration of the second step, the only difference being that the flat-approximation is replaced by the tilt-approximation, e.g. the boundary conditions are based on the corner values of the net currents.

Figure 4.2-B shows the difference between the approximated power distribution and the reference solution. Table 4.1 contains the results of the detailed investigation of the difference between the two power distributions.

In the fourth step the tilt-approximation is replaced by the parabolic approximation. The result of this step is shown in Fig. 4.2-C and Table 4.1.

The same calculational procedure is used on test cases two and three. Making this examination on

$$J_{NET},\ J^{+},\ J^{-},\ \emptyset,\ \frac{J}{\emptyset},\ \text{and}\ \frac{J}{\emptyset}(\lambda)$$

means that one has to perform 72 assembly calculations. Table 4.1 summarizes the results of all boundary parameter investiga-

tions. What is immediately evident when looking more closely at Table 4.1 is the large error in the predicted local pin powers that may be as great as 75% when the J^- approximation is used as boundary parameter.

The reason that the J^- approximation is so much in error compared with the J^+ approximation can be understood by looking at the theory described in Appendix B. As shown in this appendix the source term in the J^- approximation is expressed as:

$$S_G = \frac{1}{\frac{\Delta}{2D_G} - 2} \cdot \frac{J_G^-}{\Delta}$$

with the boundary conditions

$$J_G^S = \frac{1}{\frac{\Delta}{2D_G} - 2} \cdot \phi_G^M$$

(The symbols are defined in Appendix B).

From these equations it can be seen that problems arise when $\frac{\Delta}{2D_G} = 2$. With the chosen mesh dimensions this problem arises in one of the thermal groups, and the effect is that the fluxes in this particular group becomes negative in some of the nodes when the shape approximations are used as boundary conditions.

Table 4.1 also shows the errors in the local pin powers when the Normalization Method is used as pin power model. Comparing these errors with those from the Flux-lupe Method makes it clear that one cannot in general improve the local pin power determination by considering average values of the boundary parameters, e.g., zero net neutron current boundary conditions are in some cases a better approximation than the flat approximation based on the average boundary parameters.

Table 4.1 also shows that the $J/\phi(\lambda)$ approximation in general gives the best determination of local pin power distributions. When the flat approximation of $J/\phi(\lambda)$ is used, the maximum error in the local pin powers lies in the 8.6%-14.5% range. The

tilt approximation reduces the maximum errors to 1.8-9.3%. As shown in Table 4.1, this reduction is caused mainly by the improved shape approximations on the faces next to the narrow water gaps. This observation cannot be used in the Flux-lupe Method, but we will make use of it in Chapter 5 where the Superposition Method is examined. The maximum error in the local pin powers in case of the parabolic approximation is about 0.9%.

4.3 Summary

The investigations in Chapter 3 showed that the knowledge of the "actual" boundary conditions on the assemblies was required if the local pin power distribution was to be accurately determined all over the reactor core. The Flux-lupe investigation described in this chapter has made it clear that knowledge of the average values of the boundary parameters cannot in general improve the accuracy of the Normalization Method. An accurate determination of local pin powers requires knowledge of the spatial shape of the boundary parameters. In some cases the average values of the boundary parameters will result in an overestimation of the leakage rates in the corner nodes of the assembly. In these cases the determination of local pin powers will therefore be less accurate than when the Normalization Method is used where we assume zero net current boundary conditions.

Another conclusion to be drawn from the Flux-lupe investigation is that the $J/\Phi(\lambda)$ approximation in general makes up the best way of approximating the "actual" shape of the boundary parameters from the converged global solution.

Last but not least, the investigation performed shows that the Flux-lupe Method constitutes an accurate way to calculate pin powers, if the "actual" shape of the boundary parameters is known. The only problem is that the efficiency of the method is quite poor. However, the Flux-lupe Method will constitute a good way of calculating pin powers, if these local pin powers have to be determined in only a few assemblies.

5. THE SUPERPOSITION METHOD

5.1 Introduction

The Superposition Method to be described in this chapter is a theoretically exact method of calculating local pin power distributions. The superposition principle consists in solving the diffusion theory equation by dividing the problem into a number of subproblems all having different boundary values. First, these subproblems are solved; next, the final solution is obtained by combining all the solutions to the subproblems. The number of subproblems required depends on how detailed the shapes of the boundary parameters are to be approximated and the number of energy groups in which the boundary parameters are represented.

The Superposition Method has a certain conformity with response matrix methods (Ref. 4). However, it is more flexible, because it need not be the parameter derived from the global solution, which is used as boundary parameter in the subproblem definition. Neither are there requirements about a unique relation between the number of boundary parameters derived from the global solution and the number of subproblems. If the number of global boundary parameters exceeds the number of subproblems the final solution is defined to be the one in which the combination of boundary values in the subproblems makes the best match to the boundary parameters from the overall solution.

In the particular case where the subproblems are defined so that the parameter used as a boundary condition is unity on one part of the boundary and zero on the remaining part, and furthermore if the parameter derived from the converged global solution is to be used to define the boundary conditions for the subproblems, then the Superposition Method and response matrix method will be alike.

The idea behind the Superposition Method is based on the results from the Flux-lupe investigation. Here it was shown that $J/\emptyset(\lambda)$ boundary conditions made the best way of combining the local pin power determination with the global reactor solution. As described in the theory-section of this chapter one cannot make response matrices based on $J/\emptyset$-boundary conditions. Hence, the restriction requiring the global boundary parameter to be the same as the parameter defining the boundary conditions in the subproblem definition has to be omitted if the $\frac{J}{\emptyset}(\lambda)$-approximation is to be used as boundary parameter.

The question of whether the results from the Flux-lupe investigation can be transferred to the response matrix methods will be examined in Section 5.3 where the accuracy of the Superposition Method based on $\frac{J}{\emptyset}(\lambda)$-parameters is compared with the response matrix method based on J or $\emptyset$ parameters.

The Superposition Method will be examined and described in greater detail than the other methods in this thesis, because it is quite new, and not reported elsewhere. Recently, a pin power investigation in which the response matrix method is used as pin power model has been started at MIT. Based on superficial knowledge (Ref. 5) of MIT's pin power model (the method has not been publicized yet) it can be stated that the pin power determination is based on a response matrix modification of the zero net current assembly solution. The response matrix generation is performed using the scalar flux as boundary parameter specification.

5.2 Theory

One of the fundamental and widely encountered methods of solving complicated differential equations is to divide the problem into a number of simple parts or subproblems. First, these parts are solved; next, the final solution is obtained by combining all of the solutions to the subproblems. In order to illustrate this method we will look briefly at the solution of the Dirichlet problem for a rectangle. The problem is formulated as follows

(Ref. 6): "To find a function u that is harmonic in the given region D, taking assigned values on the closed contour L bounding D". The boundary conditions are defined as:

$$u = \begin{cases} \phi_1(x) \text{ for } y = \dfrac{b}{2} \\ \phi_2(x) \text{ for } y = -\dfrac{b}{2} \\ \phi_1(y) \text{ for } x = 0 \\ \phi_2(y) \text{ for } x = a \end{cases}$$

The solution of this problem can be obtained as the sum of the solutions of the subproblems, $u_1 + u_2$, where

$$u_1 = \begin{cases} \phi_1(x) \text{ for } y = -\dfrac{b}{2} \\ \phi_2(x) \text{ for } y = \dfrac{b}{2} \\ 0 \text{ for } x = 0 \text{ and } x = a \end{cases}$$

and

$$u_2 = \begin{cases} 0 \text{ for } y = \pm\dfrac{b}{2} \\ \phi_1(y) \text{ for } x = 0 \\ \phi_2(y) \text{ for } x = a \end{cases}$$

The simplicity of these subproblems is evident because their solutions vanish on two adjacent sides of the rectangle. Despite a simplification of many complicated problems by this approach, this method can also be advantageous if we are dealing with a differential equation, or a number of coupled differential equations, where we wish to solve a number of boundary-value problems, all having a unit global eigenvalue. Faced with such a problem, one can solve a reasonable number of the boundary value problems, and find the solutions to the remaining ones

by combining the solutions already determined. Used on the pin power problem this method will be called "superposition".

In the two-dimensional problem defined above we use fluxes as boundary conditions for the differential equation. We could also have used the first derivative of the fluxes as boundary parameter and the method would still be valid. The only requirement is that the parameter used for defining the boundary conditions be expressed in different values of the same parameter.

For instance,

$$\emptyset_A(x) = \emptyset_1(x) + \emptyset_2(x) + \emptyset_3(x)$$

or

$$J_A(x) = J_1(x) + J_2(x) + J_3(x)$$

This means that the extrapolation factor J/Ø cannot be used as boundary parameter because if

$$J_A(x) = J_1(x) + J_2(x) + J_3(x)$$

and

$$\emptyset_A(x) = \emptyset_1(x) + \emptyset_2(x) + \emptyset_3(x)$$

then

$$\frac{J_A(x)}{\emptyset_A(x)} \neq \frac{J_1(x)}{\emptyset_1(x)} + \frac{J_2(x)}{\emptyset_2(x)} + \frac{J_3(x)}{\emptyset_3(x)}$$

In order to illustrate the basic principle of the Superposition Method we use a transfer matrix representation of a one-dimensional two-group problem.

Equation 5.1 forms the basis of this transfer matrix representation.

$$\begin{Bmatrix} a_{11}(x) & a_{12}(x) & a_{13}(x) & a_{14}(x) \\ a_{21}(x) & a_{22}(x) & a_{23}(x) & a_{24}(x) \\ a_{31}(x) & a_{32}(x) & a_{33}(x) & a_{34}(x) \\ a_{41}(x) & a_{42}(x) & a_{43}(x) & a_{44}(x) \end{Bmatrix} \cdot \begin{Bmatrix} \phi_1(a) \\ \phi_2(a) \\ J_1(a) \\ J_2(a) \end{Bmatrix} = \begin{Bmatrix} \phi_1(x) \\ \phi_2(x) \\ J_1(x) \\ J_2(x) \end{Bmatrix} \quad (5.1)$$

The values of the elements in the transfer matrix depend on the position "x" to which the boundary fluxes and currents at "a" are transferred, and the two-group parameters for the cell materials. "a" and "b" constitute the position of the boundaries of the subregion concerned.

As we are dealing with critical configurations, the solution of the one-dimensional problem is uniquely determined knowing only four of the following eight boundary values: $\phi_1(a)$, $\phi_2(a)$, $J_1(a)$, $J_2(a)$, $\phi_1(b)$, $\phi_2(b)$, $J_1(b)$, and $J_2(b)$.

Consequently, we can find four solutions, "base-solutions", which equal four arbitrarily chosen linearly independent sets of boundary values, each set consisting of four boundary values. For example:

$$(1) \quad \begin{Bmatrix} \phi_1(a) \\ \phi_2(a) \\ J_1(a) \\ J_2(a) \end{Bmatrix} \rightarrow \begin{Bmatrix} (1)\phi_1(x) \\ (1)\phi_2(x) \end{Bmatrix}$$

$$(2) \quad \begin{Bmatrix} \phi_1(a) \\ \phi_2(a) \\ J_1(a) \\ J_2(a) \end{Bmatrix} \rightarrow \begin{Bmatrix} (2)\phi_1(x) \\ (2)\phi_2(x) \end{Bmatrix}$$

$$(3)\ \begin{Bmatrix} \emptyset_1(a) \\ \emptyset_2(a) \\ J_1(a) \\ J_2(a) \end{Bmatrix} \rightarrow \begin{Bmatrix} (3)\emptyset_1(x) \\ (3)\emptyset_2(x) \end{Bmatrix}$$

$$(4)\ \begin{Bmatrix} \emptyset_1(a) \\ \emptyset_2(a) \\ J_1(a) \\ J_2(a) \end{Bmatrix} \rightarrow \begin{Bmatrix} (4)\emptyset_1(x) \\ (4)\emptyset_2(x) \end{Bmatrix}$$

If we now set ourselves the task of calculating the solution for a fifth set of boundary values, we can use the Superposition Method to find the solution, hence avoiding the solving of a new boundary value problem. Using the Superposition Method we merely have to solve the following linear equation system:

$$\begin{bmatrix} {}^{(1)} & {}^{(2)} & {}^{(3)} & {}^{(4)} \\ \emptyset_1(a) & \emptyset_1(a) & \emptyset_1(a) & \emptyset_1(a) \\ \emptyset_2(a) & \emptyset_2(a) & \emptyset_2(a) & \emptyset_2(a) \\ J_1(a) & J_1(a) & J_1(a) & J_1(a) \\ J_2(a) & J_2(a) & J_2(a) & J_2(a) \end{bmatrix} \cdot \begin{Bmatrix} K_1 \\ K_2 \\ K_3 \\ K_4 \end{Bmatrix} = \begin{Bmatrix} {}^{(5)} \\ \emptyset_1(a) \\ \emptyset_2(a) \\ J_1(a) \\ J_2(a) \end{Bmatrix} \quad (5.2)$$

A knowledge of the constants K_1, K_2, K_3, and K_4 leads us to the final solution shown in Equation 5.3.

$$\begin{aligned} {}^{(5)}\emptyset_1(x) &= K_1 \cdot {}^{(1)}\emptyset_1(x) + K_2 \cdot {}^{(2)}\emptyset_1(x) + K_3 \cdot {}^{(3)}\emptyset_1(x) + K_4 \cdot {}^{(4)}\emptyset_1(x) \\ {}^{(5)}\emptyset_2(x) &= K_1 \cdot {}^{(1)}\emptyset_2(x) + K_2 \cdot {}^{(2)}\emptyset_2(x) + K_3 \cdot {}^{(3)}\emptyset_2(x) + K_4 \cdot {}^{(4)}\emptyset_2(x) \end{aligned} \quad (5.3)$$

It is clear that the Superposition Method in this case will give the exact solution to the one-dimensional problem.

Even if the extrapolation factor J/Ø (as mentioned earlier) cannot be summed, the base-solutions can nevertheless be calculated using J/Ø as boundary condition. The only requirement is that fluxes or currents or their combination are used to calculate

the constants K_1 - K_4 in Equation 5.2. If the extrapolation factor is used for these calculations as shown in Equation 5.4, Equation 5.3 will no longer constitute the exact solution to the one-dimensional problem.

$$\begin{matrix} & (1) & (2) & (3) & (4) \end{matrix}$$

$$\begin{Bmatrix} \frac{J_1(a)}{\phi_1(a)} & \frac{J_1(a)}{\phi_1(a)} & \frac{J_1(a)}{\phi_1(a)} & \frac{J_1(a)}{\phi_1(a)} \\ \frac{J_2(a)}{\phi_2(a)} & \frac{J_2(a)}{\phi_2(a)} & \frac{J_2(a)}{\phi_2(a)} & \frac{J_2(a)}{\phi_2(a)} \\ \frac{J_1(b)}{\phi_1(b)} & \frac{J_1(b)}{\phi_1(b)} & \frac{J_1(b)}{\phi_1(b)} & \frac{J_1(b)}{\phi_1(b)} \\ \frac{J_2(b)}{\phi_2(b)} & \frac{J_2(b)}{\phi_2(b)} & \frac{J_2(b)}{\phi_2(b)} & \frac{J_2(b)}{\phi_2(b)} \end{Bmatrix} \cdot \begin{Bmatrix} K_1 \\ K_2 \\ K_3 \\ K_4 \end{Bmatrix} = \begin{Bmatrix} \frac{J_1(a)}{\phi_1(a)} \\ \frac{J_2(a)}{\phi_2(a)} \\ \frac{J_1(b)}{\phi_1(b)} \\ \frac{J_2(b)}{\phi_2(b)} \end{Bmatrix} \qquad (5.4)$$

As only four "base solutions" are needed to be able to develop the solution following an abitrary choice of boundary values, the Superposition Method is clearly very advantageous in its application to one-dimensional problems.

If we use the Superposition Method on two-dimensional problems, the number of base-solutions required depends on how accurately the fluxes and currents are calculated on the four faces of the node. If we take note of the reference solution to the three two-dimensional benchmark problems in Chapter 2, the ten segments on each of the assembly faces are treated individually. Thus, it would require 200 base-solutions in order for that Superposition Method to be able to calculate the exact solution to five group reference problems. It is clear that the Flux-lupe Method described in in Chapter 3 would require less computational effort than the Superposition Method in such cases. On th other hand, if the overall calculation is performed using a coarse-mesh code, where the spatial shapes of the boundary conditions are approximated as either flat, linear, second order polynomial, etc., and where the calculation is performed in fewer energy-groups, the number of base-solutions required will be reduced considerably. For example, if the overall calculation is performed in two energy groups the number of base-solutions will reduce to 80. If the shape of the boundary values is assumed to be flat only 8 base-solutions are required. A

further reduction would be achieved if the overall solution were performed in 1 or $1\frac{1}{2}$ energy groups. In this case only 4 base-solutions need be calculated for each type of assembly. The symmetry of the assembly could further reduce this number. In the case where 180 degree rotational symmetry is present, the required number of base solutions will be reduced by a factor of two.

Only if the required number of base-solutions can be held at a reasonable level without making the pin power determination too much in error, will the Superposition Method become an efficient way of calculating local pin powers. One of the questions to be examined in this chapter is therefore how to estimate the number of base-solutions needed to attain a certain level of accuracy in the pin power determination.

5.3 Generation of the base-solutions to the two-dimensional benchmark problem

The base-solutions to the two-dimensional benchmark problem are generated using a modified version of the box-code CDB (Ref. 7) called CDB/BASE. The difference between the normal version of CDB and CDB/BASE can be summarized in the following four points:

1) CDB/BASE makes it possible to use J^+, J^-, $J/\Phi(\lambda)$, and Φ as boundary parameters (compare Appendix B).

2) In CDB/BASE the parameters J^-, J^+, J/Φ, and Φ can be calculated both on the surface of the assembly and on the surface of subregions inside the assembly.

3) CDB/BASE makes it possible to generate a number of base-solutions with different boundary values in one assembly calculation. The flux distribution from the preceding boundary value problem is used as first estimate in the succeeding boundary value problem.

4) In CDB/BASE it is possible to solve the equation system

directly, e.g. without iteration.
(This feature is accessible only for source calculations).

The only thing the user has to do in excess of normal CDB-input generation is to choose the parameter to be approximated on the boundary of the assembly, and to specify the shape-approximation (either "flat" or "tilt"). On output CDB/BASE will deliver a disk file called BASIS/SUPER/(NO) containing information about: 1) assembly type, 2) burnup levels, 3) void, 4) boundary parameter values, and the local pin powers to match.

Figure 5.1 summarizes the calculation procedure in case of a "flat" approximation of the J/Ø-parameter.

In order to be consistent with the reference solution the base-solution generation is performed in five energy groups and the mesh division is the same as in case of the reference solution (compare Fig. 2.3).

5.4 The "LOCAL-SUPERPOSITION" code.

In this section the basic principles of the "LOCAL-SUPERPOSITION" code will be described. The input data to "LOCAL-SUPERPOSITION" is contained on two disk files "OVERALL/LOCAL" and "BASIS/SUPER/ (NO)". As mentioned earlier, "BASIS/SUPER/(NO)" contains all the base-solutions. The generation of "BASIS/SUPER/(NO)" (described in Section 5.3) is performed on the assembly homogenization state of the reactor physical calculation. "OVERALL/LOCAL", on the other hand, is generated when the global three-dimensional solution is known. "OVERALL/LOCAL" is a shortened version of the disk file "OVERALL" which contains the results from the three-dimensional coarse-mesh nodal solution. For each assembly in the core and for each vertical mesh the following parameters have been stored in "OVERALL":
1) Assembly type, 2) burnup, 3) void, 4) boundary parameter values, and 5) average powers.

The reason why "OVERALL" has been shortened is that one usually is interested in local details only at specific points or certain regions of the reactor core. This selection is performed with the code "SELECT". The code "SELECT" reads the file "OVERALL", selects the interesting nodes, and stores the information about these nodes on OVERALL/LOCAL. The selection of the interesting nodes from the global solution depends on what one is looking for. If the local pin powers are to be tested against detector signals the interesting nodes can easily be pointed out. On the other hand, if one searches for maximum pin powers or maximum changes in pin powers during time-dependent ramps, the problem has a different aspect. In these cases, the selection of the interesting assemblies must be based on experience to a great extent. In this thesis all twenty-four assemblies are regarded as interesting ones, and the files OVERALL and OVERALL/LOCAL are alike.

Knowing the input files to "LOCAL/SUPERPOSITION" we can now proceed with a fast reading of the code itself. The basic subprograms in "LOCAL-SUPERPOSITION" are shown in the following:

1. INPUT
2. MATCH
3. SUPER
4. NORM
5. OUTPUT

1. INPUT

The subroutine INPUT reads the input files "OVERALL/LOCAL" and BASIS/SUPER/(NO). First the type, burnup, void, boundary parameter value, and average nodal power are read on "OVERALL/LOCAL". Next, the file "BASIS/SUPER/(NO)" is scanned looking for a set of base-solutions with the same type, burnup, and void as the node taken from "OVERALL/LOCAL". When the set of base-solutions in question is found, INPUT will read the boundary parameter values and the local pin powers to match.

2. MATCH

The subroutine MATCH solves Equation 5.2. There is no restriction requiring an equal number of equations and unknowns. The only demand is that the number of equations be equal to or larger than the number of unknowns. If the number of equations exceeds the number of unknowns the solution is defined using the following equations:

$$\underline{\underline{A}} \cdot \underline{x} = \underline{b}$$

The best match is defined to be the minimum of

$$||\underline{\underline{A}}\underline{x} - \underline{b}||_2$$

This norm can be written as:

$$||\underline{\underline{A}}\underline{x} - \underline{b}||_2 = (\underline{\underline{A}}\underline{x} - \underline{b})^T \cdot (\underline{\underline{A}}\underline{x} - \underline{b}) =$$

$$\underline{x}^T \cdot \underline{\underline{A}}^T \cdot \underline{\underline{A}} \cdot \underline{x} - 2 \cdot \underline{b}^T \cdot \underline{\underline{A}} \cdot \underline{x} + \underline{b}^T \cdot \underline{b}$$

On differenciating this equation, we obtain

$$2\underline{\underline{A}}^T \cdot \underline{\underline{A}} \cdot \underline{x} - 2\underline{b}^T \cdot \underline{\underline{A}}$$

The minimum is defined by

$$2\underline{\underline{A}}^T \cdot \underline{\underline{A}} \cdot \underline{x} - 2\underline{b}^T \cdot \underline{\underline{A}} = 0 \quad \Rightarrow$$

$$\underline{\underline{A}}^T \cdot \underline{\underline{A}} \cdot \underline{x} = \underline{b}^T \cdot \underline{\underline{A}} \qquad (5.4)$$

Equation 5.4 forms the basis of the subroutine MATCH.

3. SUPER

The subroutine SUPER performs the superposition of the local pin power distributions as shown in Equation 5.2.

4. NORM

In a practical use of LOCAL/SUPERPOSITION the subroutine NORM normalizes the local pin power distribution to the average value from the global solution. In the investigation performed here NORM normalises the local pin power distribution to an average value of 1000 in order to obtain a standard of reference for all twenty-four assemblies.

5. OUTPUT

The subroutine OUTPUT writes the local pin power distribution on the disk file PIN/POWER.

The pin powers determined using LOCAL-SUPERPOSITION are compared with the normalized pin powers (average 1000) from the reference solution. This comparison is performed with the code "COMPAR".

5.5 The accuracy and efficiency of the Superposition Method compared with the Response Matrix Method.

The objective of this section is to determine which of the parameters Ø, J, and J/Ø should be used to define the boundary conditions in the base-solution definition in "CDB/BASE" in order to make the pin power determination accurate and efficient. The Flux-lupe investigation showed that the parameter J/Ø gave the most accurate pin power determination in the case of a new assembly calculation with the boundary conditions determined from the converged global solution.

The question to be answered in this section is whether or not this situation is valid also in the case of the Superposition Method. In the following, the response matrix version of the Superposition Method will be used in the case of the parameters Ø and J. This means, as mentioned in Section 5.1, that there is a similar correspondence between the number and type of boundary parameter derived from the global solution and the number of

base-solutions and the type of parameter used to define the base-solutions. Hence, the number of energy groups in which the boundary conditions have to be defined in the base-solution generation has to be equal to the number of groups in the overall two-dimensional solution of the benchmark problems. Consequently the response matrix has to be generated in five energy groups. The dimension of the response matrix generated by "CDB/BASE" can be calculated using the following equations:

DIMENSION : NP x NB

where

NP: The number of pins in the assembly.

NB: The number of base-solutions, equal the number of boundary parameter values from the converged global solution.

$$NB = NS \cdot NG$$

where

NS: Total number of shape-approximations on all faces of the node.

NG: Number of energy groups in which the boundary parameter is represented.

In this investigation:

NP = 63 (only pin powers different from zero are considered)

$$NS = \begin{cases} 4 & \text{(Flat-approximation of the shape)} \\ 8 & \text{(Tilt-approximation of the shape)} \end{cases}$$

NG = 5

The appearance of the response matrix in the case of a flat approximation of the boundary parameter is shown below

$$\begin{bmatrix} P_1(1) & P_2(1) & P_3(1) & \cdots & P_{19}(1) & P_{20}(1) \\ P_1(2) & P_2(2) & P_3(2) & \cdots & P_{19}(2) & P_{20}(2) \\ P_1(3) & P_2(3) & \cdot & & \cdot & \cdot \\ P_1(4) & \cdot & \cdot & & \cdot & \cdot \\ \cdot & \cdot & \cdot & & \cdot & \cdot \\ \cdot & \cdot & \cdot & & \cdot & \cdot \\ \cdot & \cdot & \cdot & & \cdot & \cdot \\ \cdot & \cdot & \cdot & & \cdot & \cdot \\ \cdot & \cdot & \cdot & & \cdot & \cdot \\ P_1(62) & \cdot & \cdot & & \cdot & P_{20}(62) \\ P_1(63) & \cdot & \cdot & & P_{19}(63) & P_{20}(63) \end{bmatrix}$$

$P_N(M)$: The power in pin no. M in the $N^{'th}$ base-solution.

The final pin power solution (sol) is determined by

$$\underline{sol} = \underline{\underline{P}} \cdot \underline{b}$$

where

$\underline{\underline{P}}$: Response matrix

$\underline{b}$: The "actual" values of the global boundary parameter (ϕ or J)

The situation is different in the case of the J/ϕ-approximation. In the first place, the parameter J/ϕ cannot be used to generate a response matrix (Section 5.2). Secondly, experience has shown that the ratio, $\nabla\phi_G/\phi_G$, is nearly constant in all energy groups on the faces of assemblies lying in the interior of the core. For instance, in the case of a five energy group representation the following relation can be stated:

$$\frac{\nabla\phi_1}{\phi_1} \approx \frac{\nabla\phi_2}{\phi_2} \approx \frac{\nabla\phi_3}{\phi_3} \approx \frac{\nabla\phi_4}{\phi_4} \approx \frac{\nabla\phi_5}{\phi_5}$$

However, on faces adjoint to the reflector the situation will differ. In these regions there will be leakage out of the face in the fast groups and into the region in the thermal groups.

Hence, the ratio $\nabla\Phi_G/\Phi_G$ has to be divided in a fast part where the ratio is constant in the fast groups,

$$\frac{\nabla\Phi_1}{\Phi_1} = \frac{\nabla\Phi_2}{\Phi_2} = \frac{\nabla\Phi_3}{\Phi_3} = \lambda \qquad \text{(positive value)}$$

and a thermal part in which the ratio is constant in the thermal groups,

$$\frac{\nabla\Phi_4}{\Phi_4} = \frac{\nabla\Phi_5}{\Phi_5} = \lambda \qquad \text{(negative value)}$$

If the ratio $\nabla\Phi_G/\Phi_G$ fulfils the postulate noted above, the base-solution generation can be carried out in a "one group" representation of the boundary parameter J/Φ in the interior nodes, and in a "two group" representation for nodes lying next to the reflector.

A "one group" representation of J/Φ means in this connection that the base-solution generation is performed in five energy groups (in order to be consistent with the reference solution), but each shape-approximation on the four faces is carried out in only one energy group using the following definition

$$\frac{\nabla\Phi_1}{\Phi_1} = \frac{\nabla\Phi_2}{\Phi_2} = \frac{\nabla\Phi_3}{\Phi_3} = \frac{\nabla\Phi_4}{\Phi_4} = \frac{\nabla\Phi_5}{\Phi_5} = \lambda \qquad \text{(eigenvalue)}$$

A "two-group" representation of the boundary parameter J/Φ means that two sets of base-solutions are generated for each shape-approximation on the four faces of the node, one with

$$\frac{\nabla\Phi_G}{\Phi_G} = \lambda \qquad \text{in the fast groups}$$

$$\frac{\nabla\Phi_G}{\Phi_G} = 0 \qquad \text{in the thermal groups}$$

and one with

$$\frac{\nabla \phi_G}{\phi_G} = 0 \qquad \text{in the fast groups}$$

$$\frac{\nabla \phi_G}{\phi_G} = \lambda \qquad \text{in the thermal groups}$$

In Section 5.6 we will examine the group dependence of $\frac{\nabla \phi}{\phi}$ in more detail.

In the case of the Superposition Method two matrices are generated by "CDB/BASE", one in which the boundary parameters are stored, $\underline{\underline{B}}$, and one containing the pin powers to match $\underline{\underline{P}}$. The dimensions of these matrices can be calculated using the following equation:

DIMENSION OF $\underline{\underline{B}}$: NBP x NB

DIMENSION OF $\underline{\underline{P}}$: NP x NB

where

NBP: Number of boundary parameter values from the converged global solution.

NP : Number of pins in each assembly.

NB : Number of base-solutions.

NB = NS x NG

NS : Total number of shape-approximations on all faces of the node.

NG : Number of energy groups in which the boundary parameter is represented in the base-solution generation.

NBP = 2·JG·NS

JG : Number of energy groups in the converged global solution.

In this investigation:

JG = 5

NP = 63

$$NS = \begin{cases} 4 \text{ (Flat-approximation of the shape)} \\ 8 \text{ (Tilt-approximation of the shape)} \end{cases}$$

$$NG = \begin{cases} 1 \text{ (Interior assemblies)} \\ 2 \text{ (Assemblies adjoining the reflector region)} \end{cases}$$

The appearance of matrices $\underline{\underline{B}}$ and $\underline{\underline{P}}$ is shown below in the case of a flat approximation of the parameter J/Ø on an interior node in the core

$$\begin{Bmatrix} \underline{J_1}(a) & \underline{0} & \underline{0} & \underline{0} \\ \underline{0} & \underline{J_2}(b) & \underline{0} & \underline{0} \\ \underline{0} & \underline{0} & \underline{J_3}(c) & \underline{0} \\ \underline{0} & \underline{0} & \underline{0} & J_4(d) \\ \underline{\emptyset_1}(a) & \underline{\emptyset_2}(a) & \underline{\emptyset_3}(a) & \underline{\emptyset_4}(a) \\ \underline{\emptyset_1}(b) & \underline{\emptyset_2}(b) & \underline{\emptyset_3}(b) & \underline{\emptyset_4}(b) \\ \underline{\emptyset_1}(c) & \underline{\emptyset_2}(c) & \underline{\emptyset_3}(c) & \underline{\emptyset_4}(c) \\ \underline{\emptyset_1}(d) & \underline{\emptyset_2}(d) & \underline{\emptyset_3}(d) & \underline{\emptyset_4}(d) \end{Bmatrix} = \underline{\underline{B}}$$

where

$$\underline{J_N}(x) = \begin{Bmatrix} J_1(x) \\ J_2(x) \\ J_3(x) \\ J_4(x) \\ J_5(x) \end{Bmatrix} \qquad \underline{\emptyset_N}(x) = \begin{Bmatrix} \emptyset_1(x) \\ \emptyset_2(x) \\ \emptyset_3(x) \\ \emptyset_4(x) \\ \emptyset_5(x) \end{Bmatrix} \qquad \underline{0} = \begin{Bmatrix} 0 \\ 0 \\ 0 \\ 0 \\ 0 \end{Bmatrix}$$

N = 1, 2, 3, 4

x = a, b, c, d

$J_{GR}(x)$: the average value of the current on face x in Group GR.

$\emptyset_{GR}(x)$: the average value of the flux on face x in Group GR.

GR = 1, 2, 3, 4, 5

$$\left\{\begin{array}{cccc} P_1(1) & P_2(1) & P_3(1) & P_4(1) \\ P_1(2) & P_2(2) & P_3(2) & P_4(1) \\ P_1(3) & P_2(3) & . & . \\ P_1(4) & . & . & . \\ . & . & . & . \\ . & . & . & . \\ . & . & . & . \\ . & . & . & . \\ . & . & . & . \\ P_1(62) & P_2(62) & . & P_4(62) \\ P_1(63) & P_2(63) & . & P_4(63) \end{array}\right\} = \underline{\underline{P}}$$

In the case of the Superposition Method the local pin power distribution is calculated using the following equations:

$$\text{minimum of } ||\underline{\underline{B}} \cdot \underline{x} - q||_2 \qquad \text{(compare Section 5.4)}$$

$$\underline{sol} = \underline{\underline{P}} \cdot \underline{x}$$

where q contains the boundary parameter values from the converged global solution and $\underline{sol}$ is the predicted local pin powers.

An investigation of the efficiency of the Superposition Method compared with the Response Matrix Method shows that the former is approximately a factor of five faster than the latter as most of the computer time is taken up by the generation of the base-solution.

The Superposition Method is also superior to the Response Matrix Method with regard to the demand of storage requirements. The ratio of the number of values stored in a superposition calculation to that of a response matrix calculation is approximately 1:3 in the flat approximation case.

One can thus maintain that the Superposition Method in this particular case makes a more efficient way of calculating local pin powers than the Response Matrix Method.

The question that still must be answered is how the accuracy of the Superposition Method compares with the Response Matrix Method. In order to answer this question we use box 5 in the three benchmark problems defined in Chapter 2 as test cases. Both the tilt and the flat approximations are considered. Concerning the J/Ø-approximation, the one-group representation is used in test cases 1 and 2, whereas the two-group representation is used in test case 3.

Table 5.1 summarizes the results of this investigation. Also shown in this table is the number of base-solutions required for each shape-approximation.

From this investigation it can be concluded that when the boundary fluxes are applied in generating the base-solution the shape approximation must be more accurately defined than a "tilt"-approximation if the accuracy of the pin power prediction is to lie below 10%. The number of base solutions required is therefore of such a magnitude that the efficiency of the Superposition Method will be very poor.

Concerning the J-approximations it can be stated that the "tilt"-approximation of the boundary shapes is required if the maximum pin power error is to be below 10%. On the other hand, if the "tilt"-approximation is adopted the error will be less than 5% in the interior assemblies. This is invalid for the assemblies lying close to the reflector. With respect to these assemblies the "flat"-approximation will be superior to the "tilt"-approximation in the case of both the J- and the J/Ø-approximations. This finding agrees well with the results obtained in the Fluxlupe investigation.

The most important thing to be deduced from the investigation described above is that if the Superposition Method is adopted and the base-solutions are defined using J/Ø-approximations of

the boundary conditions one can get pin power predictions that are nearly as accurate as those with the Response Matrix Method and with far fewer base-solutions in the former case. The reason for the superiority of the J/Ø-approximations to both the Ø- and J-approximations is that in the combined approximation one does not fix the shape of either fluxes or currents on the boundaries. Hence, local heterogeneities inside the assembly will form the shape of boundary currents and fluxes. As a consequence, the boundary shapes of the base-solutions will be in better agreement with the global heterogeneous shapes, than in case of the J- and Ø-approximations, because the global shapes are influenced by the same local heterogeneities.

5.6. The relationship between the accuracy of the pin power determination and the number of base-solutions

In Section 5.2 it was indicated that the feasibility of the Superposition Method was dependent on the required number of base-solutions. Only if the required number of base-solutions can be held at a reasonable level without causing the pin power determination to be too much in error will the Superposition Method become an efficient way of calculating local pin powers. The object of this section is therefore to find out how many base-solutions are required in order to obtain a certain level of accuracy in the pin power determination.

As mentioned earlier, the number of base-solutions is defined by

$$NB = 4 \cdot NG \cdot NS$$

where NG is the number of energy groups in which the boundary parameters are represented.

NS is the shape-approximation factor

$$NS = \begin{cases} 1 & \text{"FLAT" approximation} \\ 2 & \text{"TILT" approximation} \\ 3 & \text{"PARABOLIC" approximation} \\ 10 & \text{"reference solution to the benchmark problem"} \end{cases}$$

In the two-dimensional benchmark problem the number of base-solutions is given by

$$NG = 5$$

$$\Rightarrow \quad NB = 200$$

$$NS = 10$$

and the "full" equation system to be solved by LOCAL/SUPERPOSITION can be set up as:

$$\underline{\underline{B}} \cdot \underline{x} = \underline{b}$$

$$\underline{sol} = \underline{\underline{P}} \cdot \underline{x}$$

where $\underline{\underline{B}}$ is a 200 × 200 matrix containing the boundary parameter values from the 200 base-solutions

$\underline{b}$ is a vector containing the 200 boundary parameter values from the global solution

$\underline{\underline{P}}$ is a 63 × 200 matrix containing the pin power distributions for the 200 base-solutions.

There are no special difficulties in solving this equation system; the problem lies within the generation of the two hundred base solutions. The computational effort required in order to perform all these solutions is of a magnitude such that the Flux-lupe Method will make up a better pin power method even if local pin power distributions are to be determined all over the reactor core.

On the other hand, if the overall calculation is performed using a coarse-mesh code, one cannot expect to be able to get such de-

tailed information about the shape of the boundary parameter values. Typically, only the average values of the boundary parameters in two energy groups can be derived from a converged coarse-mesh solution.

In the Flux-lupe investigation it was shown that an accurate pin power determination requires information about corner values of the boundary parameter values. How these corner values can be approximated based on average values of boundary fluxes and currents and the average nodal fluxes is described in Ref. 8. In this thesis we will assume that Koebke's extrapolation scheme (Ref. 8) is able to deliver the correct heterogeneous corner values of fluxes and currents; hence, we use the values from the reference solution condensed to two energy groups. It is these condensed reference values of fluxes and currents which will be used as "global" boundary parameter values in the remainder of this thesis.

Hence, if nothing else is stated, the pin power determination will be based on the 48-global parameter values contained in vector $\underline{b}$ defined by:

$$\underline{b} = \begin{vmatrix} \underline{b}_1 \\ \underline{b}_2 \\ \underline{b}_3 \\ \cdot \\ \cdot \\ \cdot \\ \underline{b}_{12} \end{vmatrix}$$

$$\underline{b}_n = \begin{vmatrix} \phi_1 \\ \phi_2 \\ J_1 \\ J_2 \end{vmatrix} \qquad n = 1,2,3,\ldots,11,12$$

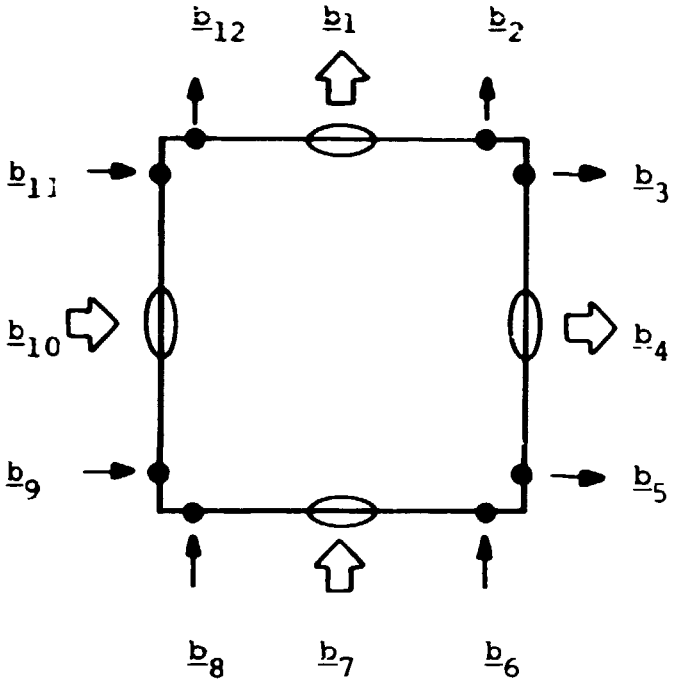

The condensation of the boundary parameter values to two energy groups has to be followed by a proportional reduction in the number of energy groups in which the boundary conditions of the base-solutions are defined, in order to obtain a direct correspondence between the local pin power problem and the global coarse-mesh solution. As the number of energy groups in the assembly calculation cannot be reduced without causing errors in the homogenized cross section generation that are too large, one has to maintain a fixed relationship between the J/Ø ratios in the fast groups and a fixed relationship between the J/Ø ratios in the thermal groups.

The approximation applied in this thesis is the commonly employed assumption of equal extrapolation distances in the fast groups, and equal extrapolation distances in the thermal groups. The group relation between the boundary conditions is hereby defined as:

$$\frac{\nabla\emptyset_1}{\emptyset_1} = \frac{\nabla\emptyset_2}{\emptyset_2} = \frac{\nabla\emptyset_3}{\emptyset_3} \qquad \text{(fast energy groups)}$$

$$\frac{\nabla\emptyset_4}{\emptyset_4} = \frac{\nabla\emptyset_5}{\emptyset_5} \qquad \text{(thermal energy group)}$$

The size of the equation system is hereby reduced:

$\underline{\underline{B}}$ is now a 24 × 24 matrix

$\underline{\underline{P}}$ is a 63 × 24 matrix

Even though the number of base-solutions is reduced from 200 to 24 the Superposition Method requires so much computational effort that the efficiency of the method still is very poor. Only a further reduction can make the Superposition Method an efficient way of calculating pin powers.

As mentioned earlier, the number of base-solutions does not have to be equal to the number of global boundary parameter values in the superposition scheme. Hence, the number of base-solutions can be reduced further and still we can use all 48 global values to determine the pin power distribution.

In Section 5.4 it was mentioned that if the number of global boundary parameters exceeds the number of base-solutions the solution is defined by the minimum of the Euclidean norm:

$$\underline{x} = \min \{||\underline{\underline{B}} \cdot \underline{x} - \underline{b}||_2\}$$

where $\underline{\underline{B}}$ is an NBP × NB matrix (NBP > NB).

The "error" vector, f, is defined by

$$\underline{f} = (\underline{\underline{B}} \cdot (\underline{\underline{B}}^T \cdot \underline{\underline{B}})^{-1} \cdot \underline{\underline{B}}^T - \underline{\underline{E}}) \cdot \underline{b}$$

When further approximations are introduced in the base-solution generation these approximations have to be defined in a way that minimizes the "error" vector $\underline{f}$. What makes the minimalization of the error vector f problematic is the dependence of the solution on where the assembly is placed in the reactor core through the influence of the vector $\underline{b}$. However, if there is a fixed relation between some of the global boundary parameter values, for each assembly type throughout the core this relationship can be utilized in order to minimize the error-vector $\underline{f}$.

In this thesis we will not look for fixed relations in the reference solution, which could be utilized in order to find the minimum of $\underline{f}$, because the question of whether or not such fixed relations exist depends on the reactor design and cannot be generalized. If we adjust the base-solutions to the reference solution, we could certainly improve the accuracy of our pin power determination, but the result of our investigation would not give a real picture of the accuracy of the general use of the Superposition Method. Instead, we will use commonly employed approximations to define the boundary conditions in the generation of base-solutions.

There are two ways of further reducing the number of base-solutions. Firstly, the number of energy groups in which the boundary parameters are represented can be reduced by stipulating a fixed relation between the J/Ø-ratios in the fast and thermal groups. Secondly, the shape of the boundary parameter values can be approximated as either being "flat" or having a "tilt".

Let us first consider the group reduction problem. In all the investigations performed in the remainder of this chapter we will assume that the group fluxes are zero at the same extrapolated distance in those energy groups which have leakage rates that differ from zero. Hence, only two possible values of the extrapolation distance can be used on each of the four faces of the assembly:

$$\frac{\nabla \emptyset_G}{\emptyset_G} = \begin{cases} \lambda & \text{(the eigenvalue)} \\ 0 & \text{(zero net current boundary condition)} \end{cases}$$

One thing of which one must be aware is that even if the group relation between the boundary conditions are fixed in the base-solution generation, these fixed values will not be transferred to the final superposed solution. Hence, it is possible to adjust the group relation between the combined extrapolation factors to the "actual" values from the global coarse-mesh solution. This would have been impossible if either the fluxes or the currents had been used to define the boundary conditions for the

base problems, because a fixed relation between the group-boundary conditions would have been transferred to the final solution.

In the following we will investigate three different group approximations. In all three cases the boundary shape is approximated as "flat". In the first place, we assume that the thermal leakage can be neglected. Hence, we have a one-group approximation requiring only four base-solutions. In the second test case we assume that the fast extrapolation distance is equal to the thermal extrapolation distance. Also, in this case we have only to calculate four base-solutions. In the third test case we use the two-group approximation where the leakage rates are divided into fast and thermal parts. Eight base-solutions are required in order to approximate this separation.

Figure 5.2 shows the results of the above-mentioned three test cases applied on the three benchmark problems defined in Chapter 2. It appears from the figure that the maximum error in the pin power prediction is 12.9% in test one, 19.1% in test two, and 20.5% in test three if we assume that the thermal currents can be neglected in the base-solution generation. If the thermal extrapolation distance is assumed to be equal to the fast extrapolation distance the corresponding errors will be 9.5%, 12.2%, and 27.4%. By separating the leakage terms using the two-group approximation these errors can be reduced to 8.9%, 10.5%, and 12%.

From this investigation it can be concluded that the two-group approximation does not improve the pin power determination appreciably in the interior assemblies compared with the one-group approximation when we assume equal extrapolation distances in the two groups. However, in the assemblies lying close to the reflector region the pin power determination will be improved by a factor of two when the two-group approximation is applied. This is because the thermal extrapolation distances are negative on the faces adjoining the reflector, while the corresponding fast extrapolation distances are positive. Clearly, one can improve the pin power predictions in the assemblies lying close to the reflector by using the two-group approximation.

Based on the "group-reduction" investigation one can conclude that if we want to determine local pin powers with an accuracy below 10%, we have to approximate the boundary shapes in more detail than in case of the "flat"-approximation. In the following, different shape approximations will be investigated. There will be made use of the results from the group reduction investigation by separating the examination in an "interior" problem (tests one and two) and a "close-to-the-reflector" problem (test three). In the "interior" problem we will apply the one-group approximation and in the "close-to-the-reflector" problem the two-group approximation will be used.

In the Flux-Type investigation it was shown that the shape approximation on the faces adjoining the broad water gap was only slightly improved by applying the "tilt"-approximation compared with the "flat"-approximation. One of the questions to be answered in this section is whether or not this fact also is valid in case of the Superposition Method.

Three different shape approximations are examined in case of the "interior" problem:

SUPER/6 : "Tilt"-approximation on the narrow water gap faces and "flat"-approximation on broad water gap faces (6 base-solutions).

SUPER/8T: "Tilt"-approximation on all four faces (8 base-solutions).

SUPER/12: Combined "tilt"- and "flat"-approximations on all four faces (12 base-solutions).

The boundary conditions for each of the three test cases are summarized in detail in Fig. 5.3. Figure 5.4 shows the result of the three test cases applied to the two interior benchmark problems. Also shown in this figure are the results from the "flat"-approximation used in a one-group representation (SUPER/4). It appears that SUPER/6 can almost predict the local pin powers to the same accuracy as SUPER/8T and SUPER/12. This result is in

good agreement with the Flux-lupe investigation with respect to SUPER/6 and SUPER/8T. Concerning SUPER/12 we would have expected a more marked reduction in the errors compared with SUPER/8T. In Section 5.7 we will show that it is possible to reduce the error in the pin power determination based on SUPER/12. This further reduction of the maximum error will confirm the results of the Flux-lupe investigation.

Let us now turn to the "close-to-the-reflector" problem. In the investigations dealing with the group dependence of the maximum pin power error it was shown that concerning the assemblies lying close to the reflector, the two-group approximation had to be applied in order to make the Superposition Method superior to the one based on normalization. Even when the two-group approximation is applied the maximum error will still lie above 10%. The question to be answered in the remainder of this section is whether or not it is possible to reduce the maximum error in order to get it well below 10%. In Section 5.5 it was demonstrated that the "flat"-approximation was superior to the "tilt"-approximation in the case where the assemblies lying close to the reflector. Hence, if we want to improve the pin power determination this cannot be done by introducing the "tilt"-approximation, as was done in the case in the interior assemblies. Clearly, the pin power determination can be improved by using the "parabolic"-approximation, but this means that one has to calculate 24 base-solutions.

On comparing the results in Table 5.1 with those in Fig. 5.2, we find that the base-solution set SUPER/8 gives different results when used on the "same" problem. In Table 5.1 the maximum error in box 5 is 7.8% while the corresponding error in Fig. 5.2 is 12%. This difference results from use of only average values of the boundary parameters in yielding 7.8% rather than all 48 boundary parameter values as in the case of the 12% error. Hence, it turns out to be possible to improve the pin power determination by neglecting some of the boundary parameter values from the global solution. This topic will be investigated in more detail in Section 5.7.

Let us conclude this section by repeating the most interesting findings: The maximum error in the local pin power determination can be held at about 5% in the interior assemblies using only 6 base-solutions. In the assemblies lying next to the reflector the two-group approximation has to be applied. Considering only average values of the global boundary parameters and using the "flat"-approximation the error will be limited to about 7%.

5.7. The relationship between maximum errors in the local pin power determination and the number of boundary parameter values

The investigations performed in Section 5.5 were based on all 48 global boundary parameter values. However, it was demonstrated that in the case where the assemblies lie next to the reflector one could improve the pin power determination by considering only average values of boundary-fluxes and currents. The object of this section is to find out if it is possible, in general, to improve the pin power determination by considering only part of the global boundary parameter values. Furthermore, the investigation will give a picture of how accurately the pin power distribution can be predicted, if only part of the boundary parameter values can be derived from the converged global coarse-mesh solution.

In the following we will make use of the results obtained in the previous section by considering only the base-solution set SUPER/6" in the interior assemblies and "SUPER/8" in the assemblies lying close to the reflector.

The possibility of using weight factors in "LOCAL/SUPERPOSITION" has been applied. The weight factors of the boundary parameter values which are to be neglected are set to zero. All other parameters have a unit weight factor. The following boundary parameter values and combinations of boundary parameter values have been examined on the three benchmark problems:

1) $\bar{\phi}_1$, $\bar{\phi}_2$, $\bar{J}_1$, and $\bar{J}_2$ (only average values)

2) ϕ_1 (corner) + $\bar{\phi}_1$ (average)

3) ϕ_2 (corner) + $\bar{\phi}_2$ (average)

4) ϕ_1 (corner) + ϕ_2 (corner) + $\bar{\phi}_1$ (average) + $\bar{\phi}_2$ (average)

The results of this examination are summarized in Fig. 5.5.

ad 1
If only the average values of the boundary parameter values are applied in the matching procedure the maximum error will increase from 6.3% to 13.4% in the interior assemblies. With respect to the assemblies lying next to the reflector the accuracy of the pin power prediction will increase from 12.0% to 7.7%.

ad 2
If only the fast fluxes are used in the matching procedure the maximum error will increase to 11.8% in the interior asemblies and to 156.3% for the assemblies lying next to the reflector.

ad 3
If only the thermal fluxes are considered the corresponding errors will be 10.2%, and 19.6%.

ad 4
Using both thermal and fast fluxes in the matching procedure the maximum errors will be reduced to 5.4% in the interior assemblies. The maximum error will be unaltered at 12.0% in the assemblies lying next to the reflector.

The four test cases have also been applied to the base-solution set "SUPER/12", and it has been shown that if thermal fluxes alone are considered during the matching procedure in "LOCAL/SUPERPOSITION" the maximum error can be reduced by a factor of two (Fig. 5.6) in the interior nodes. With this reduction the maximum error in the pin power determination using the parabolic approximation presented in "SUPER/12" will reach a level which is in agreement with the results from the Flux-lupe investigation.

In order to demonstrate if a further reduction in the maximum pin power error can be achieved by allowing weight factors different from zero and unit, a "trial and error" investigation has been performed on the three benchmark problems. The base-solution set SUPER/6 is applied in the interior assemblies and SUPER/8 is used in case of the assemblies lying close to the reflector. Figure 5.7 summarizes the results of this investigation. It appears that by choosing the "right" weight factors the maximum error can be reduced from 5.4% to 3.5% in the interior assemblies, and from 7.7% to 7.0% in the case of those assemblies lying next to the reflector.

5.8. Summary

The Superposition Method has proved to be both an efficient and accurate pin power model. If the base-solutions are defined using J/Ø parameters as boundary conditions, one can predict pin powers with a maximum error of about 5% using only six base-solutions. The computational effort required to generate these base-solutions is not a factor of six greater than the assembly calculation that was performed to determine the homogenized parameters. Firstly, symmetry in the pin enrichment can reduce the number of calculations by a factor of two or four. Secondly, computing time is saved by using the flux distribution from the preceding boundary value problem as a first estimate in solving the succeeding boundary value problem. The computing time required in order to generate the six base-solutions in "SUPER/6" is measured to be about a factor of two greater than the "normal" assembly calculation; due to symmetry in the pin enrichment we have to solve only three boundary value problems.

One question which still remains to be answered is whether or not it is possible to give an opinion on the maximum error without knowing the reference solution. This problem has been examined.

Three possible relationships have been proposed:

1) The Eucleadian norm ~ maximum pin power error

$$||\ \ ||_2 \sim \Delta P_{max}$$

2) The maximum norm ~ maximum pin power error

$$||\ \ ||_\infty \sim \Delta P_{max}$$

3) The normalization factor in subroutine "NORM" (compare Section 5.4) ~ maximum pin power error

$$P_{NORM} \sim {}^{\Delta}P_{max}$$

It has been shown that it is possible to predict errors above 10% with all three schemes, but there are no unique relationships between the three methods and maximum errors in the range 0-10%. Perhaps a combination of the three schemes will make it possible to predict errors below 10%, but this has not yet been demonstrated.

6. THE MODULATION METHODS

6.1. Introduction

The modulation technique is well known in relationship to field theory where wave functions with different frequencies are superimposed by a multiplicational procedure. In its connection with the problem of predicting local pin powers, the modulation methods will describe a common designation for all pin power models which basically defines the pin powers by multiplying two or more sets of form functions.

In this chapter the efficiency and the accuracy of a modulational scheme proposed by K. Koebke and M. Wagner (Ref. 2) will be examined. The theory behind this method relates closely to the problem of generating consistent sets of equivalent diffusion theory constants, because, as we shall see, the homogenized assembly solution is used in order to define the form functions.

A theoretically correct use of Koebke's and Wagner's modulation scheme requires a more sophisticated homogenization method. However, in this chapter we will examine if it is possible to use Homogeneous-Heterogeneous Modulation based on flux-volumen weighted homogenized cross sections.

Finally, a new method designed especially for PWR and developed at MIT (Ref. 9) will be described.

6.2. Homogeneous-Heterogeneous Modulation (HHM)

As mentioned in the introduction to this chapter, the Homogeneous-Heterogeneous Modulation scheme is closely related to the problem of determining homogenized cross sections, because the local heterogeneous flux distribution is defined as:

$$\phi_G^{HET}(x,y) = \frac{\phi_G^{HET*}(x,y)}{\phi_G^{HOM*}(x,y)} \cdot \phi_G^{HOM}(x,y)$$

where $\phi_G^{HET*}(x,y)$ is the solution to the transport or the diffusion theory equation with fixed net current boundary conditions.

$\phi_G^{HOM*}(x,y)$ is the corresponding homogenized solution (with the same net current boundary conditions as in case of ϕ_G^{HET*}).

$\phi_G^{HOM}(x,y)$ is the homogenized assembly solution based on the boundary parameter values from the global coarse-mesh solution.

It appears from this equation that Koebke's and Wagner's modulation scheme is theoretically exact if and only if the ratio $\phi_G^{HET*}(x,y)/\phi_G^{HOM*}(x,y)$ is independent of the outer boundary conditions. There is no reason why this ratio-function should be independent of the boundary conditons if the $\phi^{HOM*}(x,y)$ solution is based on flux-volumen weighted cross sections. On the other hand, if the homogenization scheme is designed in order to make this ratio fixed or nearly fixed then the HHM-method is able to predict local pin powers very accurately. A new homogen-

ization scheme has been developed at KWU in Germany (Ref. 10), primarily to improve the average nodal power determination, but also in order to be able to reconstruct a good approximation of the local heterogeneous power distribution. A unique feature of the method is that flux continuity between adjacent homogenized regions is no longer postulated. The discontinuity of the flux is represented by an additional equivalence parameter, the heterogeneity factor. For the description of the interaction between rectangular assemblies, it is necessary to use the directional dependence of the diffusion coefficients and also of the heterogeneity factors. The theory behind this homogenization scheme is called "equivalence theory", and it is described and examined in Chapter 8.

In this section we will examine Koebke's claim that the ratio of the known heterogeneous flux distribution to the equivalence few-group distribution

$$F_g^{HET}(x,y) = \frac{\phi_g^{HET}(x,y)}{\phi_G^{HOM}(x,y)}$$

is relatively independent of the outer boundary conditions (Ref. 10). If Koebke's claim is valid also for BWR then the heterogeneous flux distribution can be regained by applying HHM.

Before we proceed with the above-mentioned investigation, one problem still remains to be solved: In Ref. 10 Koebke claims that in the case of non-symmetric boundary conditions the diffusion coefficients and the heterogeneity factors will be uniquely defined. Though Koebke does not mentioned it explicitly, he must assume that only equivalence flux shapes that are positive everywhere in the region to be homogenized can be regarded as solutions to the equivalence equation system. Otherwise, there will be an infinite number of solutions (compare Chapter 8). However, if only flux solutions that are positive everywhere are considered then there will exist problems for which no solution can be found. Our experience has shown that the equivalence flux shape always will be negative in the corners where control rods are placed; this is because of the large flux

gradients across controlled assemblies. Hence, if only positive fluxes are considered then the equivalence equation system will be inapplicable in the case of controlled assemblies. The simplest approach for alleviating this difficulty is to allow negative homogenized flux shapes and choose the one and only solution which has the least negative flux shape.

Of course, this will lead to an unphysical homogenized flux solution. However, the nature of equivalence theory is unphysical because the diffusion coefficients are treated as totally artificial quantities. Hence, there are no theoretical reasons for requiring the homogenized flux shapes to be everywhere positive.

One of the questions to be answered in the remainder of this section is whether or not it is possible to regain the heterogeneous pin powers using homogenized flux shapes that are <u>not</u> positive everywhere.

The test cases used in order to examine the relationship between form factor distributions and the outer boundary conditions differ slightly from the three benchmark problems. For simplicity, the leakage rates out of or into the subregions are defined so that there exists a symmetry line from the upper left corner to the lower right. In the following we will concentrate only on box 5; hence, the above-mentioned simplification means that we must calculate merely one set of equivalence parameters for each test case, because the directional-dependent diffusion coefficient has the same value in both directions. Furthermore, we are considering only average currents both in the reference solution generation and in the form factor generation, in order to avoid inaccuracies in the local pin power determination which could be derived from errors in the shape approximation. Hence the reference solution for box 5 is defined to be the solution of an assembly calculation with the average values of net currents from the global solutions used to define the boundary conditions.

Three buffer-zone configurations are considered for Test 1 and Test 2 (compare Chapter 2) defining six new test cases:

Test 1/I	Test 2/I
Test 1/II	Test 2/II
Test 1/III	Test 2/III

Throughout this investigation, the heterogeneous calculations are performed in five energy groups, whereas the homogenized problems are defined in two energy groups. The calculation procedure is, in short:

1) The solution of the symmetric versions of the benchmark problems (Test 1 and Test 2) are calculated using "CDB", and the average net currents on the boundaries of box 5 are determined and condensed to two energy groups.

2) Six assembly calculations with the five-group average net currents as boundary conditions are performed with CDB. Beyond the defining of the heterogeneous solutions $\emptyset_G^{HET}(x,y)$ these assembly calculations will also produce the two-group equivalence parameters Σ_α. These parameters are calculated using the flux-volumen weighting scheme.

3) The diffusion coefficients and the heterogeneity factors are determined by an iterational use of "CDB" on the homogenized problems with the two-group net currents from point 1 as boundary conditions. At each step in the iteration, the heterogeneity factors are calculated on both surfaces of the assembly, and whether or not these factors are identical on both surfaces is examined. If the conditions have not been met, new values of the diffusion coefficients are computed, and the process repeated until convergence is achieved. The flux- and power distributions in the final solution make up the homogenized solution $\emptyset_G^{HOM*}(x,y)$.

4) Finally, the heterogeneous flux solutions are condensed to two energy groups, and the form factor distributions $F_G(x,y)$ are calculated for each of the six test cases.

Figure 6.1 shows the average values of the heterogeneous boundary fluxes and currents for the six test cases. The corresponding equivalence parameters are represented in Table 6.1. It appears from the table that the fast diffusion coefficients are positive in all six test cases, whereas the thermal diffusion coefficient is always negative. The corresponding heterogeneity factors lie in the 0.9306-1.5219 range. The table also shows that the equivalence diffusion coefficients depend very much on the heterogeneous boundary conditions. This is especially evident in case where the assemblies are uncontrolled, and where the fast diffusion coefficient then varies in the 0.7015-23.51 range.

Figure 6.2 summarizes the fast form factor distributions for the controlled assemblies Test 1/I, Test 1/II, and Test 1/III. It appears that there are only small differences in the three distributions. The situation is quite different with respect to the thermal form factor distributions (Fig. 6.3). Large oscillations in the form factor distributions occur in the corner where the control rod is placed. Although the shape of these oscillations are similar in all three cases, the magnitude varies very much. Hence, the postulate of an independency of the form factor distribution of the outer boundary conditions is invalid in the case of controlled assemblies with negative homogenized flux distributions.

Figures 6.4 and 6.5 show the fast and thermal form factor distributions for the uncontrolled assembly, respectively. It appears that the shape and magnitude of the fast form factor distributions are similar in all three cases, whereas the thermal distribution has similar shape and magnitude only in Test 2/II and Test 2/III. The large differences between the form factor distribution for Test 2/I, Test 2/II, and Test 2/III is caused by the large differences in the equivalence parameters (compare Table 6.1).

The Homogeneous-Heterogeneous Modulation Method has been examined using Test 1/II and Test 2/II as basis solutions ($\phi_G^{HET*}(x,y)$, $\phi_G^{HOM*}(x,y)$ and Test 1/I, Test 1/III, Test 2/I, and Test 2/III as overall solutions ($\phi^{HET}(x,y)$, $\phi^{HOM}(x,y)$. Figure 6.6 summarizes

a comparison between the heterogeneous power distributions to Test 1/I, Test 1/III, Test 2/I, and Test 2/III and the corresponding modulated power distributions (Eq. 6.1)

$$P_{MOD}(x,y) =$$

$$K \cdot \left(\Sigma_{f1} \cdot \frac{\phi_1^{HET*}(x,y)}{\phi_1^{HOM*}(x,y)} \cdot \phi_1^{HOM}(x,y) + \Sigma_{f2} \cdot \frac{\phi_2^{HET*}}{\phi_2^{HOM*}} \cdot \phi_2^{HOM}(x,y) \right) \tag{6.1}$$

Table 6.2 summarizes the maximum errors in the modulated pin powers compared with the maximum errors using the Normalization Method with Test 1/II and Test 2/II as base solutions. It appears that the maximum error in the modulated pin power distribution is 15.23% for Test 1/I and 16.88% for Test 1/III whereas the errors caused by the use of the simpler Normalization Method are 14.66% and 4.43%, respectively. With respect to the uncontrolled assembly the maximum errors will be 54.75% (Test 2/I) and 0.64% (Test 2/III) in case of the modulated pin powers and 15.03% and 2.76% in case of the normalized pin powers.

From this investigation it can be concluded that homogenized flux solutions with negative values cannot be used in order to regain the heterogeneous pin powers applying the HHM method. Large oscillations in the form factor distribution will occur at places where the equivalence flux distribution changes sign, causing large errors in the modulated pin power distribution. From the uncontrolled assembly investigation it can be concluded that the accuracy of the modulated pin powers depends very much on how much the boundary currents in the overall solution differs from the base values. Only if the shape of the overall net currents are similar to the shape of the base values, will the HHM method make up an accurate way of calculating pin powers.

6.3. Homogeneous-Heterogeneous Modulation based on flux-volumen weighted homogenized cross sections

In this section we will investigate if it is possible to use flux-volumen weighted homogenized cross sections in connection with HHM. As mentioned earlier, there is no theoretical basis for HHM if the homogenized flux distribution is based on flux-volumen weighted cross sections. The reason why we still are interested in making the above-mentioned investigation is that HHM would be much more accessible if the ordinary way of calculating homogenized cross sections could be applied without causing excessive errors in the local pin power determination. Of course, one can object that the flux-volumen weighting homogenization scheme in any case has to be replaced by a more accurate homogenization method just in order to make the average nodal power determination fairly accurate (compare Chapter 7). However, if HHM, based on flux-volumen weighted homogenized cross sections, could predict the local pin powers accurately, then the more simple homogenization method proposed by K. Smith (compare Chapter 8 and Ref. 11) can be applied instead of the somewhat difficult method proposed by Koebke.

The accuracy of HHM is examined using the three benchmark problems defined in Chapter 2. The calculation procedure consists of two assembly calculations for each type of assembly, a heterogeneous and a homogeneous calculation both having the same net current distribution on the boundaries. Next the form factor distribution is defined as the ratio between the heterogeneous- and homogeneous solution. The "actual" net current boundary conditions are derived from the global reference solution, condensed to two energy groups and approximated by a quadratic. Then a new homogenized assembly calculation is performed with the approximated net currents as boundary conditions. The solution to this boundary value problem is multiplied with the precomputed form functions and the resulting power distribution is renormalized to an average value of 1000. Finally, the renormalized power distribution is compared with the renormalized reference solution. Both flux modulation (Equation 6.1) and power modulation (Equa-

tion 6.2) are considered.

$$P_{MOD}(x,y) = \frac{pHET^*(x,y)}{pHOM^*(x,y)} \cdot p^{HOM}(x,y) \qquad (6.2)$$

Figure 6.7 summarizes the result of this investigation. First of all it appears that the flux- and power-modulation schemes give quite similar results. We will make use of this result by only considering the simpler power modulation scheme in the remainder of this chapter except for the investigation of the homogenized flux interpolation method.

Further, it appears that the maximum error in modulated pin power distribution varies in the 1.0-15.0% range. However, in 22 of the 24 assemblies the maximum error is below 8%. Thus, HHM based on flux-volumen weighted homogenized cross sections appears to be fairly accurate.

If only the average values of the net currents on the four faces of the assembly were considered in the modulation scheme the corresponding errors would lie in the 3.4-23.7% range (Fig. 6.8) and 11 of the 24 assemblies would have maximum errors above 10%. Hence, if HHM is to be applied as a local pin power model, then the corner values of net currents have to be known from the converged global coarse-mesh solution in order to get an accurate pin power determination.

Until now the homogenized two-group solution has been obtained using the finite difference code "CDB". These solutions could also be obtained in a more direct way. In the following, three different schemes will be described and tested:

1) A two-group, two-dimensional homogenized problem with spatial approximations for the net currents on the boundaries can be solved analytically (compare Section 8.3). If this analytical solution scheme is applied in HHM, then the maximum error will be nearly the same as in case of the "CDB" solutions.

2) A non-separable fourth-order polynomial $\phi(x,y)$ with 21 coefficients C_{ij}

$$\phi_g(x,y) = \sum_{i,j=0}^{4} C^g_{ij}\, x^i \cdot y^j$$

where $C^g_{33} = C^g_{34} = C^g_{43} = C^g_{44} = 0$

can be constructed as an approximation for the local flux shape in the node (Ref. 8).

For every energy group g the 21 coefficients, C^g_{ij} can be expressed in terms of linear functions of 21 base values, namely the 9 nodal averages of fluxes and net currents on the boundaries, and 12 local corner values.

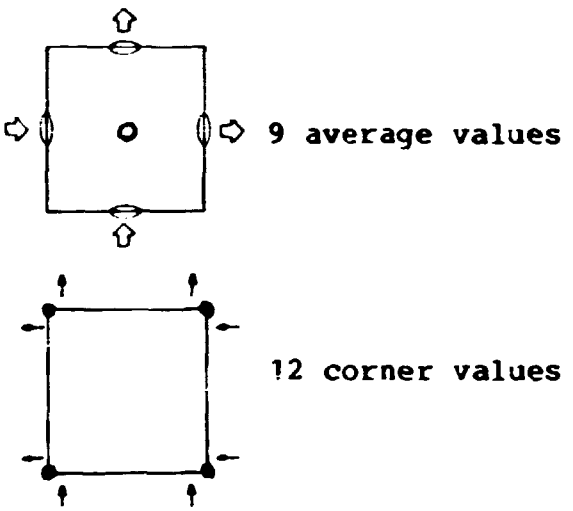

If the homogenized solutions to be used in HHM are obtained using the polynomial approximation where the 21 base values are taken from the heterogeneous reference solutions, the maximum pin power errors will lie in the 4.7% - 96.5% range (Fig. 6.9). The very large errors are caused by the lack of neither mathematical nor physical explanation for the approximated solution. As will be shown in Chapter 8, one cannot define homogenized cross sections which in a multidimensional calculation preserves 1) the group reaction rates, 2) the group surface currents, 3) the group surface fluxes, and 4) the group average fluxes.

If generalized equivalence boundary values are used instead of the heterogeneous reference values the maximum errors will be reduced. Figure 6.10 shows a comparison of the maximum error in the local pin power determination when the equivalence solutions are found by using either "CDB" or the polynomial approximation based on generalized equivalence parameters. Only the average values of the net currents have been considered in both cases.

3) A scheme (Ref. 12) determining the homogenized solution by applying an interpolation procedure has been investigated. The average nodal fluxes are concentrated in the center points of the assemblies, and the homogenized flux distribution in each assembly is determined by interpolating between the following 9 average values:

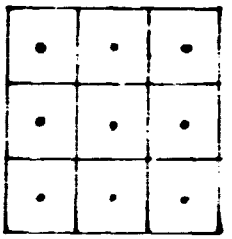

A problem in connection with HHM is that the form factor distribution cannot be determined by performing only assembly calculations. The assembly has to be enlarged with a buffer zone in order to use the interpolation scheme in the form factor generation.

A possible way to overcome this problem is to perform the assembly calculation with zero net current boundary conditions. The form factor distribution will equal the heterogeneous flux distribution in this case except for a constant factor. Figure 6.11 shows a comparison of the maximum error in the pin power determinal using HHM (flux) based on the interpolation scheme. Two different form factor distributions are considered, one based on zero net current boundary

conditions, the other one is taken from the HHM investigation using CDB (page 63).

The investigation shows large errors in the pin power determination (~ 20-40%) for controlled assemblies and for assemblies lying next to the reflector region, whereas the maximum pin power errors for the uncontrolled assemblies placed in the interior of the core will lie in the 5-18% range. The maximum errors in controlled assemblies can be reduced slightly using net currents different from zero in the form factor generation. Based on this investigation, it can be concluded that it is insufficient to use average assembly fluxes in the homogenized flux approximation scheme. The average value of boundary net currents and fluxes together with corner currents and fluxes are required in order to obtain an accurate pin power determination.

6.4. Heterogeneous-Heterogeneous Modulation

Recently a Heterogeneous-Heterogeneous Modulation method has been developed at MIT by C.L. Hoxie and A.P. Henry (Ref. 9). In this method the form function for each assembly is defined by

$$F_g(\underline{r}) = \frac{\phi_g^{HET}(\underline{r})}{A_g^{HET}(\underline{r})}$$

where $A_g^{HET}(\underline{r})$ is a flux shape for the assembly, with all heterogeneities represented explicitly but obtained using zero net current boundary conditions

$\phi_g^{HET}(\underline{r})$ is the heterogeneous solution with the "actual" boundary conditions.

With the $A_g^{HET}(\underline{r})$ precomputed, the $\phi_g^{HET}(\underline{r})$ can be constructed if the $F_g(\underline{r})$ can be inferred from the global coarse-mesh solution. One approach to finding approximate expressions for the $F_g(\underline{r})$ is to base their mathematical forms on the differential equations which they obey. Thus, if $A_g^{HET}(r) \cdot F_g(r)$ is substi-

tuted in the defining equation for $\phi_g^{HET}(\underline{r})$, and the defining equations for $A_1^{HET}(r)$ and $A_2^{HET}(\underline{r})$ are multiplied by $F_1(r)$ and $F_2(r)$, subtraction and rearrangement yields

$$-\nabla\cdot D_1\nabla F_1 + \left\{\left(\frac{1}{\lambda_A} - \frac{1}{\lambda_\phi}\right)\nu\Sigma_{f1} + \frac{1}{\lambda_A R}\nu\Sigma_{f2}\right\}\cdot F_1 - \frac{1}{\lambda_\phi\cdot R}\cdot\nu\Sigma_{f2}\,F_2$$

$$= \frac{2D_1}{A_1}\nabla F_1\cdot\nabla A_1$$

$$-\nabla\cdot D_2\nabla F_2 + R\Sigma_{1\to 2}(F_2-F_1) = \frac{2D_2}{A_2}\nabla F_2\cdot\nabla A_2$$

where

$$R \equiv \frac{A_1(x,y)}{A_2(x,y)}$$

and λ_ϕ is the eigenvalue of the global solution and λ_A that for the assembly solution. If it were not for the cross gradient terms on the right-hand sides of these equations, they would be analogous to two group diffusion equations and could be attacked by standard methods. In principle, the equation system can be solved for the F_g using homogeneous boundary conditions from the nodal problem. To avoid expense, however, an approximated solution is defined by neglecting the term $\nabla F_g\cdot\nabla A_g$ and assuming that the value of R, the ratio of fast-to-slow assembly flux, and the group parameters are constant throughout the assembly. With these assumptions the equation system becomes two coupled Helmholts equations with constant coefficients. If now accurate inhomogeneous boundary conditions for the F_g on the surface of the assembly can be inferred from the nodal solution, the F_g can be found, and good approximations to ϕ_g^{HET} can be reconstructed by

$$\phi_g^{HET}(\underline{r}) = F_g(\underline{r})\cdot A_g^{HET}(\underline{r})$$

Numerical tests for small two-dimensional benchmark problems yield maximum errors in local pin powers at the beginning of life of ~ 5% (Ref. 13).

The method is designed for PWR and therefore has not been tested on the BWR benchmark problems defined in this thesis.

6.5. Summary

For the past 4 years the Homogeneous-Heterogeneous Modulation method proposed by K. Koebke and M. Wagner has been applied to determine local heterogeneous power and flux distributions in PWR's. In this chapter the method has been tested on BWR's and we have demonstrated that HHM based on Koebke's equivalence theory is very sensitive to differences in the sign of the base net currents and the overall net currents on the four assembly faces. In the case of controlled asemblies no solution with a positive flux shape everywhere could be found. Applying the least negative equivalence flux distribution in the HHM scheme gave large errors in the pin power determination. Hence, we can conclude that negative equivalence flux distributions cannot be used in order to regain the heterogeneous pin power distribution. The simplest approach for alleviating this difficulty is to enlarge the homogenization area such that four assemblies are regarded as a node. If these enlarged areas are chosen in a way such that the control rods always lie in the centre of the node, then the large heterogeneous flux gradients across the area to be homogenized can be avoided, and a solution that is positive everywhere can be found. An objective for further investigations is therefore to examine the modulation method on such enlarged homogenization areas.

Also shown in this chapter was the HHM scheme based on Generalized Equivalence Theory.

The only difference between this homogenization scheme and the ordinary flux-volumen weighting method is that the area to be homogenized is imbedded in its natural environment and that four "new" homogenized parameters are added: The discontinuity factors. Applying this homogenization method in HHM has proven to give fairly accurate pin power predictions with maximum errors ~ 8%.

7. PIN POWER DETERMINATION BASED ON "HOMOGENIZED" BOUNDARY PARAMETER VALUES.

7.1 Introduction

In this chapter, we will investigate the practical use of the local pin power models described in the previous chapters. Until now the boundary parameter values from the global solution have been derived from the heterogeneous finite-difference solution. This is impossible in a practical use, for if the heterogeneous solution to the problem were known, there would be no need for a local pin power model.

As mentioned in the introduction the explicit modeling of a full heterogeneous reactor core is avoided by treating large "nodes" as homogeneous regions. The most commonly employed procedure for determining the homogenized parameters in these regions is to flux-volumen weight the heterogeneous cross sections. The basic principle of flux-volumen weighting consists of preserving the reaction rates in all energy groups. The theory behind this scheme is described in Refs. 1 and 11.

In this section we will examine the accuracy of the average power determination and the boundary parameter value determination in the case of the "homogenized" benchmark problem compared with the heterogeneous reference solution. Moreover, the influence of prospective errors in the boundary parameter values, if any, on the accuracy of the local pin power determination will be explained.

7.2 The average power distribution in the "homogenized" solution compared with the heterogeneous reference solution

Test case one from the benchmark definition in Chapter 2 is used to define the "homogenized" problem examined in this section.

The solution procedure is identical to an ordinary global coarse-mesh calculation. First the homogenized cross sections are calculated in five energy groups for each of the seven node-types shown in Fig. 7.1. The global "coarse-mesh" solution can be calculated from the homogenized cross sections. In this case the "coarse-mesh" calculation is a finite difference one with the same mesh-division as in case of the heterogeneous reference problem. The only difference between the reference and homogenized problems is the five-group cross section in the 1600 nodes. Hence, the only source of error in the homogenized solution compared with the reference solution is the way the homogenized parameters are calculated.

The results of the above-mentioned investigation are described in the following: Figure 7.2 shows the average pin powers (normalized to an unit average value), based on the homogenized solution. Also shown in this figure are the corresponding average powers based on the reference solution. It appears that the maximum difference in the average powers occurs at box 1, and is 0.11.

A determination of the net currents on the node-boundaries in the homogenized solution shows that the error in the average power determination is due mainly to an overprediction of the thermal currents on faces where there are control rods in the heterogeneous problem. The effect of the overpredicted thermal neutron currents is that the power distribution tends to be less oscillating in the homogenized case. This result is in agreement with investigations performed at MIT (Ref. 11) which shows errors up to 17% in the average power determination in the case of BWR.

Two questions arise: Why is the flux-volumen weighting scheme so much in error? Which of the assumptions made on the homogenization stage are invalid? In order to answer them one has to look more closely at the theory behind the flux-volumen weighting scheme (Ref. 11). In this paper we will look briefly at only one of the assumptions made in the flux-volumen weighting scheme, the flux-volumen weighting of the diffusion coefficients.

The homogenized diffusion coefficients are defined such that

$$\frac{1}{\bar{D}_g} \equiv \frac{\int_{V_i} \frac{1}{D_g(r)} \cdot \phi_g(r)\, dr}{\int_{V_i} \phi_g(r)\, dr}$$

The justification for this approximation is that $1/D_g(r)$ is proportional to the macroscopic neutron transport cross section, and it is desired to preserve the neutron transport rate. Under close scrutiny; however, it is clear that the transport cross section is a function of the net current. Hence, weighting the transport cross section by the flux does not preserve the transport rate.

The "ideal" homogenized diffusion coefficients which preserves all group currents can be defined as (Ref. 11):

$$\bar{D}_g \equiv - \frac{\int_S J_g^u(r) \cdot d\underline{s}}{\int_S \frac{d}{dv} \bar{\phi}_g(\underline{r}) \cdot d\underline{s}}$$

where

$J_g^u(\underline{r})$ ≡ net neutron current in direction u and group g.

$\bar{\phi}_g(r)$ ≡ scalar "homogenized" flux in group g.

The evaluation of the "ideal" homogenized diffusion coefficients requires a priori knowledge of the net currents for each region to be homogenized. Secondly, even if these quantities are assumed known, the flux shape, $\bar{\phi}_g(\underline{r})$, which results from the use of the homogenized constants must also be known. Since the homogenized flux shape is strongly coupled to the values of the homogenized parameters, a nonlinearity is introduced into the process of evaluating homogenized parameters. If conventional continuity conditions of scalar flux and net current are imposed on all nodal surfaces, the values of D_G will be different for each surface of the node. Thus, it appears to be impossible to define spatially constant values of D_G which preserve the con-

dition of a preservation of net currents on each of the node-faces, except for very special cases. Consequently, this situation dictates that additional degrees of freedom must be added to the homogenized parameters if the net currents on the faces of the region to be homogenized are to be preserved.

Many prescriptions for eliminating the inaccuracy which result from the use of flux-volumen weighted parameters have been developed (Ref. 11).

Three of these "new" homogenization schemes are described in Chapter 8. Here, in this section, we will proceed with the investigation concerning the practical use of the local pin power models if the boundary parameter values from the global "coarse-mesh" solution are based on the flux-weighted homogenization scheme.

7.3 Form factor determination using local pin power models in the framework of the homogenized "coarse-mesh" solution

In Section 7.2 it was shown that the predicted average powers could be in error by as much as 11% if the homogenized parameters were calculated using the flux-volumen weighting scheme. These errors in the average power determination will, of course, be transferred to the local pin power determination in the sense that the predicted form factor distribution is normalized to this average value. The investigation described in the following will show the error in the pin power determination due to the inaccuracy of the boundary parameter values in the homogenized solution, compared with the reference solution.

The Normalization Method makes no use of the boundary parameter values; hence the form factor determination will be unaffected by the inaccuracy in the homogenized solution.

In the cases of the three other pin power models the boundary parameter values will be represented in the same detail as in the case of the heterogeneous solution. The base-solution set

"BASIS/ SUPER/6" (compare Section 5.6) is used in the investigation of the Superposition Method, and the finite-difference scheme with flux-weighted homogenized parameters is used in the case of the Modulation Method.

Table 7.1 summarizes the results of the investigation mentioned above. Also shown in Table 7.1 is the corresponding results from the heterogeneous boundary parameter value calculation. It appears that the inaccuracy in the boundary parameter value determination makes the form factor prediction very much in error. The form factor prediction using the Flux-lupe, Superposition, or Modulation Methods will in some cases be less accurate as in the case of the Normalization Method.

The investigation also shows that the connexion between the errors in the form factor prediction and the inaccuracy of the boundary parameter values are more pronounced in the Superposition than in the Modulation Method. This is because the Superposition Method has a superior theoretical basis than the latter, based on the flux-weighted homogenization scheme.

7.4 Summary

As the main conclusion to the investigation performed in this chapter, it can be maintained that the flux-weighted homogenization scheme in the case of BWR analyses will tend to overpredict significantly the net currents between controlled assemblies. As a result, the predicted assembly average power may be in error by as much as 11%. Moreover, the accuracy of a practical use of the local pin power models is poor if the coarse-mesh solution is based on flux-weighted homogenized parameters. In some cases the Normalization Method will yield more accurate results than the more sophisticated pin power models. Hence, other homogenization schemes have to be introduced if the pin powers have to be accurately predicted.

8. "NEW" SPATIAL HOMOGENIZATION METHODS

8.1 Introduction

In Chapter 7 it was concluded that it was necessary to introduce a new spatial homogenization method if the local pin powers were to be determined accurately. Also mentioned in Chapter 7 is the cause of the large errors in the average power determination: the flux-weighting of the diffusion coefficient. Furthermore, that additional degrees of freedom had to be added to the homogenized parameters in order to make them fulfil the requirement of preserving the average currents into the region to be homogenized.

Three ways of defining this additional degree of freedom will be described in this chapter: The Response Matrix Homogenization Method (Ref. 14), Koebke's Equivalence Theory (Ref. 10), and Generalized Equivalence Theory (Ref. 11). The former (RMHM) and latter (GET) will be described only superficially, whereas Koebke's "equivalence theory" will be examined in more detail on account of its close relationship with the theory behind the Modulation Method.

In RMHM the additional degree of freedom lies within the diffusion coefficients which are allowed to have up- and down-scattering elements, and besides, a preservation of the average fluxes in each energy group is no longer assumed. The basic principle of the RMHM is in short: First, the response matrix is calculated in the case of the heterogeneous configuration. Next, the homogenized parameters are defined by claiming that the homogenized response matrix is equal to the heterogeneous response matrix. In the one-dimensional case the homogenized parameters obtained reproduce the neutron leakage and the integral reaction rates of the node exactly, when it becomes part of a reactor. Unfortunately, the RMHM cannot be extended to the

multidimensional case. However, some of the ideas developed in one dimension can be adapted to multidimensional homogenization problems.

In Koebke's homogenization scheme, called "equivalence theory", the additional degree of freedom lies within the postulation of flux-discontinuity between adjacent homogenized regions. The discontinuity of the flux is represented by an additional equivalence parameter, the heterogenity factor. The equivalence theory will be described in detail in Sections 8.2 and 8.3.

MIT's version of equivalence theory is called "Generalized Equivalence Theory" (GET). In GET, two discontinuity factors are defined for each region and each direction by

$$f^{HETx}\left(\pm\frac{a}{2}\right) \equiv \frac{\phi_G^{HET}\left(\pm\frac{a}{2}\right)}{\phi_G^{HOM}\left(\pm\frac{a}{2}\right)}$$

instead of Koebke's single heterogenity factor for each node and direction. Moreover, the diffusion coefficients are defined in GET to be equal the homogenized diffusion coefficients using the flux-volumen weighting scheme.

The steps involved in the implementation of GET can be summarized as follows (Ref. 11):

1) The exact solution to the heterogeneous global reactor problem is assumed to be known.

2) Flux-weighted cross sections are evaluated for each node by weighting with the local heterogeneous fluxes.

3) The diffusion coefficients are arbitrarily chosen for each node (usually computed by weighting the heterogeneous diffusion coefficients with the local heterogeneous flux).

4) One-dimensional boundary value problems are solved (with heterogeneous surface currents as boundary conditions) to obtain the one-dimensional homogenized surface fluxes for each node and each direction.

5) Discontinuity factors are computed for each surface of each homogenized region.

6) The global homogenized reactor equations are solved (allowing flux discontinuities at all surfaces), perhaps approximately, but using approximations identical to those employed in Step 4.

This homogenization method is "exact" in the sense that the solution to the homogenized reactor equations will reproduce the reactor eigenvalues (k_{eff}), all group reaction rates, and all group surface currents of the heterogeneous solution.

8.2 Equivalence Theory

In order to derive Koebke's homogenization method, one must assume that the exact global reactor solution is known. With this lone assumption, it is possible to derive, in a formal fashion, a set of homogenized differential equations whose solutions will preserve simultaneously all of the quantities (k_{eff}, group reaction rates, and group surface currents) in all homogenized regions. The neutron balance in the case of the homogeneous node,

$$\left(-\frac{a}{2} < x < \frac{a}{2} \quad \text{and} \quad -\frac{b}{2} < y < \frac{b}{2}\right)$$

can be written as:

$$-\bar{D}_G^x \frac{d^2 \bar{\phi}_G(x)}{dx^2} + (\bar{\Sigma}_{a_G} + \sum_{G'} \bar{\Sigma}_{G\to G'}) \cdot \bar{\phi}_G(x)$$

$$- \sum_{G'} (\bar{\Sigma}_{G'\to G} + \chi_G \cdot \overline{\nu\Sigma}_{fG'}) \cdot \bar{\phi}_{G'}(x) \qquad (8.1)$$

$$= \frac{J_G^T(x)}{b}$$

where

$$\bar{\phi}_G(x) = \frac{1}{b} \int_{-\frac{b}{2}}^{\frac{b}{2}} \phi_G(x,y)\, dy$$

$$J_G^T(x) = J_G^Y(x, \tfrac{b}{2}) - J_G^Y(x, -\tfrac{b}{2})$$

and the gradient of the "homogeneous" flux is connected with the known average heterogeneous currents at the interfaces

$(x = \pm \frac{a}{2})$ by:

$$J_G^{HETx}(\pm \tfrac{a}{2}) = -\bar{D}_G^x \left. \frac{d\bar{\phi}_G(x)}{dx} \right/_{x = \pm \frac{a}{2}} \qquad (8.2)$$

where the diffusion coefficient is assumed to be directionally dependent.

In Koebke's scheme the homogenized cross sections are calculated using the ordinary flux-weighted homogenization method, with the slight difference that the region to be homogenized is embedded in its typical neutron physical environment, whereas the ordinary flux-weighted scheme uses zero net current boundary conditions.

The diffusion coefficients are, however, unrelated to those of the flux-weighting methods, but rather, are treated as totally artificial quantities which can be chosen in such a manner as to match the nodal leakage terms.

By choosing the two boundary conditions for the boundary value problem defined in Equations 8.1 and 8.2 to be the values of the heterogeneous group surface currents, one is assured that the homogenized nodal flux solution will preserve the surface currents. However, one must consider that ultimately it is the global homogenized reactor equation which must be solved. In doing so, it is necessary to relate group surface currents and surface fluxes between adjacent homogenized regions. Since the heterogeneous group surface currents are continuous and since preservation of the group surface currents is postulated, it is necessary that the homogenized group surface currents be continuous at all nodal interfaces.

The situation with respect to group surface fluxes is much less clear. Any arbitrary choice for $\bar{D}_G^x$ will result in a unique solution to the boundary value problem, but unfortunately, the homogenized flux shapes will be such that the homogenized surface fluxes do not match the heterogeneous surface fluxes. Consequently, it is difficult to determine the appropriate relationship between nodal surface fluxes.

Koebke overcame this difficulty by postulating the existence of an additional homogenization parameter. He defined the ratios of the known heterogeneous surface fluxes to the homogenized surface fluxes to be "heterogeneity factors":

$$f_G^{HETx}\left(\pm\frac{a}{2}\right) = \frac{\phi_G^{HET}\left(\pm\frac{a}{2}\right)}{\bar{\phi}_G^{HOM}\left(\pm\frac{a}{2}\right)} \tag{8.3}$$

Since the values of the diffusion coefficients remained to be specified, Koebke chose to restrict the values of $\bar{D}_g^x$ such that

$$f_g^{HETx}\left(+\frac{a}{2}\right) = f_g^{HETx}\left(-\frac{a}{2}\right) \tag{8.4}$$

By virtue of the requirement that the heterogeneous surface fluxes be continuous, the homogenized flux continuity condition must be

$$\phi_{G_{i-1}}^{HOM}\left(\frac{a}{2}\right)\cdot f_{G_{i-1}}^{HETx} = \phi_{G_i}^{HOM}\left(-\frac{a}{2}\right)\cdot f_{G_i}^{HETx}$$

In (Ref. 10) Koebke maintains that the equations system (8.1, 8.2, 8.3, 8.4) for the inhomogeneous boundary value problem and for the integral heterogeneous fluxes $\phi_G^{HET}\left(\pm\frac{a}{2}\right)$ lead to a unique definition of D_G^x of f_G^x in every group. Only, if the boundary values are symmetric $\phi_G^{HET}\left(\frac{a}{2}\right) = \phi_G^{HET}\left(-\frac{a}{2}\right)$ and $J_G^{HET}\left(\frac{a}{2}\right) = J_G^{HET}\left(-\frac{a}{2}\right)$ does an infinite number of pairs of equivalence parameters (D_G^x, f_G^x) exist, which allows fulfilment of the postulate that the integral net currents and integral fluxes at the interface between adjacent regions are preserved.

8.3. The solution of the equivalence equation system both in a one-group and a two-group approach

The equation system (8.1, 8.2, 8.3, and 8.4) is solved both in a one-group one-dimensional representation in this section, and in a two-group two-dimensional representation. The equivalence boundary value problem is in the one-group one-dimensional representation defined as

$$D\nabla^2 \Phi(x) - \Sigma_a \cdot \Phi(x) + \nu\Sigma_f \cdot \Phi(x) = 0$$

$$-D \left.\frac{d\Phi}{dx}\right|_{x=0} = J_o^{HET} , \quad -D \left.\frac{d\Phi}{dx}\right|_{x=a} = J_a^{HET}$$

The solution to this differential equation can be written as

$$\Phi(x) = A \cdot \cos kx + B \cdot \sin kx$$

where

$$k^2 = \frac{\nu\Sigma_f - \Sigma_a}{D}$$

The unknowns in this solution are: A, B, and D.

Three equations are needed in order to determine these unknowns. Two of them are defined using the boundary values J_o, and J_a

$$J_o = -D(-A \cdot k \cdot \sin(k \cdot o) + B \cdot k \cdot \cos(k \cdot o)) \qquad (1)$$

$$J_a = -D(-A \cdot k \cdot \sin(k \cdot a) + B \cdot k \cdot \cos(k \cdot a)) \qquad (2)$$

The third is based on Equations (8.3) and (8.4)

$$\frac{\Phi_o^{HET}}{\Phi_o^{HOM}} = \frac{\Phi_a^{HET}}{\Phi_a^{HOM}} \Rightarrow \Phi_o^{HET} \cdot \Phi_a^{HOM} - \Phi_a^{HET} \cdot \Phi_o^{HOM} = 0$$

hence:

$$\phi_o^{HET}(A\cdot\cos(k\cdot a) + B\cdot\sin(k\cdot a)) - \phi_a^{HET}(A\cdot\cos(k\cdot o) + B\cdot\sin(k\cdot o)) = 0$$

The solution to this equation system can be written

$$A = \frac{J_a - J_o\cdot\cos(k\cdot a)}{D\cdot k\cdot\sin(k\cdot a)}$$

$$B = -\frac{J_o}{D\cdot k}$$

$$D = \frac{a^2(\nu\Sigma_f - \Sigma_a)}{\left\{\text{Arccos}\ \frac{J_o\cdot\phi_o + J_a\cdot\phi_a}{\phi_o\cdot J_a + \phi_a\cdot J_o}\right\}^2}$$

From the solution defining the diffusion coefficient, it can be seen that in the case of

$$\left|\frac{J_o\cdot\phi_o + J_a\cdot\phi_a}{\phi_o\cdot J_a + \phi_a\cdot J_o}\right| < 1$$

the homogenized diffusion coefficient can assume an infinite number of real values. On the other hand, if

$$\left|\frac{J_o\cdot\phi_o + J_a\cdot\phi_a}{\phi_o\cdot J_a + \phi_a\cdot J_o}\right| > 1$$

then the diffusion coefficient will have only one real value, and an infinite number of complex values. Moreover, it can be seen that if $\nu\Sigma_f < \Sigma_a$ then the diffusion coefficient will become negative, and if $\Sigma_a < \nu\Sigma_f$ it will become positive.

In the two-group two-dimensional case the equivalence boundary value problem is defined by

$$D_1\cdot\nabla^2\phi_1(x,y) - \Sigma_r\cdot\phi_1(x,y) + \nu\Sigma_{f1}\cdot\phi_1(x,y) + \nu\Sigma_{f2}\cdot\phi_2(x,y) = 0$$

$$D_2\cdot\nabla^2\phi_2(x,y) - \Sigma_{a2}\cdot\phi_2(x,y) + \Sigma_{1\to2}\cdot\phi_1(x,y) = 0$$

$$\Sigma_r = \Sigma_{a1} + \Sigma_{1\to2}$$

With the following definitions

$$\rho_o \equiv \frac{\Sigma_r}{D_1} - \frac{\nu\Sigma_{f1}}{D_1} \qquad K_1 = \frac{\nu\Sigma_{f2}}{D_1}$$

$$\omega_o \equiv \frac{\Sigma_{a2}}{D_2} = X^2 \qquad K_2 = \frac{\Sigma_{1\to2}}{D_2}$$

the differential equation system can be reduced to

$$\nabla^2\phi_1(x,y) - \rho_o\cdot\phi_1(x,y) + K_1\cdot\phi_2(x,y) = 0$$

$$\nabla^2\phi_2(x,y) - \omega_o\cdot\phi_2(x,y) + K_2\cdot\phi_1(x,y) = 0$$

A one-dimensional representation of this equation system can be written as

$$\frac{d^2\phi_1(x,y_o)}{dx^2} - \rho_o\cdot\phi_1(x,y_o) + K_1\cdot\phi_2(x,y_o) = Q_{1y}(x,y_o)$$

$$\frac{d^2\phi_2(x,y_o)}{dx^2} - \omega_o\cdot\phi_2(x,y_o) + K_2\cdot\phi_2(x,y_o) = Q_{2y}(x,y_o)$$

where

$$Q_{1y}(x,y_o) = -\frac{d^2\phi_1(x,y_o)}{dy^2}$$

$$Q_{2y}(x,y_o) = -\frac{d^2\phi_2(x,y_o)}{dy^2}$$

The homogeneous solution to this equation system can be written as

$$\phi_1^{HOM}(x) = A\cdot\cosh(\mu x) + B\cdot\sinh(\mu x) + C\cdot\cosh(\psi x) + D\cdot\sinh(\psi x)$$

$$\phi_2^{HOM}(x) = S_1(A\cdot\cosh(\mu x)+B\cdot\sinh(\mu x)) + S_2(C\cdot\cosh(\psi x)+D\cdot\sinh(\psi x))$$

where

$$\begin{Bmatrix}\mu^2\\ \psi 2\end{Bmatrix} = \frac{\omega_o+\rho_o}{2} \pm \sqrt{\left(\frac{\omega_o \cdot \rho_o}{2}\right)^2 - \omega_o \cdot \rho_o + K_1 K_2}$$

$$S_1 = \frac{\rho_o - \mu^2}{K_1} \qquad S_2 = \frac{\rho_o - \psi^2}{K_1}$$

If the transverse leakage rates are approximated using a first-order polynomial

$$Q_{1y}(x) = Q_{1yo} + dQ_{1y} \cdot x$$

$$Q_{2y}(x) = Q_{2yo} + dQ_{2y} \cdot x$$

then the particular solution can be written as:

$$\phi_1^{PAR}(x) = \frac{1}{\psi^2-\mu^2}\left\{-P_2(\cosh(\mu x)-1) - P_4 \cdot \frac{1}{\mu}(\sinh(\mu x)-\mu x) + P_1(\cosh(\psi x)-1) + P_3 \cdot \frac{1}{\psi}(\sinh(\psi x)-\psi x)\right\}$$

$$\phi_2^{PAR}(x) = \frac{1}{\psi^2-\mu^2}\left\{-S_1 \cdot P_2(\cosh(\mu x)-1) - S_1 \cdot P_4 \cdot \frac{1}{\mu}(\sinh(\mu x)-\mu x) + S_2 \cdot P_1(\cosh(\psi x)-1 + S_2 \cdot P_3 \cdot \frac{1}{\phi}(\sinh(\psi x)-\psi x)\right\}$$

where

$$P_1 = \frac{Q_{1yo}(\psi^2-\omega_o)-Q_{2yo} \cdot K_1}{\psi^2}$$

$$P_2 = \frac{Q_{1yo}(\mu^2-\omega_o)-Q_{2yo} \cdot K_1}{\mu^2}$$

$$P_3 = \frac{dQ_{1y}(\psi^2-\omega_o)-dQ_{2y}\cdot K_1}{\psi^2}$$

$$P_4 = \frac{dQ_{1y}(\mu^2-\omega_o)-dQ_{2y}\cdot K_1}{\mu^2}$$

This equation system has been used to generate the analytical solutions to the homogenized problems in Section 6.3. In this section it will be used in order to analytically define the two-group equivalence diffusion coefficients and the corresponding heterogeneity factors.

There are six unknowns in the solution to the two-group diffusion theory equations: A, B, C, D, D_1, and D_2; hence, six equations are required in order to determine these values. Four of these are set up using the heterogeneous net currents on the boundaries, and the remainding two are set up using Equations (8.3 and 8.4).

The following values of A, B, C, and D can be calculated based on the net currents

$$J_1^{(o)} = -D_1 \left.\frac{d\phi_1}{dx}\right|_{x=0} \qquad J_1^{(b)} = -D_1 \left.\frac{d\phi_1}{dx}\right|_{x=b}$$

$$J_2^{(o)} = -D_2 \left.\frac{d\phi_2}{dx}\right|_{x=0} \qquad J_2^{(b)} = -D_2 \left.\frac{d\phi_2}{dx}\right|_{x=b}$$

$$A = \frac{-\cosh(\mu b)\cdot\left\{\frac{S_2\cdot J_1^{(o)}}{D_1} - \frac{J_2^{(o)}}{D_2}\right\} + \left\{\frac{S_2\cdot J_1^{(b)}}{D_1} - \frac{J_2^{(b)}}{D_2}\right\}}{\mu\cdot\sinh(\mu\cdot b)\cdot(S_1-S_2)}$$

$$B = \frac{\sinh(\mu \cdot b) \cdot \left\{ \frac{J_1^{(o)} \cdot S_2}{D_1} - \frac{J_2^{(o)}}{D_2} \right\}}{\mu \cdot (S_1 - S_2)}$$

$$C = \frac{-\cosh(\psi \cdot b) \cdot \left\{ \frac{J_1^{(c)} \cdot S_1}{D_1} - \frac{J_2^{(o)}}{D_2} \right\} + \left\{ \frac{S_1 \cdot J_1^{(b)}}{D_1} - \frac{J_2^{(b)}}{D_2} \right\}}{\psi \cdot \sinh(\psi \cdot b) \cdot (S_1 - S_2)}$$

$$D = \frac{\sinh(\psi \cdot b) \cdot \left\{ \frac{J_1^{(o)} \cdot S_1}{D_1} - \frac{J_2^{(o)}}{D_2} \right\}}{\psi \cdot (S_1 - S_2)}$$

Based on these values the two nonlinear equations defining the diffusion coefficients can be written as

$$\{\phi_1^{(o)} \cdot \cosh(\mu \cdot b) - \phi_1^{(b)}\} \cdot A + \phi_1^{(o)} \cdot B - \{\phi_1^{(o)} \cdot \cosh(\psi \cdot b) - \phi_1^{(b)}\} C + \phi_1^{(o)} \cdot D + \phi_1^{(o)} \cdot L_1^{(b)} - \phi_1^{(b)} \cdot L_1^{(o)} = 0 \quad (1)$$

$$\{\phi_2^{(o)} \cdot S_1 \cdot \cosh(\mu \cdot b) - S_1 \phi_2^{(b)}\} \cdot A + S_1 \cdot \phi_2^{(o)} \cdot B - \{\phi_2^{(o)} \cdot S_2 \cdot \cosh(\psi \cdot b) - S_2 \cdot \phi_2^{(b)}\} \cdot C + S_2 \cdot \phi_2^{(o)} \cdot D + \phi_2^{(o)} \cdot L_2^{(b)} - \phi_2^{(b)} \cdot L_2^{(o)}$$

where $\phi_1^{(o)}$, $\phi_2^{(o)}$, $\phi_1^{(b)}$, and $\phi_2^{(b)}$ are the heterogeneous flux values on the boundary of the area to be homogenized and $L_1^{(o)}$, $L_2^{(o)}$, $L_1^{(b)}$, $L_2^{(b)}$ represents the transverse leakage terms.

This equation system is rather complex and the solution is not immediately evident. However, if a nonlinear method for solving these equations (Ref. 15) is applied, the numerical solutions to the equation system can be computed. This has been done, and the equation system has been tested on the four test cases defined in Section 6.2. From this investigation it appears that there are an infinite number of solutions to the nonlinear equation

system. Table 8.1 summarizes some of them. Also shown in this table are the results of an iterational use of CDB/BASE. It appears that there is good correspondence between the iterated and analytical solutions.

Figure 8.1 shows two equivalence flux solutions to Test 2/II (compare Section 6.2). It appears that the equivalence flux solutions corresponding to the diffusion coefficients (D_1 = 8.86, D_2 = -0.82) are positive everywhere. The fast flux solution in the case of the diffusion coefficients (D_1 = 4.97, D_2 = 0.24) is also positive, whereas the thermal flux solution becomes negative in the corners of the assembly. From this investigation it can be concluded that in order to define the solution to the equivalence equation system uniquely a further requirement has to be introduced. If we assume that only flux solutions that are positive everywhere are allowed then it appears as if the solution will be uniquely defined. However, further investigations are required in order to prove the existence of only one solution that is positive everywhere. Experience has shown that the requirement of positive equivalence flux solutions will result in a possibility of defining problems for which no solution can be found. For instance, the equivalence flux will always be negative in the corners where control rods are placed in the test cases we are using in this thesis. How to alleviate this difficulty is described in Section 6.5.

8.4. Summary

In this chapter, Koebke's equivalence theory homogenization method was examined. The solutions to the one-dimensional one group and the two-dimensional two-group problems were found, and it was demonstrated that an infinite number of solutions exist if equivalence flux shapes with negative values could be regarded as solutions to the equivalence equation system. Allowing only flux solutions that are positive everywhere it seems as if the solution will be uniquely defined. However, further investigations are required in order to prove the existence of only one such solution.

9. CONCLUSION

Several methods are investigated of regaining the information on local properties of single heterogeneous subassemblies after the three-dimensional coarse-mesh solution has been found. The Superposition Method proved to be superior to the other pin power models examined in this thesis provided both efficiency and accuracy are considered. If the base-solutions used in the superposition scheme are defined using J/Ø-parameters as boundary conditions, one can predict pin powers with a maximum error of ~ 5% using only six base-solutions. Due to symmetry in pin enrichment in the benchmark definitions, only three boundary value calculations need be solved in order to obtain the six base-solutions. The computing time required in order to generate the six base-solutions is measured to be about a factor of two greater than the "normal" assembly calculation.

Moreover, it has been demonstrated that an accurate determination of local pin powers requires knowledge of the heterogeneous or "equivalence" boundary parameter values from the converged global solution. Furthermore, it is not sufficient to use the average values of the boundary parameter values in the pin power models: A first- or a second-order polynomial approximation of the shape of the boundary parameters is required.

It has been shown that the accuracy of a practical use of the local pin power models is poor if the coarse mesh solution is based on flux-weighted homogenized parameters. Hence, other homogenization schemes should be introduced if the pin powers are to be accurately predicted.

One of the major findings is therefore the close connection between the homogenization scheme, the nodal coarse-mesh method, and the local pin power model. Historically, these three subjects were investigated in sequence, and it is only now after progress has been made in all three areas that the close connection can

be recognized (Ref. 13). Consequently, an iterational procedure between homogenization, coarse-mesh calculation, and pin power determination is required in order to obtain fairly accurate solutions. However, based on the results from the Superposition Method, it proves to be possible to avoid the rather time-consuming iterational procedure using the superposition scheme in the global three-dimensional coarse-mesh calculation. The idea is that if the Generalized Equivalence Theory is applied and the discontinuity factors are calculated for each boundary-value problem in the base-solution generation, then it is possible to develop the "actual" discontinuity factors using the superposition scheme during the coarse-mesh solution. This idea has not been examined in this thesis but it seems to be an interesting topic for further investigation.

REFERENCES

1) F. NISSEN (1980). Local Pin Powers, Basic Theories and Methods. Risø SRE-5-80 (Internal report in Danish).
2) K. KOEBKE and M.R.WAGNER (1977). The Determination of the Pin Power Distribution in a Reactor Core on the Basis of Nodal Coarse Mesh Calculations. Atomkernenergie 30, 136-142.
3) F. NISSEN. New Spatial Homogenization Methods for LWR. Risø-M-2350 (under preparation).
4) Z. WEISS (1977). Some Basic Properties of the Response Matrix Equations. Nucl. Sci. Eng. 63, 457-492.
5) Personal communication with A.F. HENRY (MIT) at the ANS-Winter Meeting San Fransisco (1981).
6) L.V. KANTOROVICH and V.I. KRYLOV (1958). Approximate Methods of Higher Analysis (Noordhoff, Groningen) 681 p.
7) K.E. LINDSTRØM JENSEN (1971). Development and Verification of Nuclear Calculation Methods for Light Water Reactors. Risø Report No. 235. 161 p.
8) K. KOEBKE (1976). Berechnung lokaler Fluss-und Leistungsverteilungen durch nachträgliche Interpolation nodaler Grobmaschenverfahren. In: Reaktortagung 1976, held inn Düsseldorf, 30. März - 2. April (Deutsches Atomforum, Bonn) 79-82.
9) C.L. HOXIE, A.F.HENRY (1980). Reconstruction of Heterogeneous PWR Flux Shapes from Nodal Calculations. Trans. Am. Nucl. Soc. 39, 905-906.
10) K. KOEBKE (1978). A New Approach to Homogenization and Group Condensation. In: Homogenization Methods in Reactor Physics, held in Lugano, 13-15 November 1978 (IAEA-TECDOC-231) (International Atomic Energy Agency, Wien) 303-323.
11) K.S. SMITH (1980). Spatial Homogenization Methods for Light Water Reactor Analysis. Dissertation (Ph.D.), Massachusetts Institute of Technology. 150 p.
12) S. WEBER (1981). Coresimulator. SRE-5-81. (Internal report in Danish).

13) P.J. FINCK, C.L. HOXIE, H.S. KHALIL, D.K. PARSONS, and A.F. HENRY (1982). The Application of Nodal Methods to Light Water Reactors. IN: Proceedings of the Topical Meeting on Advances in Reactor Physics and Core Thermal Hydraulics, held in Kiamesha Lake, NY, 22-24 September, 1982 (NUREG-CP-0034) Vol. 1 (US Nuclear Regulatory Commission, Washington DC) 348-364.

14) A.F. HENRY, B.A. WORLEY, and A.A. MORSHED (1978). Spatial Homogenization of Diffusion Theory Parameters. In: Homogenization Methods in Reactor Physics, held in Lugano, 13-15 November 1978 (IAEA-TECDOC-231) (International Atomic Energy Agency, Wien) 275-302.

15) M.J.D. POWELL (1970). A Hybrid Method for Nonlinear Equations. In: Numerical Methods for Nonlinear Equations. Edited by P. RABINOWITZ (Gordon and Breach, London) 87-114.

16) A.Y.C. CHENG (1981). Homogenization of BWR Assemblies by Response Matrix Methods. Dissertation (Ph.D.), Massachusetts Institute of Technology. 151 p.

APPENDIX A

Five-group cross sections for the assembly and the buffer zone defining the benchmark problems.

The mesh-division and the benchmark layout are shown in Figs. 2.3-2.4. Here the five-group cross sections for the twenty-five different compositions are described. The cross sections are presented as shown below

Composition No.					
	D_1	D_2	D_3	D_4	D_5
	Σ_{r1}	$\Sigma_{2\to1}$	$\Sigma_{3\to1}$	$\Sigma_{4\to1}$	$\Sigma_{5\to1}$
	$\Sigma_{1\to2}$	Σ_{r2}	$\Sigma_{3\to2}$	$\Sigma_{4\to2}$	$\Sigma_{5\to2}$
	$\Sigma_{1\to3}$	$\Sigma_{2\to3}$	Σ_{r3}	$\Sigma_{4\to3}$	$\Sigma_{5\to3}$
	$\Sigma_{1\to4}$	$\Sigma_{2\to4}$	$\Sigma_{3\to4}$	Σ_{r4}	$\Sigma_{5\to4}$
	$\Sigma_{1\to5}$	$\Sigma_{2\to5}$	$\Sigma_{3\to5}$	$\Sigma_{4\to5}$	Σ_{r5}
	X_1	X_2	X_3	X_4	X_5
	$\nu\Sigma_{f1}$	$\nu\Sigma_{f2}$	$\nu\Sigma_{f3}$	$\nu\Sigma_{f4}$	$\nu\Sigma_{f5}$

where $\Sigma_{rn} = \Sigma_{an} + \sum_{m} \Sigma_{n\to m}$

COMPOSITION NO. 1 (CONTROLLED ASSEMBLY)

2.23115E+00	9.17390E-01	5.79120E-01	2.03230E-01	8.27274E-02
5.32374E-02	0.	0.	0.	0.
5.15560E-02	8.38684E-02	0.	0.	0.
4.91758E-04	7.86111E-02	1.37572E-01	0.	0.
1.01645E-07	1.67691E-05	2.91585E-02	1.41378E+00	3.12394E-03
2.62347E-08	8.40718E-06	1.43493E-02	3.23816E-01	3.06330E+00
1.00000E+00	0.	0.	0.	0.
0.	0.	0.	0.	0.

COMPOSITION NO. 1 (UNCONTROLLED ASSEMBLY)

2.95823E+00	1.08252E+00	7.79878E-01	5.97004E-01	2.51106E-01
8.83339E-02	0.	0.	0.	0.
8.72153E-02	1.40575E-01	0.	0.	0.
9.39533E-04	1.40520E-01	1.28245E-01	0.	0.
1.95382E-07	3.08943E-05	8.51931E-02	6.04289E-01	4.42800E-04
5.17351E-08	1.54903E-05	4.25860E-02	6.01696E-01	1.05135E-02
8.67932E-01	1.31872E-01	1.96627E-04	3.30801E-10	4.23506E-11
0.	0.	0.	0.	0.

COMPOSITION NO. 2 (CONTROLLED ASSEMBLY)

2.23115E+00	9.17390E-01	5.79120E-01	2.03230E-01	8.27274E-02
5.32374E-02	0.	0.	0.	0.
5.15560E-02	8.38684E-02	0.	0.	0.
4.91758E-04	7.86111E-02	1.37572E-01	0.	0.
1.01645E-07	1.67691E-05	2.91585E-02	1.41378E+00	3.12394E-03
2.62347E-08	8.40718E-06	1.43493E-02	3.23816E-01	3.06330E+00
1.00000E+00	0.	0.	0.	0.
0.	0.	0.	0.	0.

COMPOSITION NO. 2 (UNCONTROLLED ASSEMBLY)

2.68005E+00	1.08663E+00	8.26160E-01	6.70785E-01	2.89458E-01
7.47155E-02	0.	0.	0.	0.
7.37006E-02	1.16034E-01	0.	0.	0.
7.73598E-04	1.15919E-01	1.07214E-01	0.	0.
1.60838E-07	2.54533E-05	7.02604E-02	4.83891E-01	4.04267E-04
4.25882E-08	1.27622E-05	3.50658E-02	4.81552E-01	9.64593E-03
8.67932E-01	1.31872E-01	1.96627E-04	3.30801E-10	4.23506E-11
0.	0.	0.	0.	0.

COMPOSITION NO. 3

2.68005E+00	1.08663E+00	8.26160E-01	6.70785E-01	2.89458E-01
7.47155E-02	0.	0.	0.	0.
7.37006E-02	1.16034E-01	0.	0.	0.
7.73598E-04	1.15919E-01	1.07214E-01	0.	0.
1.60838E-07	2.54533E-05	7.02604E-02	4.83891E-01	4.04267E-04
4.25882E-08	1.27622E-05	3.50658E-02	4.81552E-01	9.64593E-03
8.67932E-01	1.31872E-01	1.96627E-04	3.30801E-10	4.23506E-11
0.	0.	0.	0.	0.

COMPOSITION NO. 4

2.95823E+00	1.08252E+00	7.79878E-01	5.97004E-01	2.51106E-01
8.83339E-02	0.	0.	0.	0.
8.72153E-02	1.40575E-01	0.	0.	0.
9.39533E-04	1.40520E-01	1.28245E-01	0.	0.
1.95382E-07	3.08943E-05	8.51931E-02	6.04289E-01	4.42800E-04
5.17351E-08	1.54903E-05	4.25860E-02	6.01696E-01	1.05135E-02
8.67932E-01	1.31872E-01	1.96627E-04	3.30801E-10	4.23506E-11
0.	0.	0.	0.	0.

COMPOSITION NO. 5

2.54718E+00	1.08894E+00	8.56238E-01	7.05902E-01	3.19981E-01
6.71608E-02	0.	0.	0.	0.
6.62034E-02	1.02293E-01	0.	0.	0.
6.81546E-04	1.02144E-01	9.53457E-02	0.	0.
1.41675E-07	2.24068E-05	6.18332E-02	4.35090E-01	3.80196E-04
3.75139E-08	1.12347E-05	3.08208E-02	4.32853E-01	9.10280E-03
8.67932E-01	1.31872E-01	1.96627E-04	3.30801E-10	4.23506E-11
0.	0.	0.	0.	0.

```
COMPOSITION NO. 6
  2.19875E+00 1.00005E+00 7.83573E-01 7.01080E-01 3.54100E-01
  6.28966E-02 0.          0.          0.          0.
  5.91483E-02 8.53464E-02 0.          0.          0.
  5.39733E-04 8.30773E-02 8.88210E-02 0.          0.
  1.12028E-07 1.80331E-05 4.63466E-02 3.58647E-01 6.73633E-04
  2.96643E-08 9.04177E-06 2.27623E-02 3.49628E-01 4.05675E-02
  8.67932E-01 1.31872E-01 1.96627E-04 3.30801E-10 4.23506E-11
  6.41789E-03 3.11749E-04 3.36976E-03 7.56924E-03 4.73669E-02

-------------------------------------------------------------

COMPOSITION NO. 7
  2.19881E+00 9.99911E-01 7.81911E-01 6.98642E-01 3.52878E-01
  6.29173E-02 0.          0.          0.          0.
  5.91413E-02 8.54123E-02 0.          0.          0.
  5.39734E-04 8.30796E-02 8.95189E-02 0.          0.
  1.12028E-07 1.80336E-05 4.62456E-02 3.60273E-01 7.45607E-04
  2.96643E-08 9.04203E-06 2.27135E-02 3.49614E-01 4.97378E-02
  8.67932E-01 1.31872E-01 1.96627E-04 3.30801E-10 4.23506E-11
  6.49241E-03 4.49859E-04 4.84736E-03 1.08896E-02 6.67067E-02

-------------------------------------------------------------

COMPOSITION NO. 8
  2.19881E+00 9.99911E-01 7.83165E-01 6.98644E-01 3.52878E-01
  6.29173E-02 0.          0.          0.          0.
  5.91413E-02 8.54123E-02 0.          0.          0.
  5.39734E-04 8.30796E-02 8.89579E-02 0.          0.
  1.12028E-07 1.80336E-05 4.63197E-02 3.60270E-01 7.45604E-04
  2.96643E-08 9.04203E-06 2.27493E-02 3.49611E-01 4.97378E-02
  8.67932E-01 1.31872E-01 1.96627E-04 3.30801E-10 4.23506E-11
  6.49241E-03 4.49859E-04 4.85924E-03 1.08897E-02 6.67067E-02

-------------------------------------------------------------

COMPOSITION NO. 9
  2.15416E+00 9.93670E-01 7.86418E-01 7.11521E-01 3.67676E-01
  6.08212E-02 0.          0.          0.          0.
  5.68233E-02 8.04609E-02 0.          0.          0.
  5.06156E-04 7.79711E-02 8.46732E-02 0.          0.
  1.05026E-07 1.68883E-05 4.33604E-02 3.38547E-01 7.04627E-04
  2.78104E-08 8.46778E-06 2.12311E-02 3.28862E-01 4.34577E-02
  8.67932E-01 1.31872E-01 1.96627E-04 3.30801E-10 4.23506E-11
  7.02333E-03 3.43138E-04 3.71080E-03 8.34530E-03 5.19322E-02

-------------------------------------------------------------

COMPOSITION NO. 10
  2.19889E+00 9.99765E-01 7.81315E-01 6.95942E-01 3.51434E-01
  6.29403E-02 0.          0.          0.          0.
  5.91334E-02 8.54859E-02 0.          0.          0.
  5.39735E-04 8.30823E-02 8.97378E-02 0.          0.
  1.12028E-07 1.80342E-05 4.62069E-02 3.62139E-01 8.20184E-04
  2.96643E-08 9.04232E-06 2.26947E-02 3.49657E-01 5.95026E-02
  8.67932E-01 1.31872E-01 1.96627E-04 3.30801E-10 4.23506E-11
  6.57548E-03 6.04017E-04 6.50123E-03 1.45752E-02 8.72769E-02

-------------------------------------------------------------
```

COMPOSITION NO. 11

2.15189E+00	9.92168E-01	7.82046E-01	7.07420E-01	3.65237E-01
6.09952E-02	0.	0.	0.	0.
5.69651E-02	8.07842E-02	0.	0.	0.
5.07778E-04	7.82243E-02	8.62506E-02	0.	0.
1.05363E-07	1.69442E-05	4.33200E-02	3.41421E-01	7.84777E-04
2.78997E-08	8.49580E-06	2.12145E-02	3.29927E-01	5.34745E-02
8.67932E-01	1.31872E-01	1.96627E-04	3.30801E-10	4.23506E-11
7.10588E-03	4.95172E-04	5.32334E-03	1.20060E-02	7.30646E-02

COMPOSITION NO. 12

2.19889E+00	9.99765E-01	7.80082E-01	6.95941E-01	3.51435E-01
6.29403E-02	0.	0.	0.	0.
5.91334E-02	8.54859E-02	0.	0.	0.
5.39735E-04	8.30823E-02	9.02927E-02	0.	0.
1.12028E-07	1.80342E-05	4.61340E-02	3.62141E-01	8.20188E-04
2.96643E-08	9.04232E-06	2.26595E-02	3.49660E-01	5.95026E-02
8.67932E-01	1.31872E-01	1.96627E-04	3.30801E-10	4.23506E-11
6.57148E-03	6.04017E-04	6.48550E-03	1.45752E-02	8.72768E-02

COMPOSITION NO. 13

2.15197E+00	9.92011E-01	7.80035E-01	7.04366E-01	3.63465E-01
6.10203E-02	0.	0.	0.	0.
5.69564E-02	8.08650E-02	0.	0.	0.
5.07779E-04	7.82270E-02	8.70997E-02	0.	0.
1.05363E-07	1.69448E-05	4.31975E-02	3.43497E-01	8.67004E-04
2.78997E-08	8.49610E-06	2.11555E-02	3.29994E-01	6.41144E-02
8.67932E-01	1.31872E-01	1.96627E-04	3.30801E-10	4.23506E-11
7.19679E-03	6.64859E-04	7.11974E-03	1.60688E-02	9.54929E-02

COMPOSITION NO. 14

2.15205E+00	9.91807E-01	7.77596E-01	7.00654E-01	3.61178E-01
6.10514E-02	0.	0.	0.	0.
5.69459E-02	8.09645E-02	0.	0.	0.
5.07781E-04	7.82305E-02	8.81350E-02	0.	0.
1.05363E-07	1.69456E-05	4.30489E-02	3.46078E-01	9.59085E-04
2.78996E-08	8.49648E-06	2.10838E-02	3.30121E-01	7.65188E-02
8.67932E-01	1.31872E-01	1.96627E-04	3.30801E-10	4.23506E-11
7.30868E-03	8.73418E-04	9.30844E-03	2.10299E-02	1.21601E-01

COMPOSITION NO. 15

2.15197E+00	9.92011E-01	7.81538E-01	7.04367E-01	3.63465E-01
6.10203E-02	0.	0.	0.	0.
5.69564E-02	8.08650E-02	0.	0.	0.
5.07779E-04	7.82270E-02	8.64245E-02	0.	0.
1.05363E-07	1.69448E-05	4.32861E-02	3.43493E-01	8.67002E-04
2.78997E-08	8.49610E-06	2.11981E-02	3.29990E-01	6.41144E-02
8.67932E-01	1.31872E-01	1.96627E-04	3.30801E-10	4.23506E-11
7.19679E-03	6.64859E-04	7.14075E-03	1.60688E-02	9.54930E-02

COMPOSITION NO. 16

2.15197E+00	9.92011E-01	7.81455E-01	7.04367E-01	3.63465E-01
6.10203E-02	0.	0.	0.	0.
5.69564E-02	8.08650E-02	0.	0.	0.
5.07779E-04	7.82270E-02	8.64515E-02	0.	0.
1.05363E-07	1.69448E-05	4.32812E-02	3.43493E-01	8.67002E-04
2.78997E-08	8.49610E-06	2.11958E-02	3.29991E-01	6.41144E-02
8.67932E-01	1.31872E-01	1.96627E-04	3.30801E-10	4.23506E-11
7.19679E-03	6.64859E-04	7.13959E-03	1.60688E-02	9.54930E-02

COMPOSITION NO. 17

2.15205E+00	9.91807E-01	7.79065E-01	7.00656E-01	3.61178E-01
6.10514E-02	0.	0.	0.	0.
5.69459E-02	8.09645E-02	0.	0.	0.
5.07781E-04	7.82305E-02	8.74691E-02	0.	0.
1.05363E-07	1.69456E-05	4.31357E-02	3.46074E-01	9.59084E-04
2.78996E-08	8.49648E-06	2.11256E-02	3.30117E-01	7.65188E-02
8.67932E-01	1.31872E-01	1.96627E-04	3.30801E-10	4.23506E-11
7.30868E-03	8.73418E-04	9.33554E-03	2.10300E-02	1.21601E-01

COMPOSITION NO. 18

2.15205E+00	9.91807E-01	7.78985E-01	7.00656E-01	3.61178E-01
6.10514E-02	0.	0.	0.	0.
5.69459E-02	8.09645E-02	0.	0.	0.
5.07781E-04	7.82305E-02	8.75056E-02	0.	0.
1.05363E-07	1.69456E-05	4.31309E-02	3.46074E-01	9.59084E-04
2.78996E-08	8.49648E-06	2.11233E-02	3.30117E-01	7.65188E-02
8.67932E-01	1.31872E-01	1.96627E-04	3.30801E-10	4.23506E-11
7.30868E-03	8.73418E-04	9.33405E-03	2.10300E-02	1.21601E-01

COMPOSITION NO. 19

2.15438E+00	9.93162E-01	7.80186E-01	7.01962E-01	3.62092E-01
6.09000E-02	0.	0.	0.	0.
5.67965E-02	8.07136E-02	0.	0.	0.
5.06159E-04	7.79797E-02	8.72800E-02	0.	0.
1.05026E-07	1.68902E-05	4.29827E-02	3.45019E-01	9.58728E-04
2.78104E-08	8.46873E-06	2.10490E-02	3.29062E-01	7.64996E-02
8.67932E-01	1.31872E-01	1.96627E-04	3.30801E-10	4.23506E-11
7.30765E-03	8.73385E-04	9.33247E-03	2.10296E-02	1.21574E-01

COMPOSITION NO. 20

2.29930E+00	1.07253E+00	8.98779E-01	7.76077E-01	3.85897E-01
5.43577E-02	0.	0.	0.	0.
5.34822E-02	7.84616E-02	0.	0.	0.
5.23212E-04	7.82471E-02	7.50247E-02	0.	0.
1.08708E-07	1.71161E-05	4.73084E-02	3.39941E-01	3.49733E-04
2.87849E-08	8.58200E-06	2.34963E-02	3.37788E-01	8.63908E-03
8.67932E-01	1.31872E-01	1.96627E-04	3.30801E-10	4.23506E-11
0.	0.	0.	0.	0.

COMPOSITION NO. 21-25 (BUFFER ZONE)

2.21734E+00	9.98314E-01	7.65819E-01	6.59159E-01	3.42242E-01
6.15252E-02	0.	0.	0.	0.
5.81734E-02	8.55384E-02	0.	0.	0.
5.37201E-04	8.30282E-02	9.28091E-02	0.	0.
1.11472E-07	1.80089E-05	4.50762E-02	3.92077E-01	7.60282E-04
2.94505E-08	9.02953E-06	2.21825E-02	3.52776E-01	6.09519E-02
8.67932E-01	1.31872E-01	1.96627E-04	3.30801E-10	4.23506E-11
5.38130E-03	5.37056E-04	5.67197E-03	1.36420E-02	7.57153E-02

POISONED CROSS SECTIONS FOR THE BUFFER ZONE

COMPOSITION NO. 21

0.00000E-00	0.00000E-00	0.00000E-00	0.00000E-00	0.00000E-00

COMPOSITION NO. 22

3.56530E-04	3.56530E-04	3.56530E-04	3.56530E-02	7.13060E-02

COMPOSITION NO. 23

1.06910E-03	1.06910E-03	1.06910E-03	1.06910E-02	2.13820E-02

COMPOSITION NO. 24

1.06910E-04	1.06910E-04	1.06910E-04	1.06910E-03	2.13820E-03

COMPOSITION NO. 25

1.13470E-05	1.13470E-05	1.13470E-05	1.13470E-03	2.26940E-03

APPENDIX B

THE USE OF "CDB" WITH "NEW" BOUNDARY PARAMETERS

In the Flux-lupe investigation "CDB" was applied to perform the assembly calculations with either J^-, J^+, J, $\emptyset$ or $\lambda \cdot J/\emptyset$ as boundary parameter. Unfortunately, used directly "CDB" can solve only extrapolated and reflected boundary value problems. Thus, a "trick" is needed to solve problems with J^-, J^+, J, $\emptyset$, or $\lambda \cdot J/\emptyset$ as boundary condition.

The following "tricks" have been used:

1) The boundary conditions are divided into an extrapolation and source factor in the cases of J^+, J^-, and J.

2) In the case of the flux boundary value problems the flux values are held fixed (during the iteration process) in the outer nodes of the assembly.

3) In the case of the $\lambda \cdot J/\emptyset$ approximation the possibility of multiplying the eigenvalue on "poisoned" cross sections has been used. The values of the extrapolation factors are converted to "poisoned" cross sections in the outer nodes of the assembly and the eigenvalues are multiplied on these "poisoned" cross sections.

The three "tricks" mentioned above are described in more details in the following.

B1: J^-, J^+, and J (source calculation)

In (Ref. 16) the calculation procedure is described for J^+ and J used as boundary parameters in a multigroup diffusion theory finite difference code "CITATION". As it is the same solution

procedure which has been developed for "CDB", we will look only at the problem concerning the boundary parameter J^-.

In order to use "CDB" directly, the boundary conditions must either be net currents equal to zero or have the form

$$J_g^S = \frac{1}{1/C_S + \Delta/2D_g^S} \cdot \phi_g^M$$

where

J_g^S is the face average group g net current at the boundary surface

Δ is the mesh size of meshes neighbouring the boundary surface

D_g^S is the g group diffusion coefficient in those meshes neighbouring the boundary surface

ϕ_g^M is the volume-averaged group of flux in those meshes neighbouring the boundary surface

C_S is a constant that can be arbitrarily specified.

The group g net currents on those mesh faces belonging to the boundary of the assembly are given by:

$$J_g = D_g \frac{\phi_g^M - \phi_g^S}{\frac{\Delta}{2}}$$

where

ϕ_g^S is the scalar flux in group g at the boundary surface.

Using the diffusion theory approximation we have:

$$\phi_g^S = 2(J_g^{in} + J_g^{out})$$

Combining and rearranging these two equations above gives:

$$J_g^{in} - \frac{\frac{\Delta}{2} + 2D_g}{\frac{\Delta}{2} - 2D_g} \cdot J^{out} - \frac{D_g}{\frac{\Delta}{2} - 2D_g} \cdot \phi_g^M$$

and the total leakage through the boundary mesh faces is given by:

$$-J_g = -\frac{4D_g}{\frac{\Delta}{2} - 2D_g} \cdot J^{out} - \frac{D_g}{(\frac{\Delta}{2} - 2D_g)} \cdot \phi_g^M$$

Substituting the leakage expression into the differential equation and moving the term involving J_g^{out} to the right-hand side, we see that the problem that we are trying to solve is equivalence to one with distributed sources S_g, where

$$S_g = \begin{cases} \dfrac{4}{\frac{\Delta}{2D_g} - 2} \cdot \dfrac{J_g^{out}}{\Delta} & \text{in the meshes lying next to the boundary} \\ 0 & \text{elsewhere} \end{cases}$$

and with boundary conditions

$$J_g^s = \frac{1}{\frac{\Delta}{2D_g} - 2} \cdot \phi_g^M$$

In case of the J^+ boundary value problems the distributed sources and the boundary conditions are defined by (Ref. 16):

$$S_g = \begin{cases} \dfrac{4}{\frac{\Delta}{2D_g} + 2} \cdot \dfrac{J_g^{in}}{\Delta} & \text{in the meshes neighbouring the boundary surface} \\ 0 & \text{elsewhere} \end{cases}$$

$$J_g^s = \frac{1}{\frac{\Delta}{2D_g} + 2} \cdot \phi_g^M$$

The J_{NET} boundary value problems are solved by:

$$S_g = \begin{cases} \dfrac{J_g^{NET}}{\Delta} & \text{in the meshes neighbouring the boundary surface} \\ 0 & \text{elsewhere} \end{cases}$$

$$J_g^S = 0 \cdot \phi_g^M$$

B2: Flux boundary value problems

In "CDB" the finite-difference equation system (Equation B2-1) is solved by an iterational procedure.

$$\underline{\underline{A}} \cdot \underline{\phi} = \underline{S} \qquad \text{(B2-1)}$$

where the cross sections and coupling coefficients are contained in the band matrix $\underline{\underline{A}}$ and the source values are included in $\underline{S}$. $\underline{\phi}$ consists of the volume-averaged flux values in all meshes in which the assembly is divided.

By maintaining the flux values in the meshes neighbouring the boundary surface during the iteration process the final solution will be equal the solution to the differential equation system with the fixed flux values in the outer meshes as boundary conditions.

In order to illustrate the calculation procedure mentioned above, let us examine a two-dimensional one-group problem:

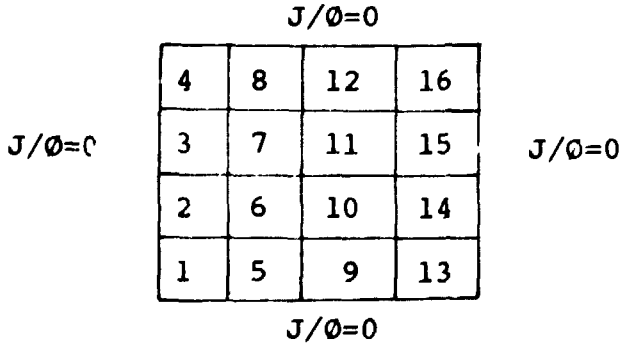

The finite-difference equation system for this problem can be written as:

$$\begin{bmatrix} a_{11} & a_{12} & 0 & 0 & a_{15} & 0 & 0 \\ a_{21} & a_{22} & a_{23} & 0 & 0 & a_{26} & \\ 0 & a_{32} & a_{33} & a_{34} & 0 & 0 & a_{37} \\ 0 & 0 & & & & & \\ a_{51} & 0 & & & & & \\ 0 & a_{62} & & & & & \\ 0 & & & & & & \\ \cdot & & & & & & \\ \cdot & & & & & & \\ \cdot & & & & & & \\ \cdot & & & & & & \\ \cdot & & & & & & \\ \cdot & & & & & & \\ & & & & & & \end{bmatrix} \cdot \begin{bmatrix} \phi_1 \\ \phi_2 \\ \phi_3 \\ \\ \\ \\ \\ \\ \\ \\ \\ \\ \\ \phi_{16} \end{bmatrix} = \begin{bmatrix} S_1 \\ S_2 \\ S_3 \\ \\ \\ \\ \\ \\ \\ \\ \\ \\ \\ S_{16} \end{bmatrix}$$

Keeping ϕ_1, ϕ_2, ϕ_3, ϕ_4, ϕ_5, ϕ_8, ϕ_9, ϕ_{12}, ϕ_{13}, ϕ_{14}, ϕ_{15}, and ϕ_{16} fixed the equation system will be reduced to one containing only four equations with four unknowns. The solution to this reduced problem will make up the solution to the problem of calculating the fluxes in the criterion four nodes when the fluxes in the meshes neighbouring the boundary faces are used as boundary conditions.

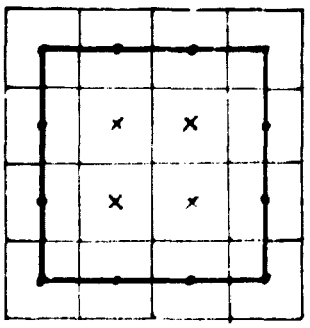

In the Flux-lupe investigation described in Chapter 4, the meshes neighbouring the boundary surface have been divided into two pieces in order to make the average fluxes in the outer meshes "equal" to the fluxes on the boundary faces. The division performed is illustrated by:

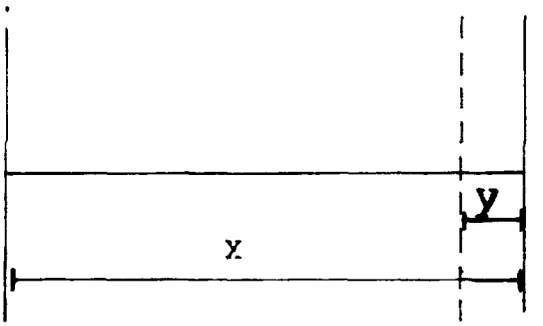

x = 1.385 cm , y = 0.05 (broad water gap)

x = 0.850 cm , y = 0.05 (narrow water gap)

Investigations has shown that the influence on the pin power distribution due to the change in mesh division described above is very weak

B3: $\lambda \cdot J/\emptyset$ used as boundary conditions

The $\lambda \cdot J/\emptyset$ extension of "CDB" makes it possible to calculate the ratio between net neutron currents and scalar fluxes on the boundary of the assembly which gives criticality. The trick we use can be explained by the following example:

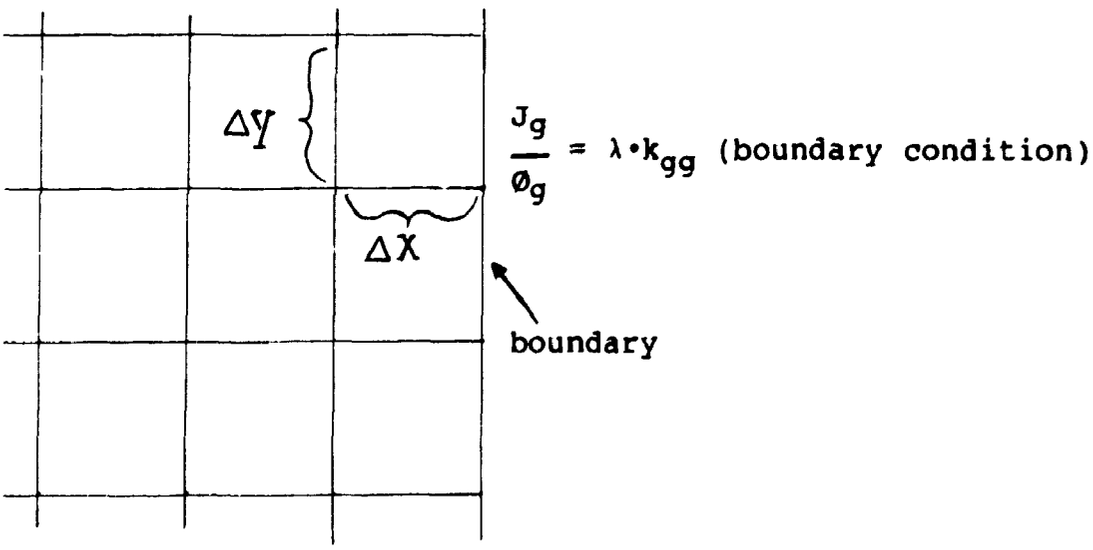

$\frac{J_g}{\emptyset_g} = \lambda \cdot k_{gg}$ (boundary condition)

The net neutron currents at the boundary surface can be expressed as:

$$\underline{J}^S = \underline{\underline{K}} \cdot \underline{\phi}^S$$

where $\underline{\underline{K}}$ is a diagonal matrix containing the elements k_{gg}

$\underline{\phi}^S$ contains the group fluxes on the boundary surface.

If the ratio between scalar fluxes at the center of the node, $\underline{\phi}^M$, and scalar fluxes on the boundary faces can be expressed as:

$$\underline{\phi}^M = \underline{\underline{T}} \cdot \underline{\phi}^S$$

then it is possible to transfer the leakage rate $J_g^S \cdot \Delta y$ to a "leakage" cross-section by:

$$\underline{J}^S \cdot \Delta y = \underline{\underline{K}} \cdot \underline{\underline{T}}^{-1} \cdot \underline{\phi}^M \cdot \Delta y \Rightarrow$$

$$\underline{\underline{P}} = \underline{\underline{K}} \cdot \underline{\underline{T}}^{-1} \cdot \frac{1}{\Delta x}$$

$\underline{\underline{P}}$ contains the equivalent leakage cross sections, $p_{GG'}$.

The differential equation system we are faced with when the "leakage" cross sections are introduced is defined as:

$$D_G \nabla^2 \phi_G - (\Sigma_{aG} + f_{G'} \Sigma_{G \to G'} + \frac{1}{\lambda} \cdot p_{GG'}) \cdot \phi_G + f_{G'} (\Sigma_{G' \to G} + \chi_G \nu \Sigma_{fG'}) \cdot \phi_{G'} = 0$$

with the boundary conditions

$$\underline{J}^S = \underline{\underline{0}} \cdot \underline{\phi}^S$$

where the elements of $\underline{\underline{0}}$ are zero.

Table 4.1. Results of the Flux-lupe investigations.

Test case	Boundary Parameter	Boundary Approximation	Average errors in the boundary approximation % of average reference value				Maximum deviation in pin powers	Average deviation in pin powers
			Fast group		Thermal group			
Number of benchmark problem			Face 2	Face 3	Face 2	Face 3	In % of average assembly power	In % of average assembly power
1	J^+	Flat	1.5	1.9	1.5	3.5	13.4	2.7
1	J^+	Tilt	1.0	0.4	2.6	4.2	11.9	3.6
1	J^+	Parabolic	0.2	0.2	0.2	1.6	1.2	0.4
2	J^+	Flat	0.7	0.6	0.9	1.5	7.5	1.7
2	J^+	Tilt	0.7	1.0	1.0	1.4	7.4	2.2
2	J^+	Parabolic	0.1	0.1	0.1	0.3	1.0	0.4
3	J^+	Flat	1.5	1.8	1.7	2.6	15.1	4.1
3	J^+	Tilt	0.8	0.9	0.5	2.7	6.7	2.0
3	J^+	Parabolic	0.1	0.1	0.3	0.3	2.1	0.6
1	J^-	Flat	2.1	2.2	1.4	3.6	40.9	12.8
1	J^-	Tilt	0.9	0.4	2.4	4.4	20.7	6.4
1	J^-	Parabolic	0.2	0.2	0.2	1.7	5.5	2.0
2	J^-	Flat	0.5	0.5	0.9	1.4	62.2	33.9
2	J^-	Tilt	0.8	0.9	1.7	1.3	63.8	36.0
2	J^-	Parabolic	0.1	0.1	0.1	0.2	6.6	3.2
3	J^-	Flat	2.2	2.2	1.6	2.3	75.2	35.2
3	J^-	Tilt	1.1	1.4	1.4	2.7	62.3	37.3
3	J^-	Parabolic	0.1	0.1	0.2	0.3	7.2	3.5
1	J	Flat	8.8	2.7	4.6	0.7	10.9	2.7
1	J	Tilt	3.1	0.5	4.3	0.7	2.2	0.7
1	J	Parabolic	3.4	0.6	1.9	0.3	0.6	0.2
2	J	Flat	8.4	1.0	4.3	0.2	10.9	2.6
2	J	Tilt	2.3	0.3	2.7	0.1	2.7	1.0
2	J	Parabolic	1.1	0.2	0.7	0.0	0.7	0.2
3	J	Flat	5.1	2.1	2.2	0.7	7.2	1.6
3	J	Tilt	8.0	2.4	4.5	0.7	25.6	12.5
3	J	Parabolic	0.5	0.8	0.6	0.3	2.9	0.9

(To be continued on next page)

Table 4.1. (continued)

Test case Number of benchmark problem	Boundary Parameter	Boundary Approximation	Average errors in the boundary approximation % of average reference value				Maximum deviation in pin powers	Average deviation in pin powers
			Fast group		Thermal group		In % of average assembly power	In % of average assembly power
			Face 2	Face 3	Face 2	Face 3		
1	Ø	Flat	1.8	2.1	1.4	3.6	15.2	3.2
1	Ø	Tilt	1.0	0.4	2.5	4.2	14.4	4.4
1	Ø	Parabolic	0.2	0.2	0.2	1.6	1.3	0.4
2	Ø	Flat	0.6	0.6	0.9	1.4	8.9	2.0
2	Ø	Tilt	0.8	0.9	1.7	1.3	10.7	3.2
2	Ø	Parabolic	0.1	0.1	0.1	0.3	1.2	0.4
3	Ø	Flat	1.8	2.0	1.7	2.5	16.9	4.9
3	Ø	Tilt	0.2	1.2	0.9	2.8	8.0	2.5
3	Ø	Parabolic	0.0	0.1	0.3	0.3	2.4	0.7
1	J/Ø	Flat	8.5	0.8	4.3	0.9	17.7	4.2
1	J/Ø	Tilt	1.6	0.8	2.4	0.5	2.9	1.1
1	J/Ø	Parabolic	0.7	0.7	0.7	0.7	0.9	0.3
2	J/Ø	Flat	8.8	1.0	4.6	0.1	9.5	2.2
2	J/Ø	Tilt	1.8	0.7	2.1	0.1	2.1	0.9
2	J/Ø	Parabolic	0.8	0.2	0.7	0.1	0.9	0.3
3	J/Ø	Flat	5.4	2.2	1.2	0.4	16.9	1.8
3	J/Ø	Tilt	6.6	2.8	1.7	0.3	22.6	10.4
3	J/Ø	Parabolic	1.6	1.0	0.3	0.1	3.7	0.9
1	λ·J/Ø	Flat	-	-	-	-	14.5	3.4
1	λ·J/Ø	Tilt	-	-	-	-	2.2	0.6
1	λ·J/Ø	Parabolic	-	-	-	-	0.9	0.3
2	λ·J/Ø	Flat	-	-	-	-	9.4	2.1
2	λ·J/Ø	Tilt	-	-	-	-	1.8	0.7
2	λ·J/Ø	Parabolic	-	-	-	-	0.9	0.3
3	λ·J/Ø	Flat	-	-	-	-	8.6	1.0
3	λ·J/Ø	Tilt	-	-	-	-	9.3	3.9
3	λ·J/Ø	Parabolic	-	-	-	-	0.9	0.2
1	J/Ø=0	Flat	-	-	-	-	8.4	2.8
2	J/Ø=0	Flat	-	-	-	-	8.8	3.1
3	J/Ø=0	Flat	-	-	-	-	23.3	8.5

Table 5.1. Results of a comparison between the Response Matrix Method and the Superposition Method.

Boundary parameter in the base-solution generation		Number of base-solution	Maximum error in the local pin power determination (% of average assembly power)		
TYPE	APPROXIMATION		Test 1	Test 2	Test 3
J/Ø	Flat	4	11.9	7.8	7.7
J/Ø	Tilt	8	6.9	3.4	16.3
J	Flat	20	13.7	12.3	5.1
J	Tilt	40	3.8	2.6	26.1
Ø	Flat	20	24.1	11.8	12.4
Ø	Tilt	40	15.9	11.2	7.8

Table 6.1. Equivalence parameters for the six test cases shown in Figure 6.1

Test case	D_1 cm	D_2 cm	F_1	F_2	$\Sigma_{a1}+\Sigma_{1\to2}$ $\cdot10^{-2}$ cm^{-1}	Σ_{a2} $\cdot10^{-2}$ cm^{-1}	$\Sigma_{1\to2}$ $\cdot10^{-2}$ cm^{-1}	$\nu\Sigma_{f1}$ $\cdot10^{-3}$ cm^{-1}	$\nu\Sigma_{f2}$ $\cdot10^{-2}$ cm^{-1}
Test 1/I	2.217	-1.188	0.955	1.064	2.885	6.039	1.918	3.840	6.965
Test 1/II	1.891	-0.943	0.958	1.125	2.886	5.825	1.933	3.885	6.945
Test 1/III	1.950	-1.006	0.957	1.110	2.875	5.876	1.931	3.871	6.953
Test 2/I	0.702	-0.109	1.013	1.522	2.813	4.142	2.161	3.895	5.808
Test 2/II	8.863	-0.819	0.933	1.289	2.822	4.094	2.174	3.858	5.714
Test 2/III	23.514	-0.905	0.931	1.290	2.820	4.102	2.172	3.868	5.731

Table 6.2. The maximum errors in the local pin power determination using HHM based on the equivalence homogenization parameters shown in Table 6.1.

Test case	Maximum error in % of the average assembly power
Test 1/I	15.2
Test 1/III	16.9
Test 2/I	54.8
Test 2/III	0.6

Table 7.1. A comparison between the maximum errors in the pin power determination for Test 1 using heterogeneous - and homogeneous boundary parameter values.

LOCAL MODEL	TYPE OF BOUNDARY	BOX NUMBER								
		1	2	3	4	5	6	7	8	9
NORMALIZ		21.1	27.2	32.3	28.1	27.0	35.2	10.3	7.1	30.3
FLUX-LUPE	HETEROG.					0.0				
FLUX-LUPE	HOMOGEN.					36.2				
SUPER/6	HETEROG.	5.5	4.6	4.7	4.9	5.5	2.9	5.2	2.8	2.0
SUPER/6	HOMOGEN.	16.8	17.8	12.0	12.8	10.7	7.8	6.8	4.8	9.9
MODULATION	HETEROG.	7.2	12.5	6.8	4.6	5.6	5.9	1.8	1.1	4.7
MODULATION	HOMOGEN.	11.2	11.0	8.0	20.1	26.3	11.6	10.3	9.5	4.0

Table 8.1. Equivalence diffusion coeficients and heterogeniety factors for the six test cases shown in Fig. 6.1.

Test case	Type of calculation	D_1 cm	D_2 cm	F_1	F_2
Test 1/I	ANALYT	2.159	-1.176	0.953	1.067
Test 1/I	ITERATION	2.217	-1.118	0.955	1.064
Test 1/I	ANALYT	-0.209	-0.043	1.041	6.435
Test 1/II	ANALYT	1.939	-0.942	0.958	1.128
Test 1/II	ITERATION	1.891	-0.943	0.958	1.126
Test 1/II	ANALYT	0.865	-0.132	0.945	1.116
Test 1/III	ANALYT	1.968	-1.001	0.956	1.112
Test 1/III	ITERATION	1.950	-1.006	0.957	1.110
Test 1/III	ANALYT	0.678	-0.304	1.076	4.644
Test 2/I	ANALYT	0.717	-0.102	1.031	1.422
Test 2/I	ITERATION	0.702	-0.109	1.013	1.522
Test 2/I	ANALYT	0.769	-0.020	1.015	1.409
Test 2/II	ANALYT	9.070	-0.815	0.934	1.288
Test 2/II	ITERATION	8.863	-0.819	0.933	1.289
Test 2/II	ANALYT	5.181	-0.229	0.966	9.392
Test 2/II	ITERATION	4.971	-0.236	0.966	8.699
Test 2/III	ANALYT	23.619	-0.898	0.931	1.289
Test 2/III	ITERATION	23.514	-0.905	0.931	1.290
Test 2/III	ANALYT	11.130	-0.235	0.948	25.881

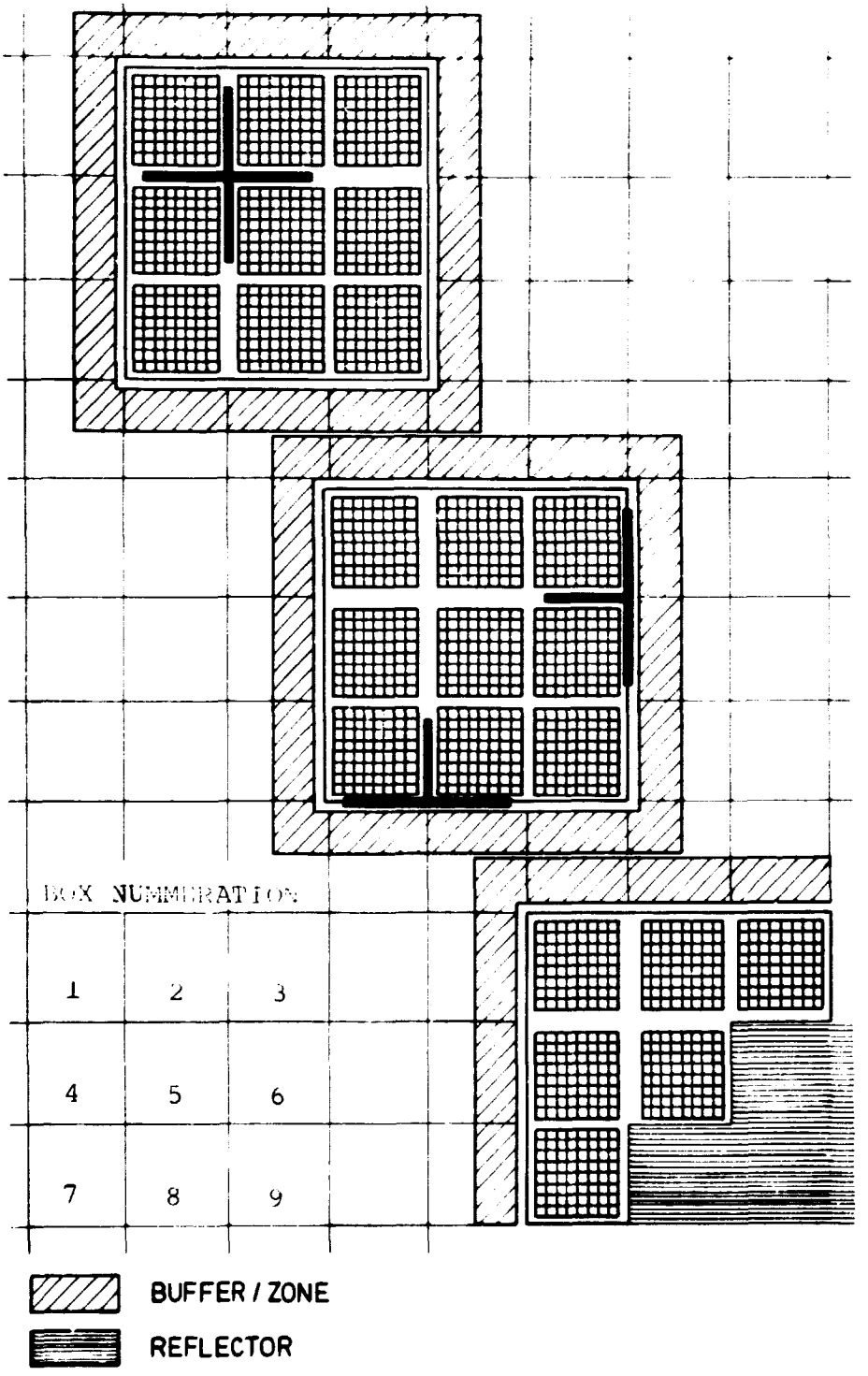

Fig. 2.1. Plan view of the three subregions of the BWR core used as benchmark problems.

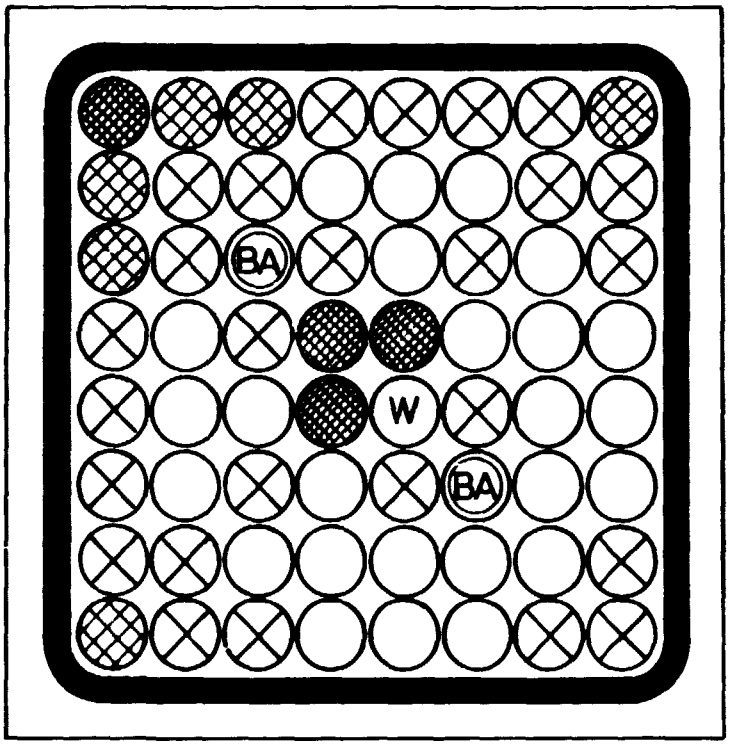

0.97 W/O U - 235

1.40 " "

1.88 " "

2.47 " "

BA 2.47 " " With BA

W Water hole

Fig. 2.2. Pin enrichment values for BWR fuel assembly.

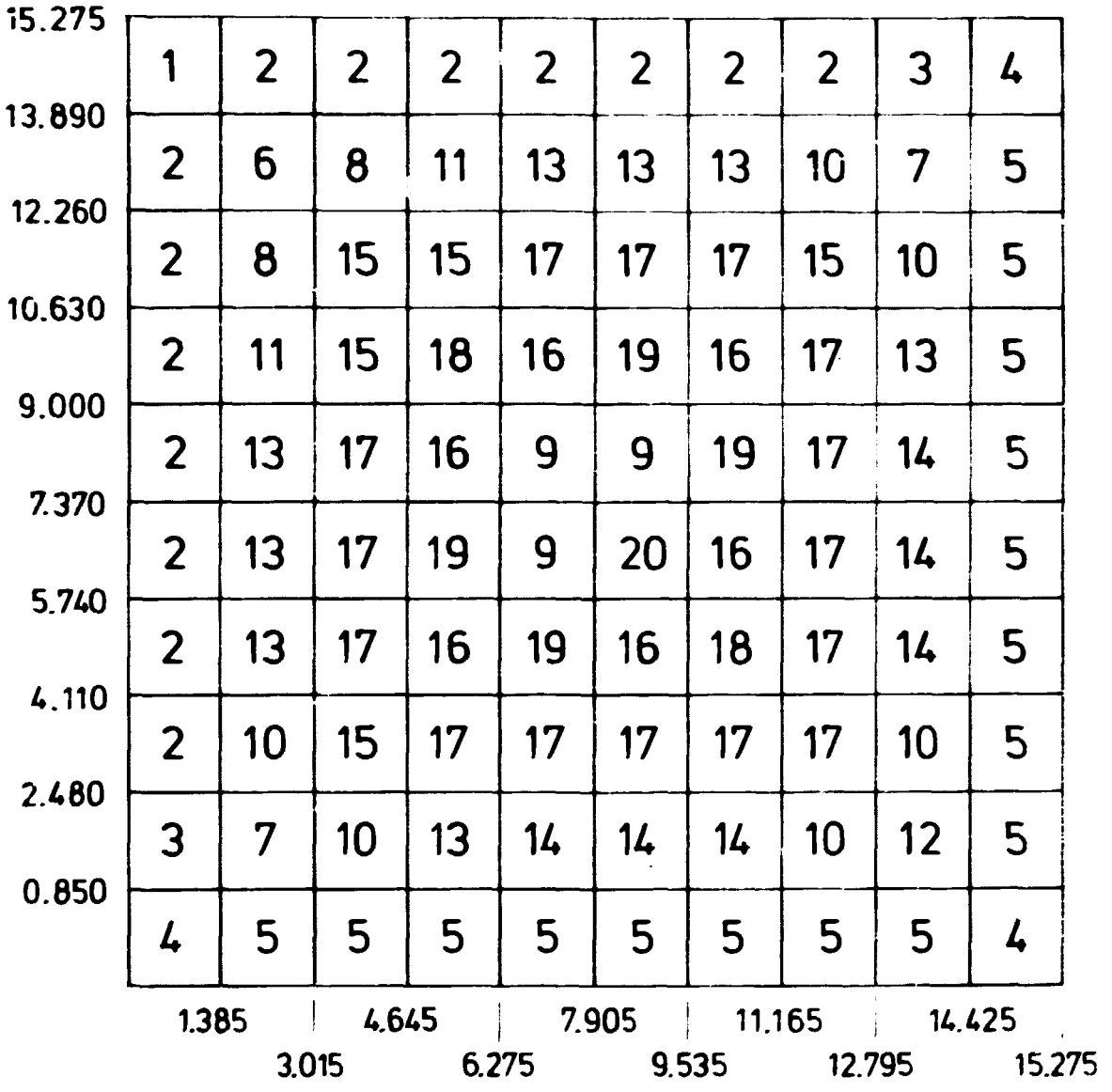

Fig. 2.3. Mesh description of the assembly.

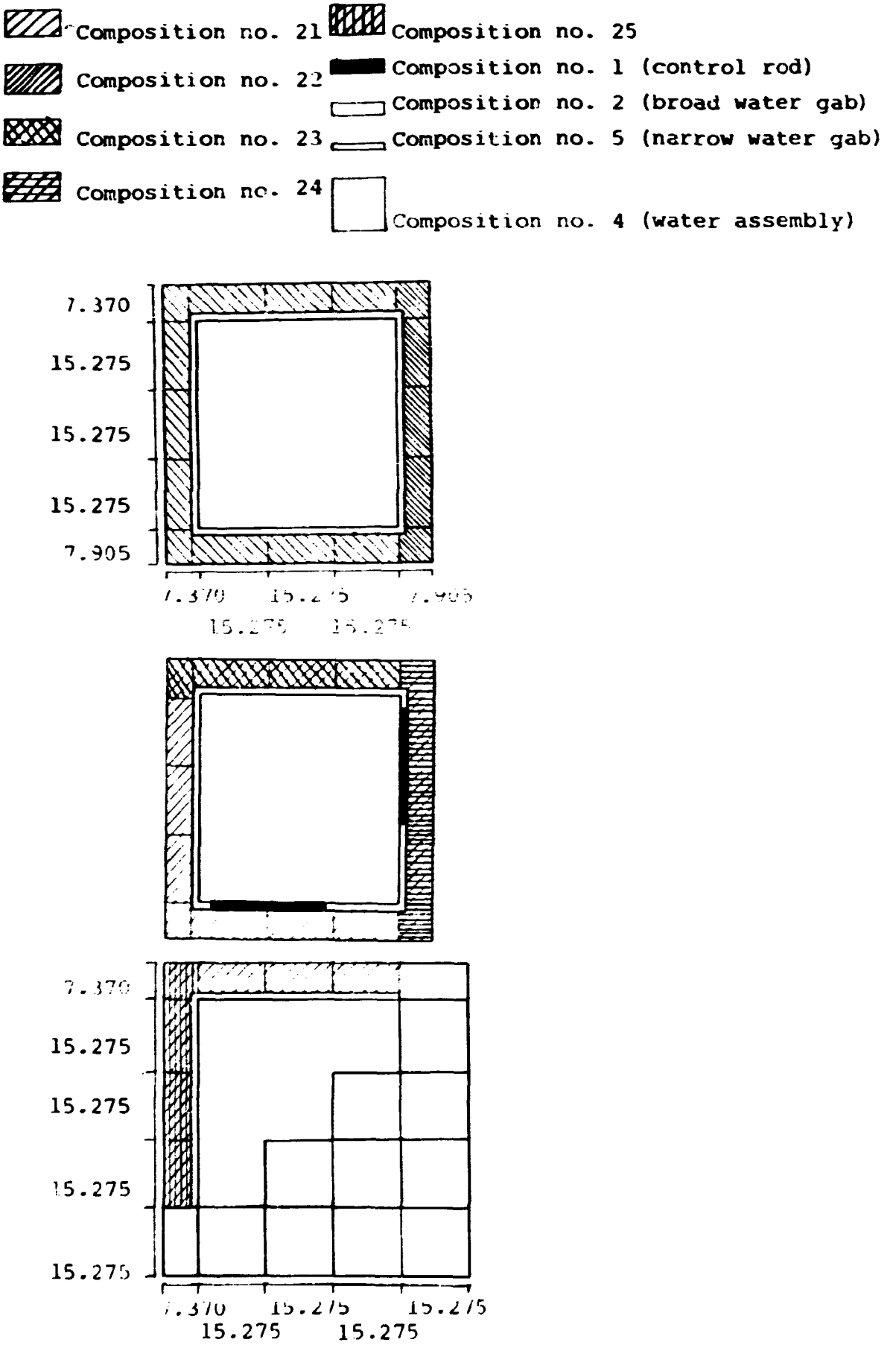

Fig. 2.4. Layout of the three buffer zone configurations.

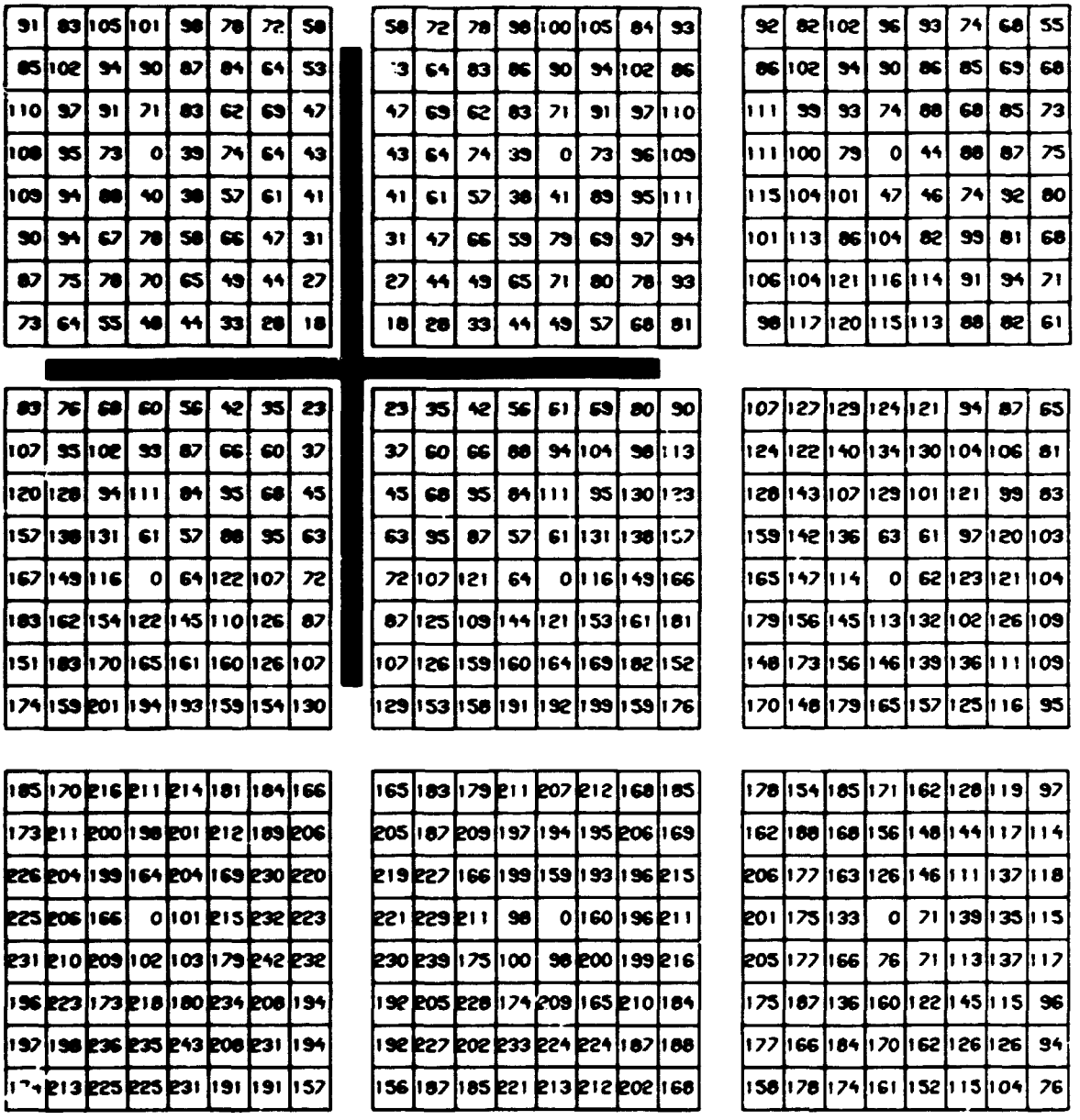

Fig. 2.5. Reference solution to Test One.
(Pin powers in % of the average power of the subregion).

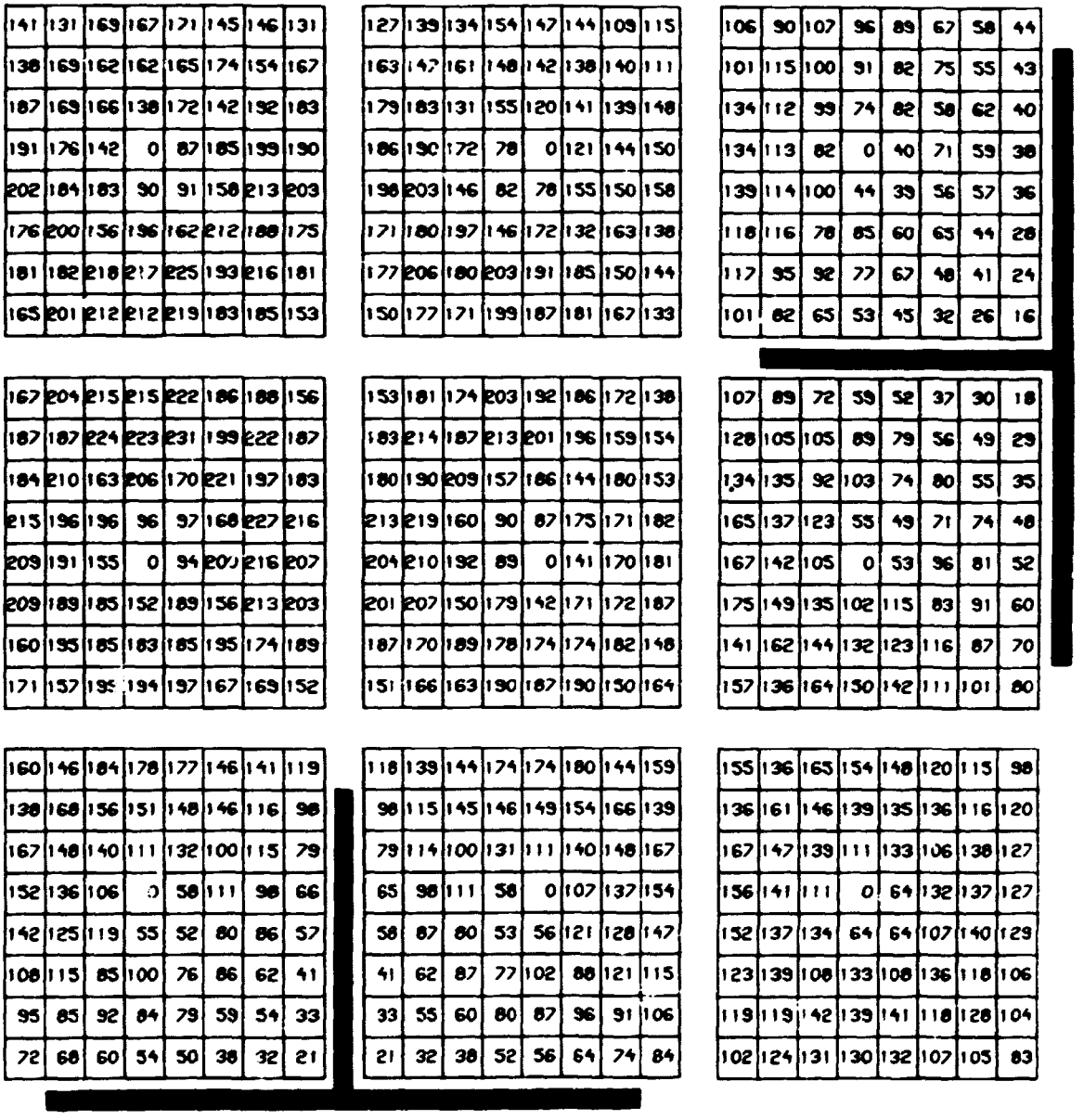

141	131	169	167	171	145	146	131
138	169	162	162	165	174	154	167
187	169	166	138	172	142	192	183
191	176	142	0	87	185	199	190
202	184	183	90	91	158	213	203
176	200	156	196	162	212	188	175
181	182	218	217	225	193	216	181
165	201	212	212	219	183	185	153

127	139	134	154	147	144	109	115
163	147	161	148	142	138	140	111
179	183	131	155	120	141	139	148
186	190	172	78	0	121	144	150
198	203	146	82	78	155	150	158
171	180	197	146	172	132	163	138
177	206	180	203	191	185	150	144
150	177	171	199	187	181	167	133

106	90	107	96	89	67	58	44
101	115	100	91	82	75	55	43
134	112	99	74	82	58	62	40
134	113	82	0	40	71	59	38
139	114	100	44	39	56	57	36
118	116	78	85	60	65	44	28
117	95	92	77	67	48	41	24
101	82	65	53	45	32	26	16

167	204	215	215	222	186	188	156
187	187	224	223	231	199	222	187
184	210	163	206	170	221	197	183
215	196	196	96	97	168	227	216
209	191	155	0	94	200	216	207
209	189	185	152	189	156	213	203
160	195	185	183	185	195	174	189
171	157	195	194	197	167	169	152

153	181	174	203	192	186	172	138
183	214	187	213	201	196	159	154
180	190	209	157	186	144	180	153
213	219	160	90	87	175	171	182
204	210	192	89	0	141	170	181
201	207	150	179	142	171	172	187
187	170	189	178	174	174	182	148
151	166	163	190	187	190	150	164

107	89	72	59	52	37	30	18
128	105	105	89	79	56	49	29
134	135	92	103	74	80	55	35
165	137	123	55	49	71	74	48
167	142	105	0	53	96	81	52
175	149	135	102	115	83	91	60
141	162	144	132	123	116	87	70
157	136	164	150	142	111	101	80

160	146	184	178	177	146	141	119
138	168	156	151	148	146	116	98
167	148	140	111	132	100	115	79
152	136	106	0	58	111	98	66
142	125	119	55	52	80	86	57
108	115	85	100	76	86	62	41
95	85	92	84	79	59	54	33
72	68	60	54	50	38	32	21

118	139	144	174	174	180	144	159
98	115	145	146	149	154	166	139
79	114	100	131	111	140	148	167
65	98	111	58	0	107	137	154
58	87	80	53	56	121	128	147
41	62	87	77	102	88	121	115
33	55	60	80	87	96	91	106
21	32	38	52	56	64	74	84

155	136	165	154	148	120	115	98
136	161	146	139	135	136	116	120
167	147	139	111	133	106	138	127
156	141	111	0	64	132	137	127
152	137	134	64	64	107	140	129
123	139	108	133	108	136	118	106
119	119	142	139	141	118	128	104
102	124	131	130	132	107	105	83

Fig. 2.6. Reference solution to Test Two.
(Pin powers in % of the average power of the subregion).

148	139	181	179	182	153	152	133
138	171	163	163	165	173	152	163
179	163	159	131	163	134	181	171
176	161	131	0	79	168	179	170
178	163	162	79	80	137	184	174
149	170	132	167	137	177	156	144
148	149	178	177	183	156	173	144
129	159	168	168	172	143	144	118

128	142	137	157	149	145	108	112
157	142	155	142	135	130	131	103
165	169	120	140	108	126	124	131
164	166	149	68	0	103	122	127
168	170	122	68	64	127	122	129
138	144	157	116	135	103	128	109
138	159	137	153	143	138	113	111
113	132	125	144	134	130	122	100

101	87	103	93	87	68	64	56
93	106	92	84	77	75	63	67
118	99	88	66	76	57	73	69
115	97	71	0	36	71	71	67
116	97	88	39	36	57	71	66
99	103	73	89	62	73	60	53
102	94	102	92	85	65	66	53
95	107	103	93	86	64	57	43

124	152	161	160	165	137	137	112
136	137	164	163	167	142	157	130
131	149	116	145	119	154	135	124
150	137	135	66	66	113	151	142
142	129	104	0	63	132	140	132
138	125	122	100	123	100	135	128
102	125	119	118	118	124	110	119
106	98	125	122	124	106	108	98

106	124	118	135	126	124	119	104
124	142	122	136	126	125	107	116
117	121	130	95	111	87	115	111
134	135	95	52	49	99	103	124
125	125	111	49	0	76	96	115
122	123	86	99	76	89	92	110
117	105	113	102	95	92	96	82
102	114	109	123	114	109	82	30

96	88	113	110	112	96	99	93
82	100	94	93	94	100	91	104
97	87	84	68	84	70	99	100
87	79	63	0	37	80	88	90
81	73	72	35	34	59	82	83
63	71	54	67	54	70	63	61
60	59	69	67	68	57	64	55
52	63	65	63	63	51	50	42

Fig. 2.7. Reference solution to Test Three.
(Pin powers in % of the average power of the subregion).

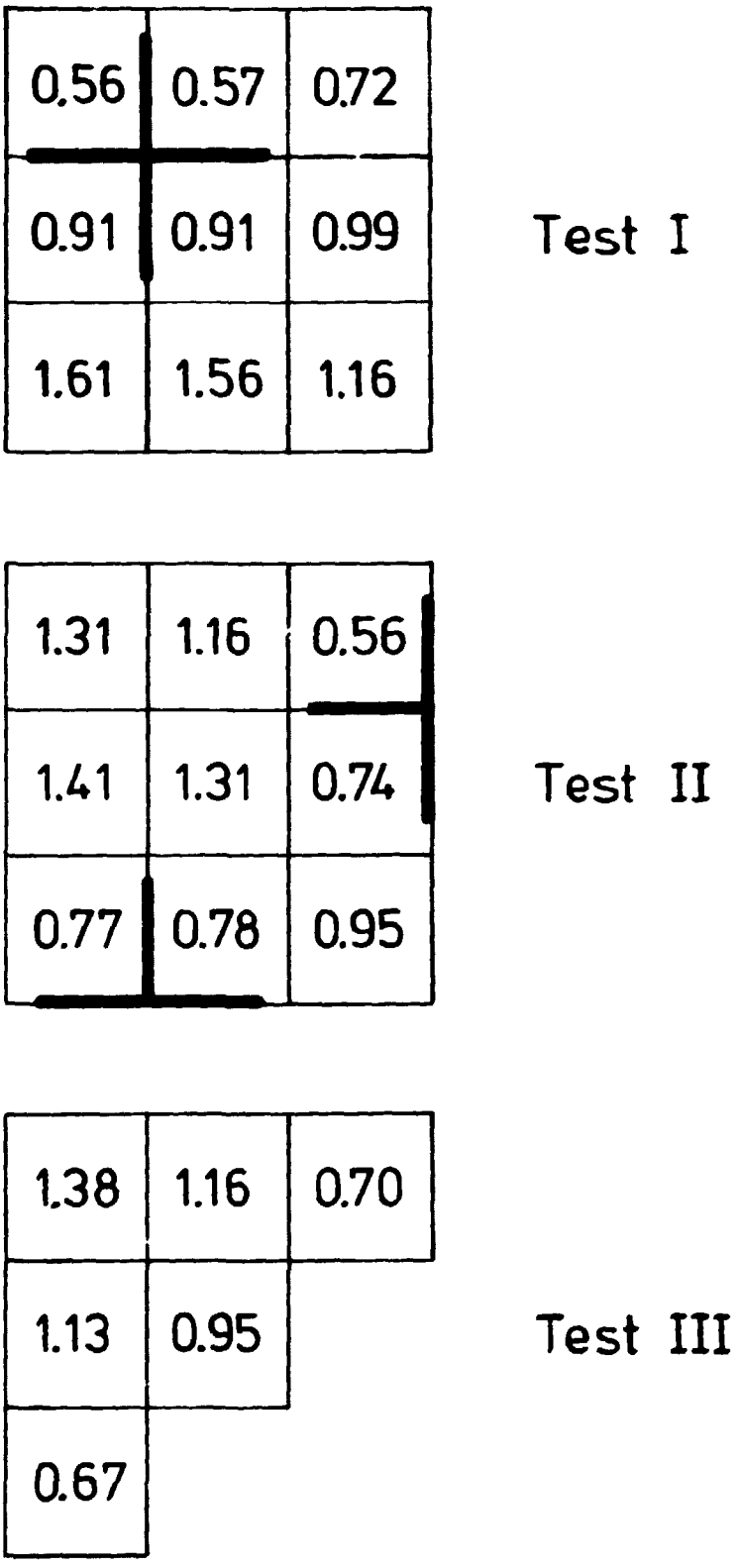

Fig. 2.8. The average assembly powers in the three subregions. (Normalized to unity).

Normalized reference solution.

Errors in % of average assembly power.

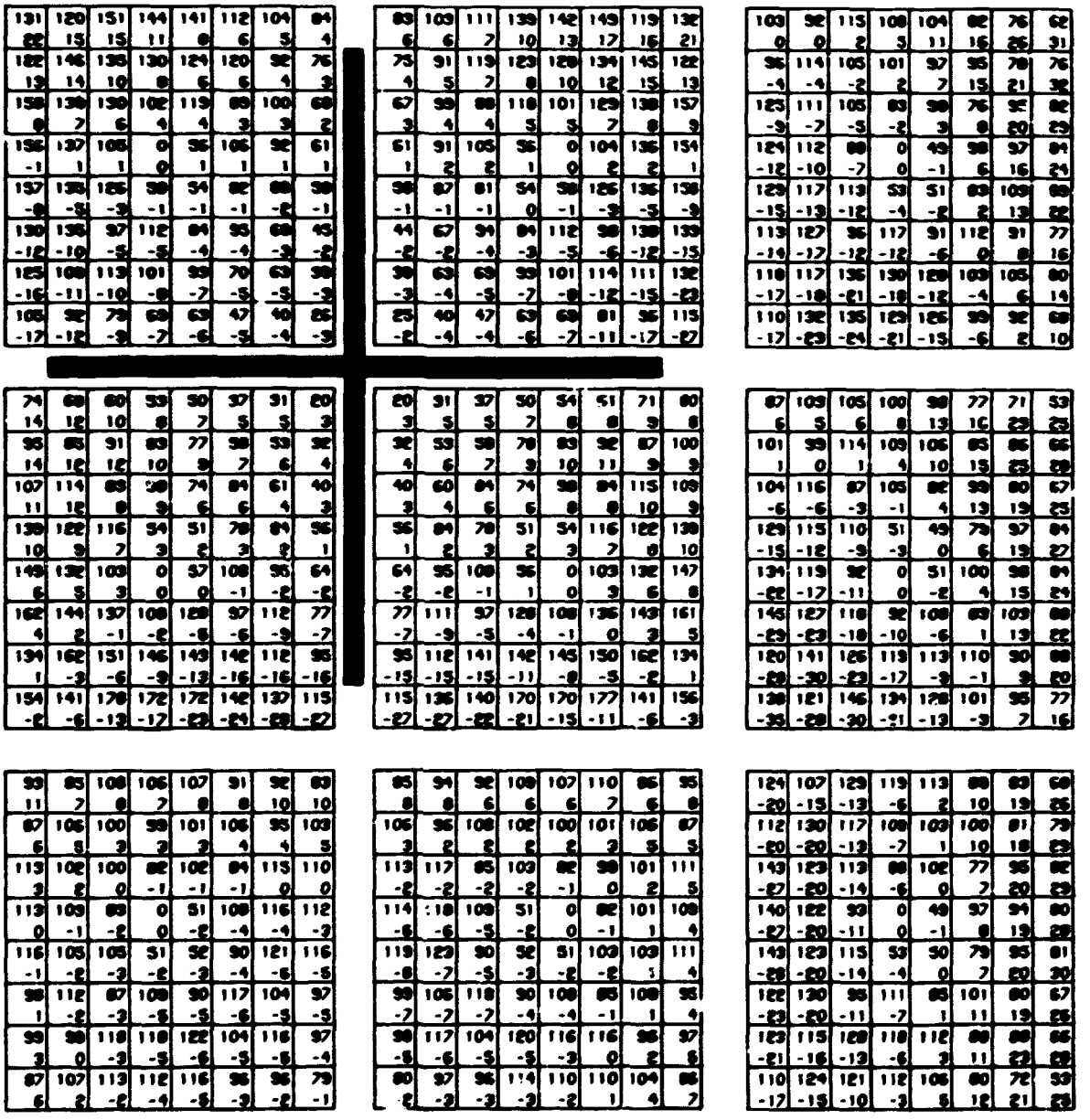

Fig. 3.1. Errors in the local pin power determination using the Normalization Method on Test One.

Normalized reference solution.

Error in % average assembly power.

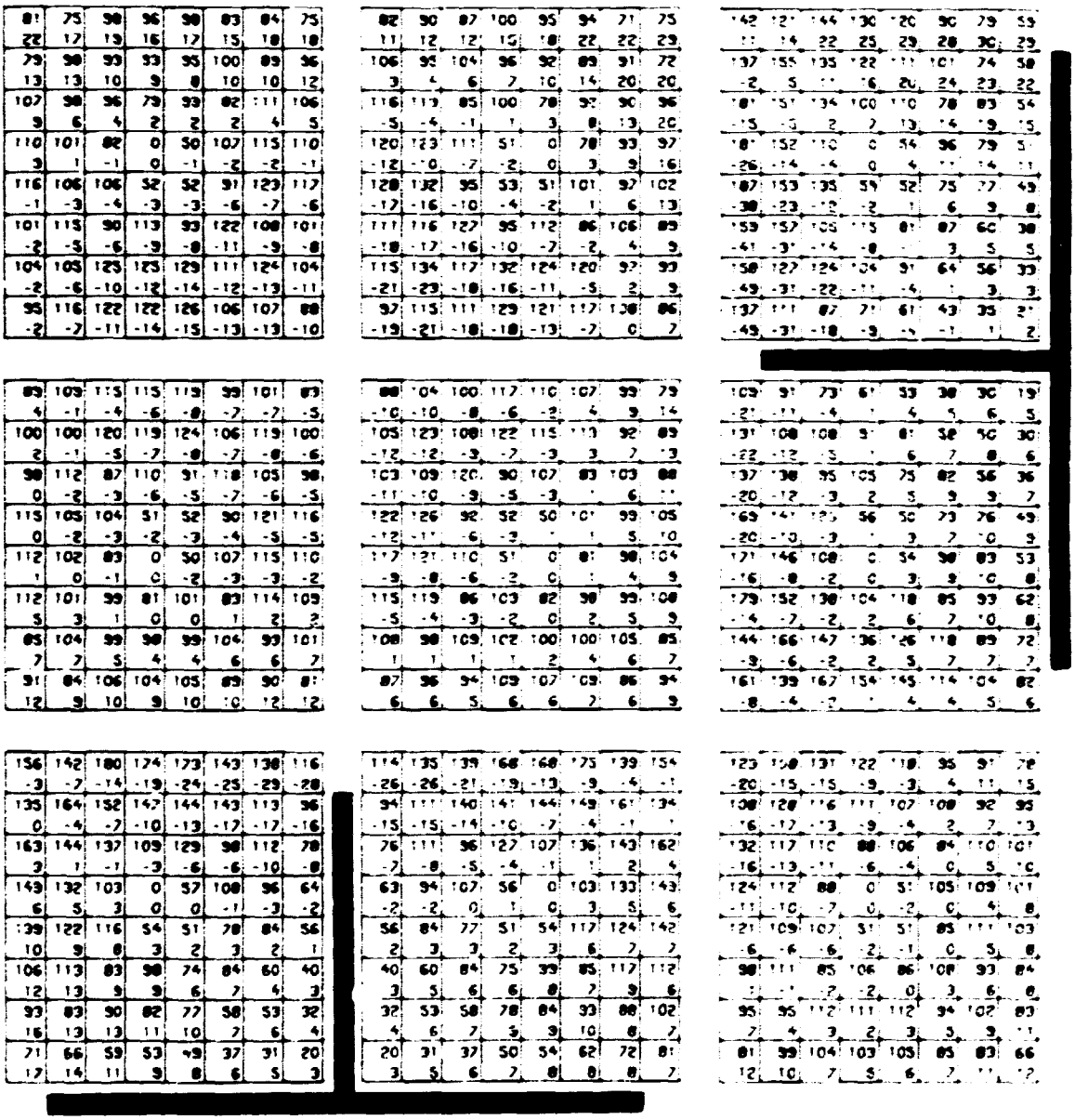

Fig. 3.2. Errors in the local pin power determination using the Normalization Method on Test Two.

Normalized reference solutions.

Error in % of average assembly power.

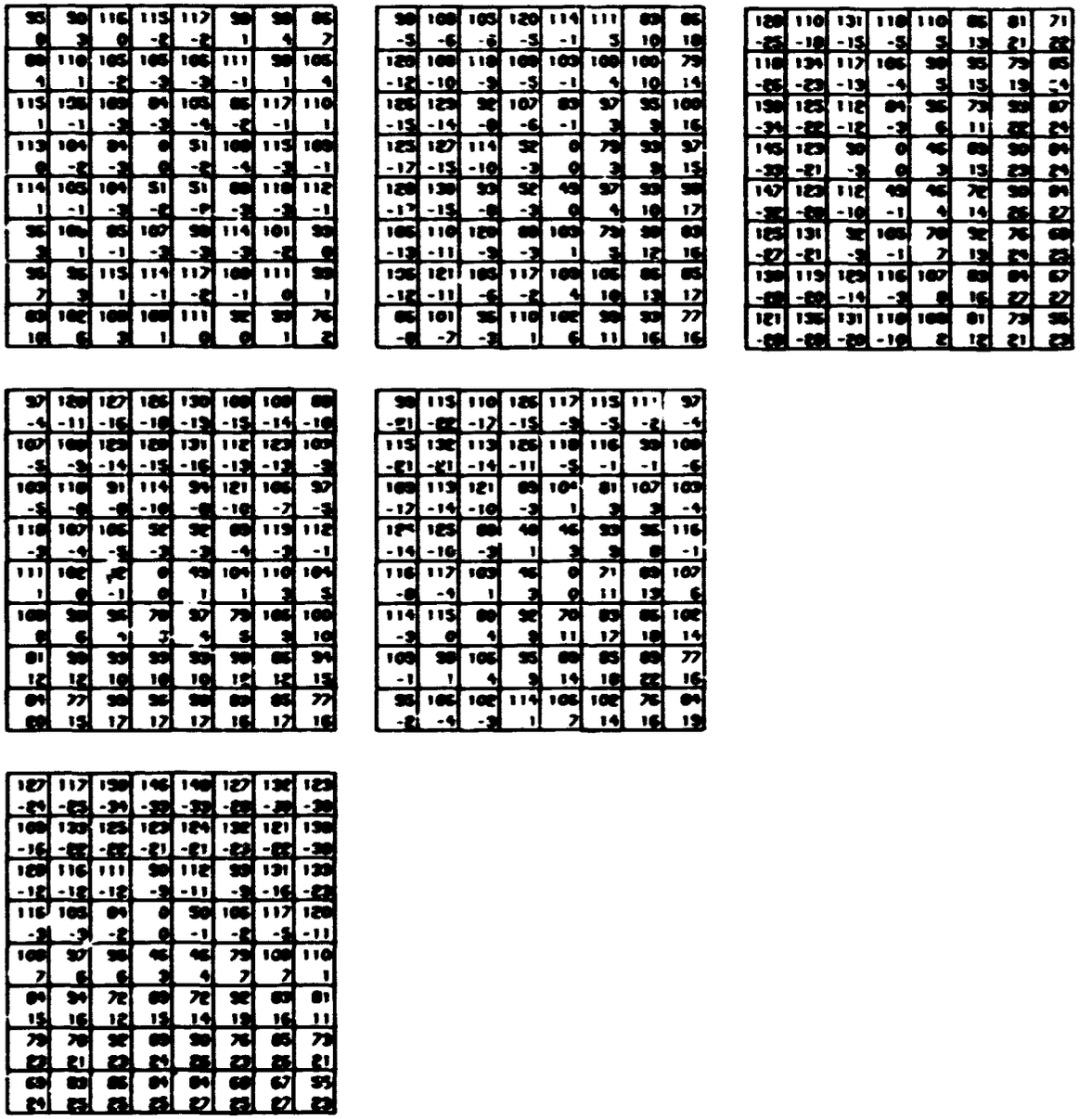

Fig. 3.3. Errors in the local pin power determination using the Normalization Method on Test Three.

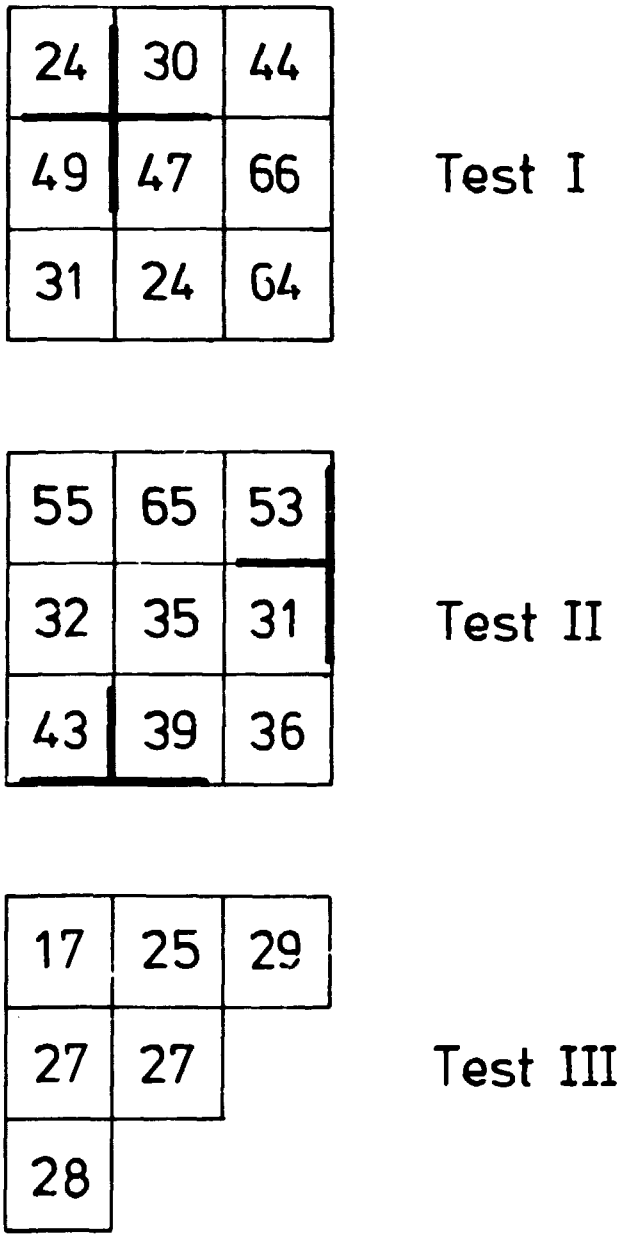

Fig. 3.4. Maximum pin power errors in the twenty-four assemblies using the Normalization Method. The average pin power for the core is assumed to be 160 cm/pin. (W/cm/pin).

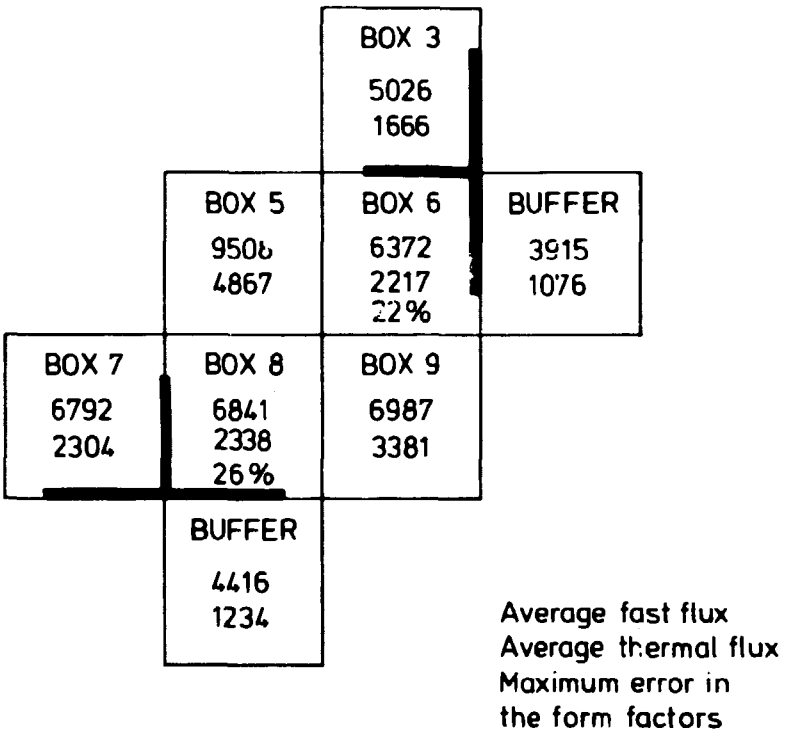

Average - and corner values of the net currents

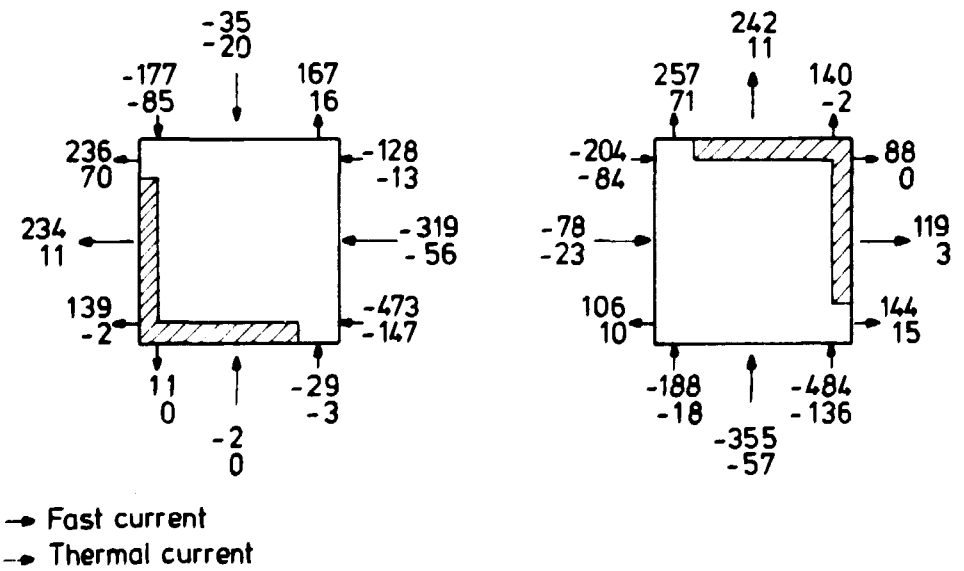

Fig. 3.5. Average - and boundary fluxes and currents in Box 6 and Box 8 of Test Two, and in the neighbouring assemblies.

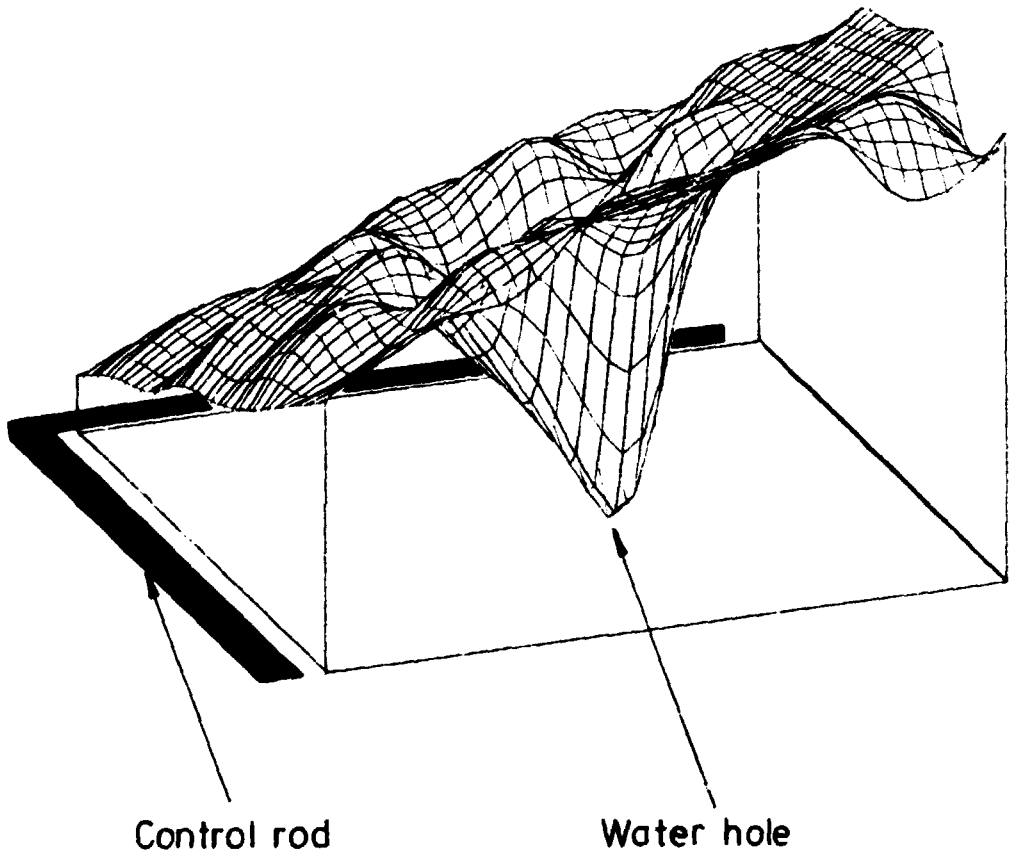

Fig. 4.1. The power distribution for the assembly using "accurate" net currents as boundary conditions. (Reference solution to Box 5 in Test One).

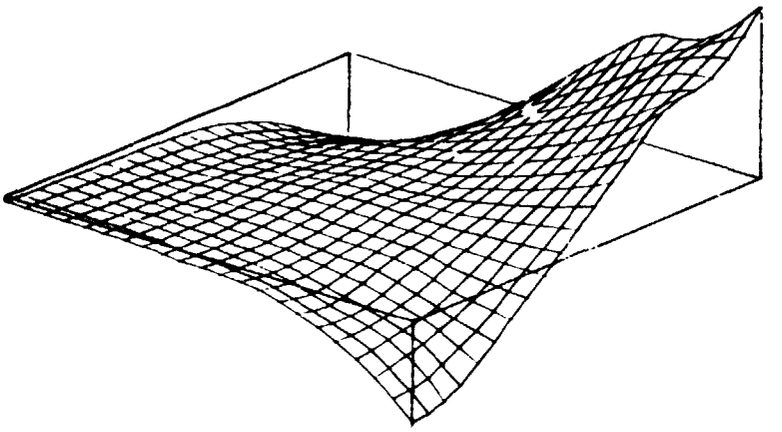

Fig. 4.2.A. The difference between the reference solution (Fig. 4.1) and the power distribution calculated using the flat approximation of the boundary conditions.

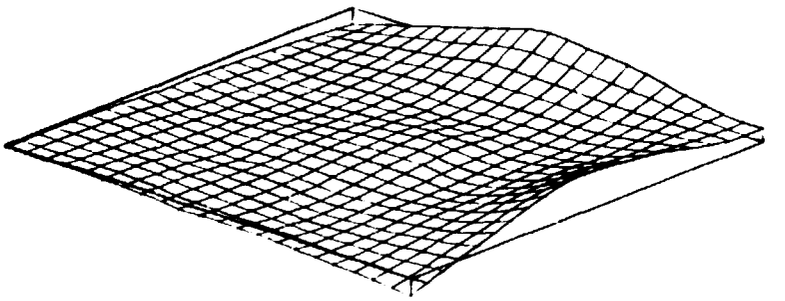

Fig. 4.2.B. The difference between the reference solution and the power distribution calculated using the tilt approximation.

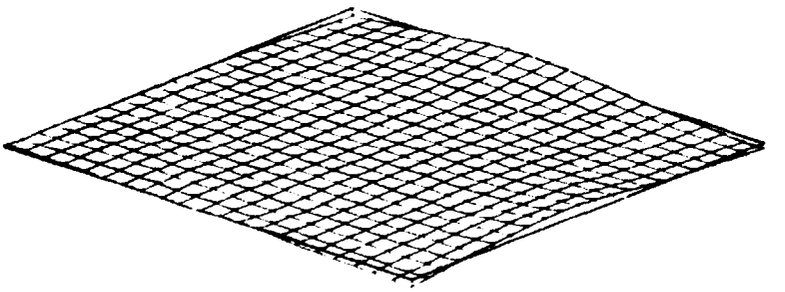

Fig. 4.2.C. The difference between the reference solution and the power distribution calculated using the parabolic approximation.

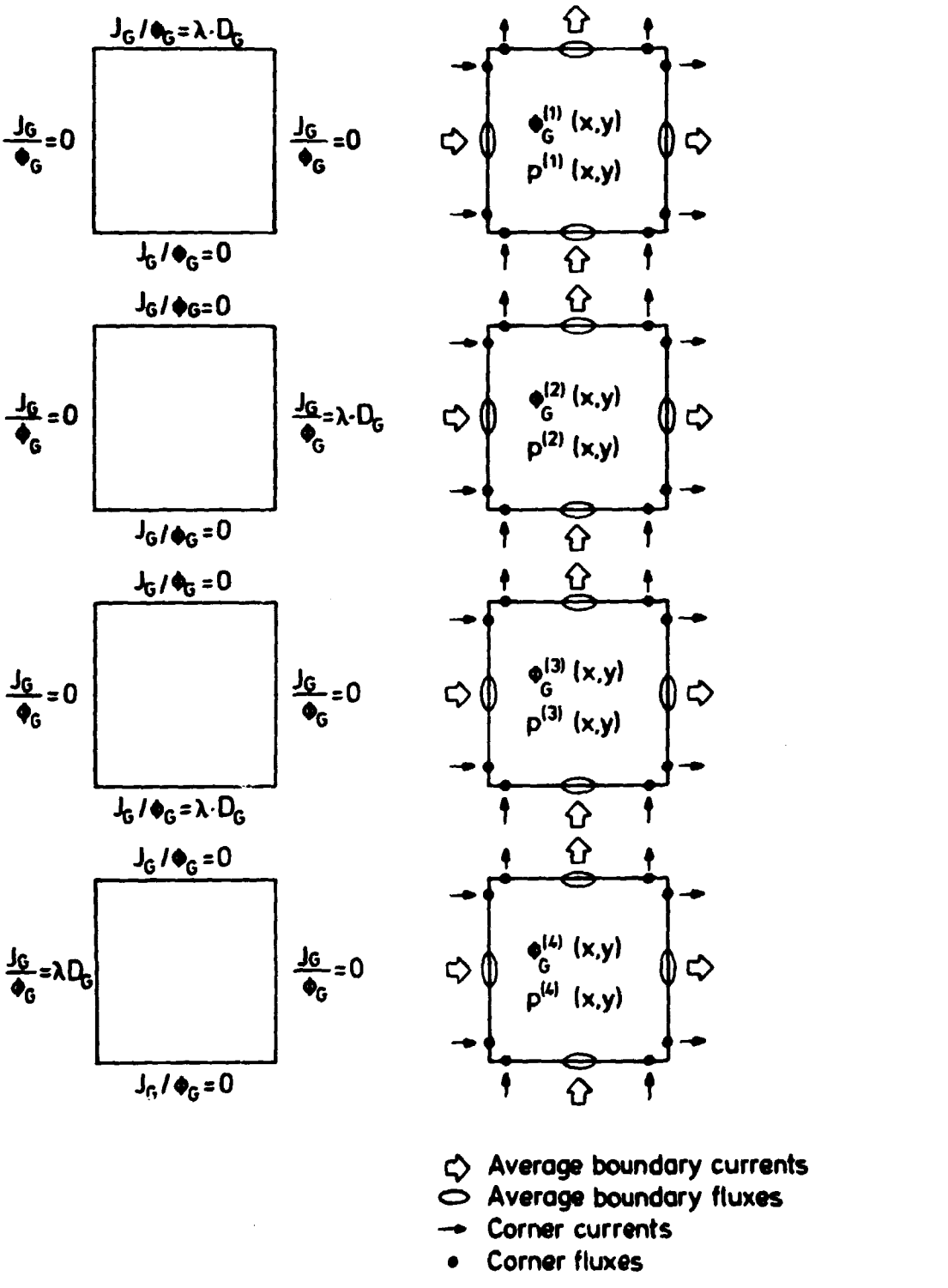

Fig. 5.1. Generation of the base solutions to the flat approximation.

10.3 8.1 6.0	12.4 7.8 8.0	8.2 4.3 2.7
12.5 8.5 8.9	12.9 9.5 5.0	9.2 7.2 7.1
7.2 5.8 3.0	6.4 4.6 3.7	6.9 2.7 2.4

Test I

8.2 5.2 5.6	9.2 7.0 6.4	19.1 12.2 10.5
6.3 5.2 4.8	8.9 7.3 8.8	11.5 9.2 5.5
12.3 7.9 8.8	13.2 9.9 5.9	11.5 10.1 9.4

Test II

7.0 5.4 5.5	7.0 6.1 9.5	14.1 13.7 8.0
7.4 6.4 9.4	20.5 27.4 12.0	
14.7 14.3 8.3		

Test III

Super/4H	Neglecting thermal leakage
Super/4	One-group approximation with $\frac{\Delta\Phi_1}{\Phi_1} = \frac{\Delta\Phi_2}{\Phi_2}$
Super/8	Two-group approximation

Fig. 5.2. Maximum errors in the local pin power determination using the flat approximation of the boundary parameters. (Error in % of average assembly power).

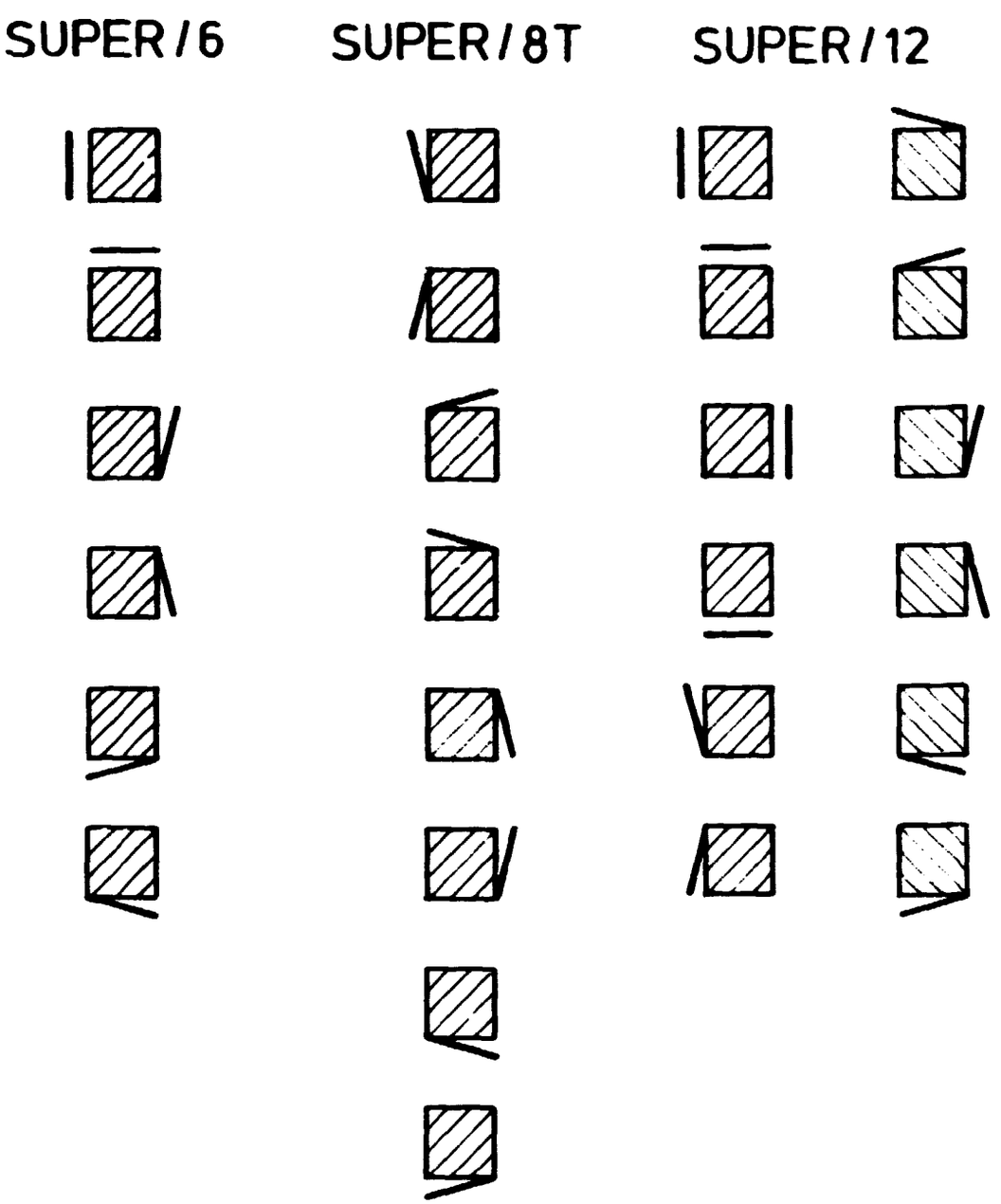

Fig. 5.3. Three different sets of boundary parameter value approximation in the base-solution generation.

8.1 5.5 5.0 4.8	7.8 4.6 4.8 4.1	4.3 4.7 5.5 3.8
8.5 4.9 4.6 4.1	9.5 5.5 5.1 4.0	7.2 2.9 3.1 2.6
5.8 5.2 5.1 3.8	4.6 2.8 3.0 2.3	2.7 2.0 2.5 1.5

Test I

5.2 4.5 4.2 3.7	7.0 4.4 4.4 3.7	12.2 6.3 6.0 5.9
5.2 4.0 3.9 3.0	7.3 3.5 3.0 2.3	9.2 5.0 4.7 3.8
7.9 4.8 4.7 4.2	9.9 5.4 5.1 4.2	10.1 4.6 4.3 3.2

Test II

Super /4
Super /6
Super /8
Super /12

Error in % of the average pin power in the core

Fig. 5.4. Maximum errors in the local pin power determination using the Superposition Method with four different shape approximations.

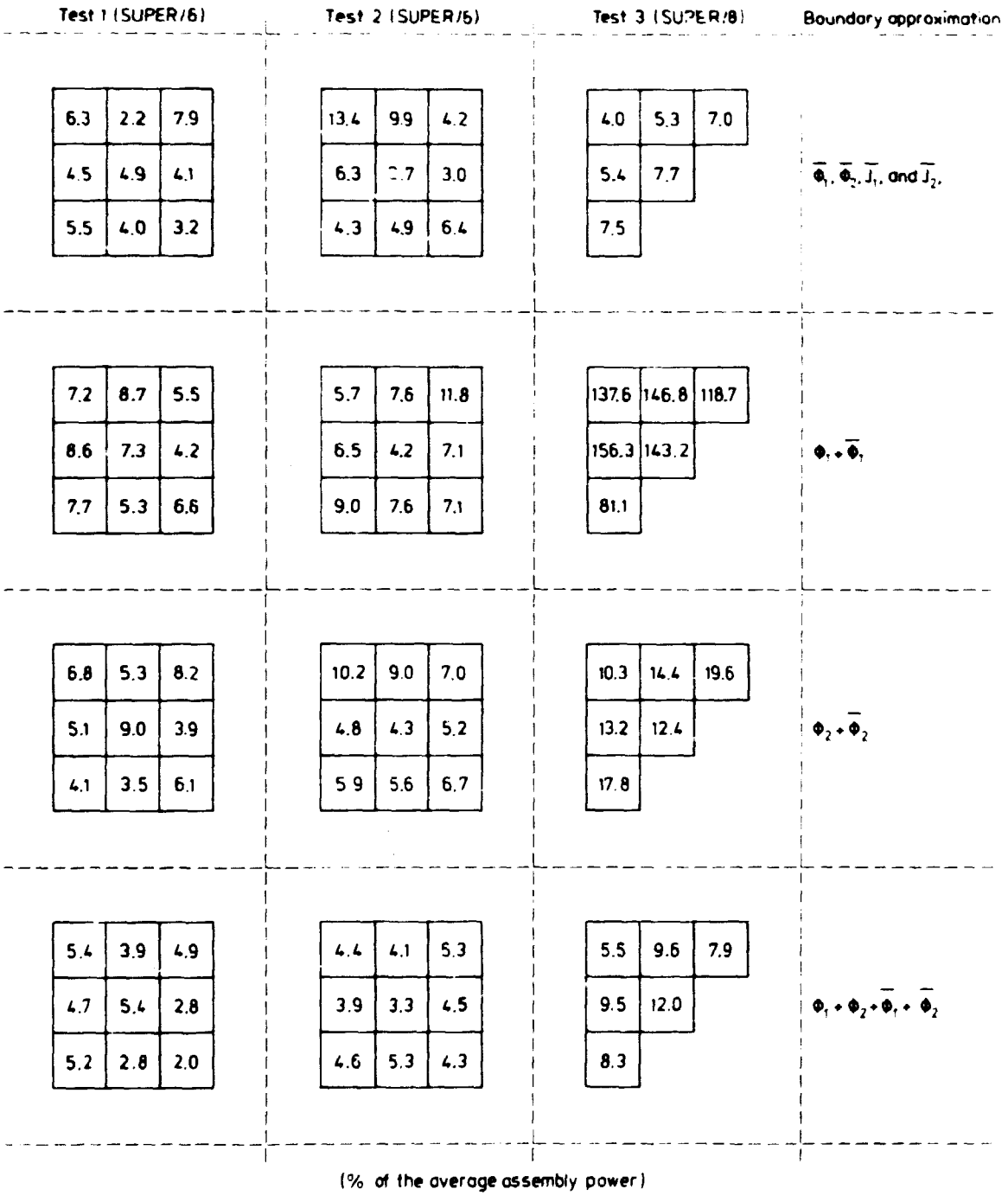

Fig. 5.5. The relationship between maximum errors in the local pin power determination and the type and number of boundary parameters.

(% of the average assembly power)

1.9	1.4	2.3
2.2	2.1	1.8
1.3	1.0	2.3

Test 1

1.7	1.7	2.3
1.0	0.6	1.3
2.5	1.2	1.3

Test 2

Fig. 5.6. The maximum errors in the local pin power determination using SUPER/12 as base-solution and $\bar{\phi}_2 + \phi_2$ as boundary parameters. (% of the average assembly power).

(% of the average assembly power)

2.5	1.4	3.2
1.6	3.2	1.5
2.8	2.0	1.6

Test 1

3.5	2.9	1.6
2.2	1.8	2.2
1.7	2.9	2.6

Test 2

2.8	3.9	5.1
3.8	7.0	
5.5		

Test 3

Fig. 5.7. Maximum errors in the local pin power determination using weight factors different from one and zero (in % of average assembly power).

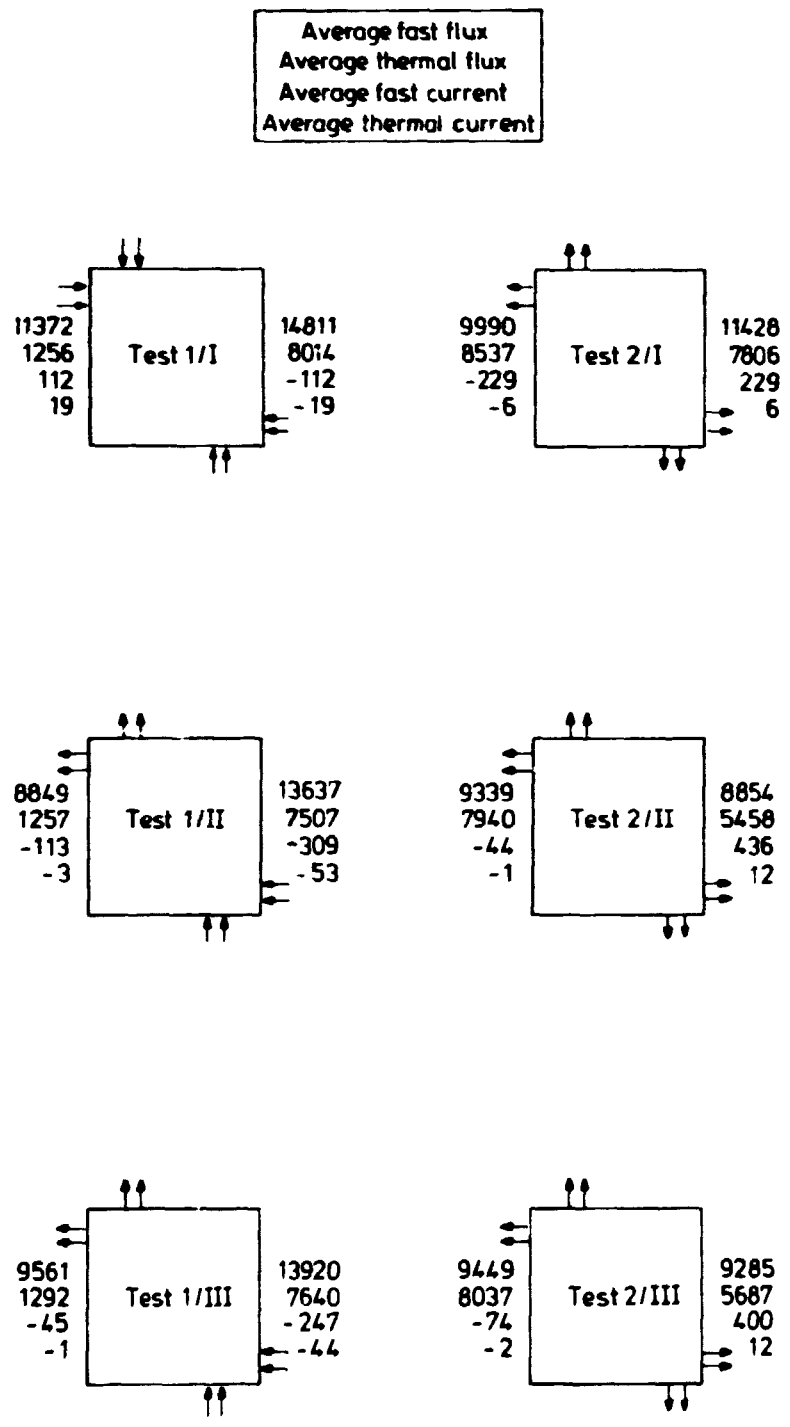

Fig. 6.1. The average heterogeneous boundary fluxes and currents in the 6 test cases.

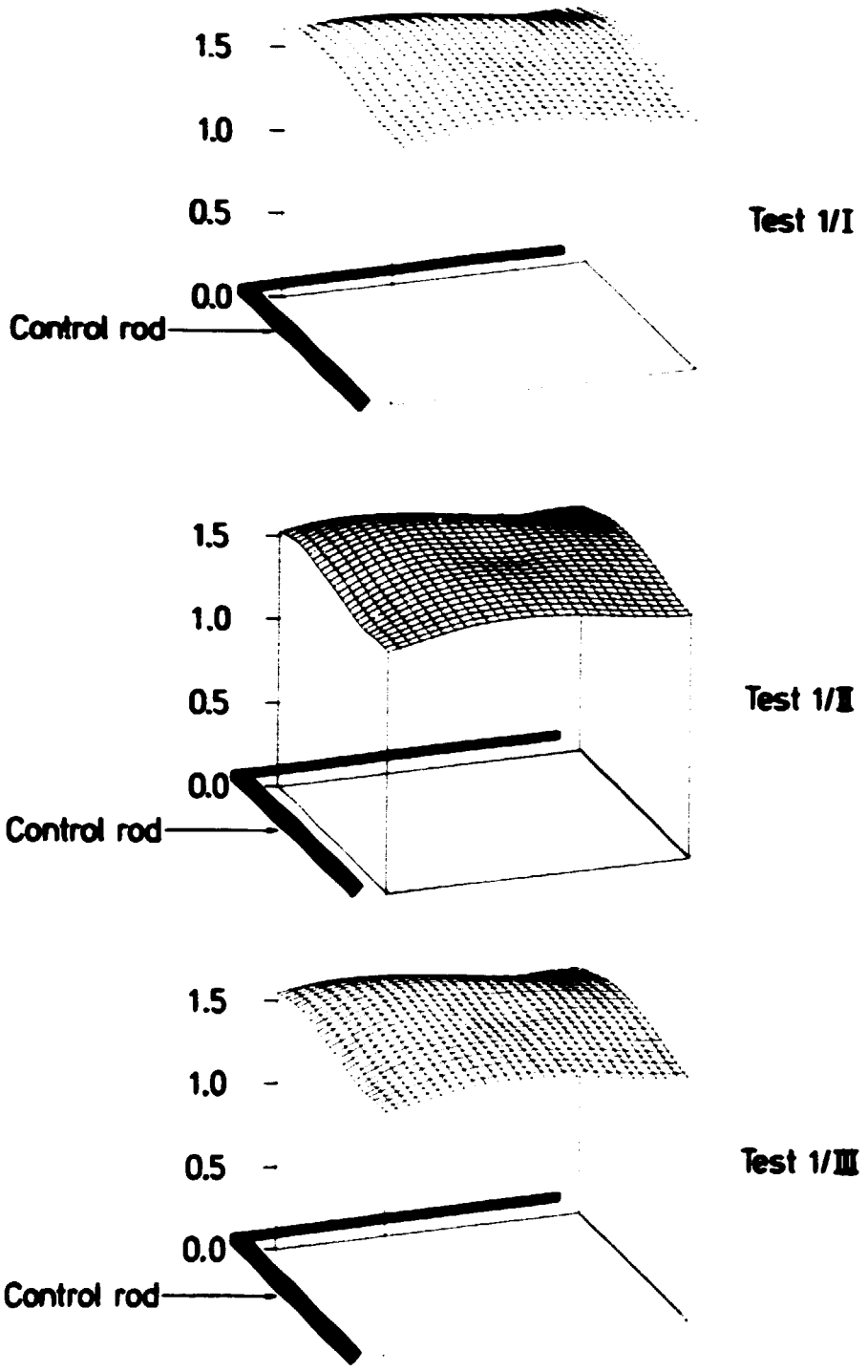

Fig. 6.2. The fast form function $\phi_1^{het} / \phi_1^{hom}$ for the rodded assembly.

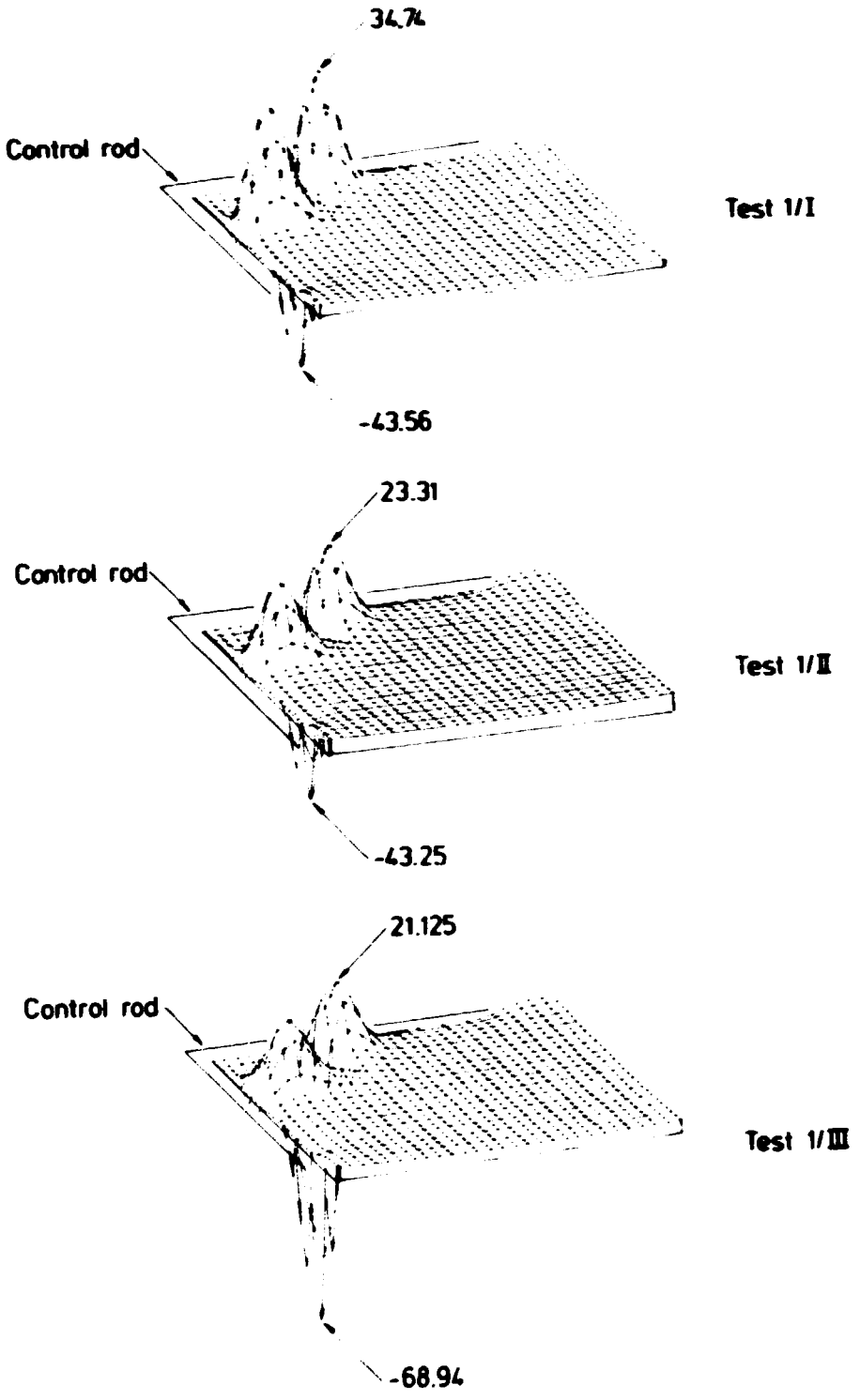

Fig. 6.3. The thermal form function $\phi_2^{het} / \phi_2^{hom}$ for the rodded assembly.

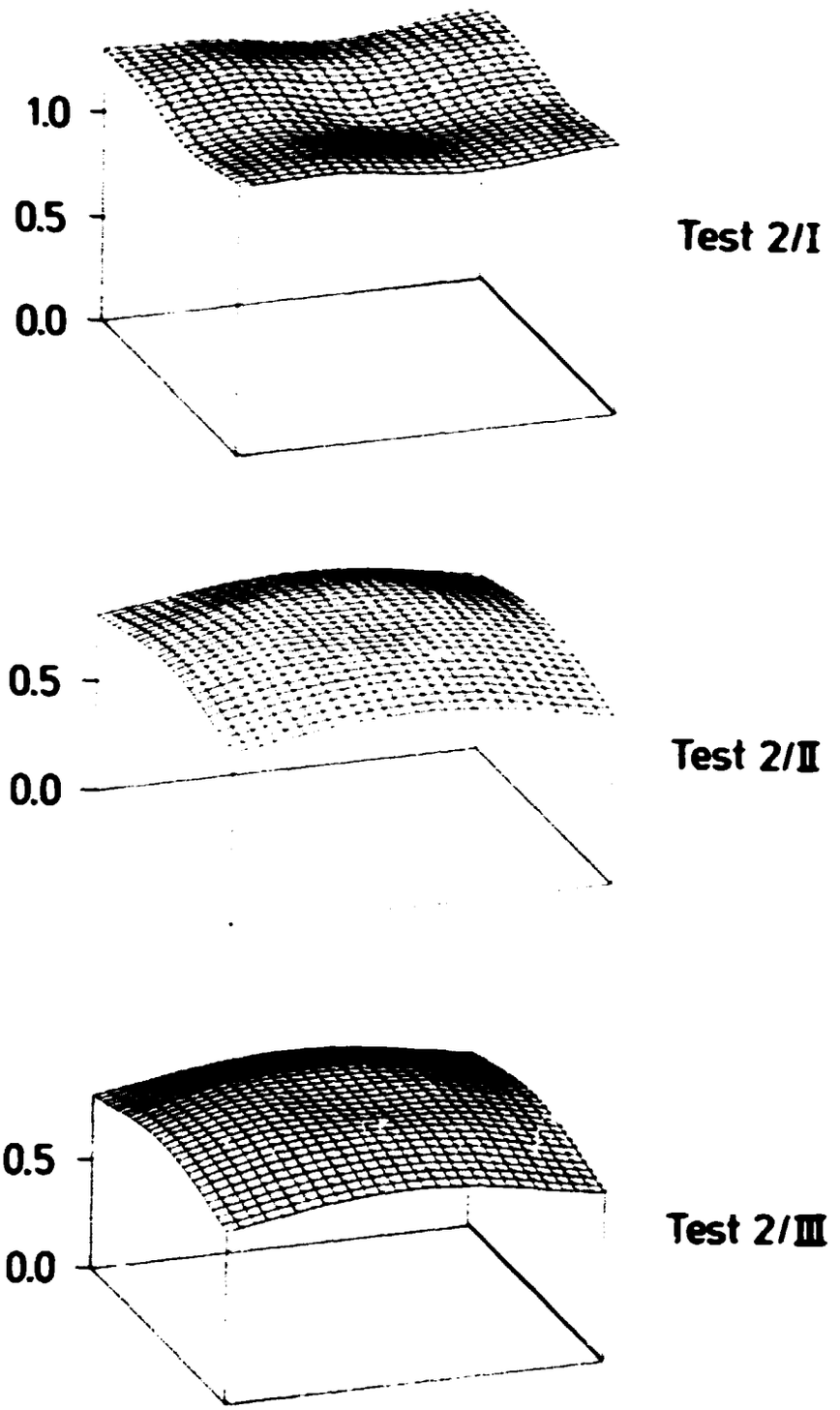

Fig. 6.4. The fast form function $\phi_1^{het}/\phi_1^{hom}$ for the unroduced assembly.

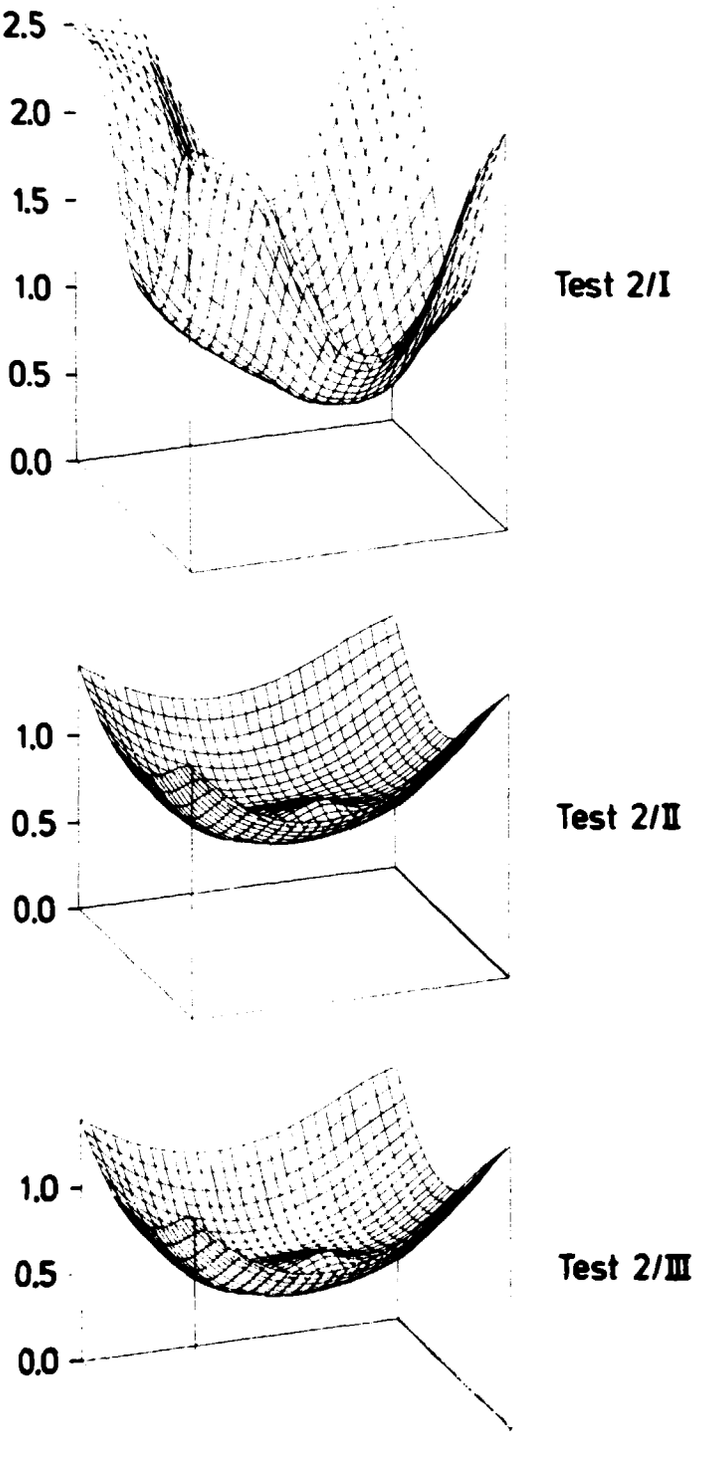

Fig. 6.5. The thermal form function $\emptyset_2^{het} / \emptyset_2^{hom}$ for the unrodded assembly.

Control rod

-1.84	-2.37	-10.50	-5.52	-4.36	-3.40	-2.27	-0.93
-2.37	1.84	-5.66	-5.87	-4.72	-3.34	-1.21	1.01
-10.50	-5.66	-5.85	-4.05	-3.75	-1.68	1.15	2.83
-5.52	-5.87	-4.05	-1.83	-1.19	-0.67	1.83	5.44
-4.36	-4.72	-3.75	-1.19	0.00	0.80	3.74	7.64
-3.42	-3.34	-1.68	-0.67	0.80	3.23	6.23	10.56
-2.29	-1.21	0.12	1.83	3.74	6.23	9.70	11.06
-0.95	0.99	2.83	5.44	7.65	10.56	11.06	15.23

Test 1/I

Control rod

-1.19	-2.38	3.76	-0.68	-0.86	-0.71	-0.40	0.10
-2.38	-16.88	0.01	-1.13	-1.12	-0.80	-0.24	0.44
3.78	0.02	-1.04	-0.99	-1.08	-0.50	0.01	0.81
-0.65	-1.12	-0.99	-0.52	-0.39	-0.33	0.39	1.42
-0.83	-1.12	-1.05	-0.39	0.00	0.06	0.88	2.01
-0.71	-0.77	-0.50	-0.32	0.08	0.75	1.60	2.86
-0.37	-0.21	0.02	0.39	0.88	1.60	2.61	3.06
0.14	0.50	0.83	1.45	2.04	2.86	3.06	4.24

Test 1/III

-30.08	-38.32	-30.02	-18.09	-3.10	1.95	-14.44	-25.42
-38.32	-47.25	-34.15	-20.94	-5.01	-3.79	-14.89	-30.00
-30.00	-34.15	-28.44	-7.32	6.57	6.84	-3.97	17.93
-18.07	-20.92	-7.30	5.13	13.21	30.48	18.93	4.05
-3.08	-5.01	6.60	13.23	0.00	41.09	39.13	25.96
-1.92	-3.75	6.87	30.48	41.12	54.75	44.54	31.60
-14.41	-14.85	-3.94	18.98	39.13	44.54	34.26	13.68
-25.40	-29.95	-17.91	4.10	26.00	31.60	13.68	-2.46

Test 2/I

-0.01	-0.07	-0.10	-0.11	-0.13	-0.13	-0.21	-0.30
-0.07	-0.15	-0.17	-0.19	-0.14	-0.15	-0.20	-0.34
-0.08	-0.17	-0.23	-0.16	-0.13	0.07	-0.12	-0.21
-0.10	-0.21	-0.14	-0.07	-0.02	0.11	0.07	-0.07
-0.11	-0.14	-0.11	-0.01	0.00	0.23	0.29	0.20
-0.13	-0.14	-0.07	0.09	0.25	0.44	0.47	0.47
-0.20	-0.20	-0.12	0.07	0.29	0.47	0.64	0.50
-0.30	-0.31	-0.23	-0.04	0.23	0.47	0.50	0.55

Test 2/III

Fig. 6.6. Errors in the pin power determination coarsed by the use of HHM with Test 1/II and Test 2/II as base-solutions. (Error in % of average assembly power).

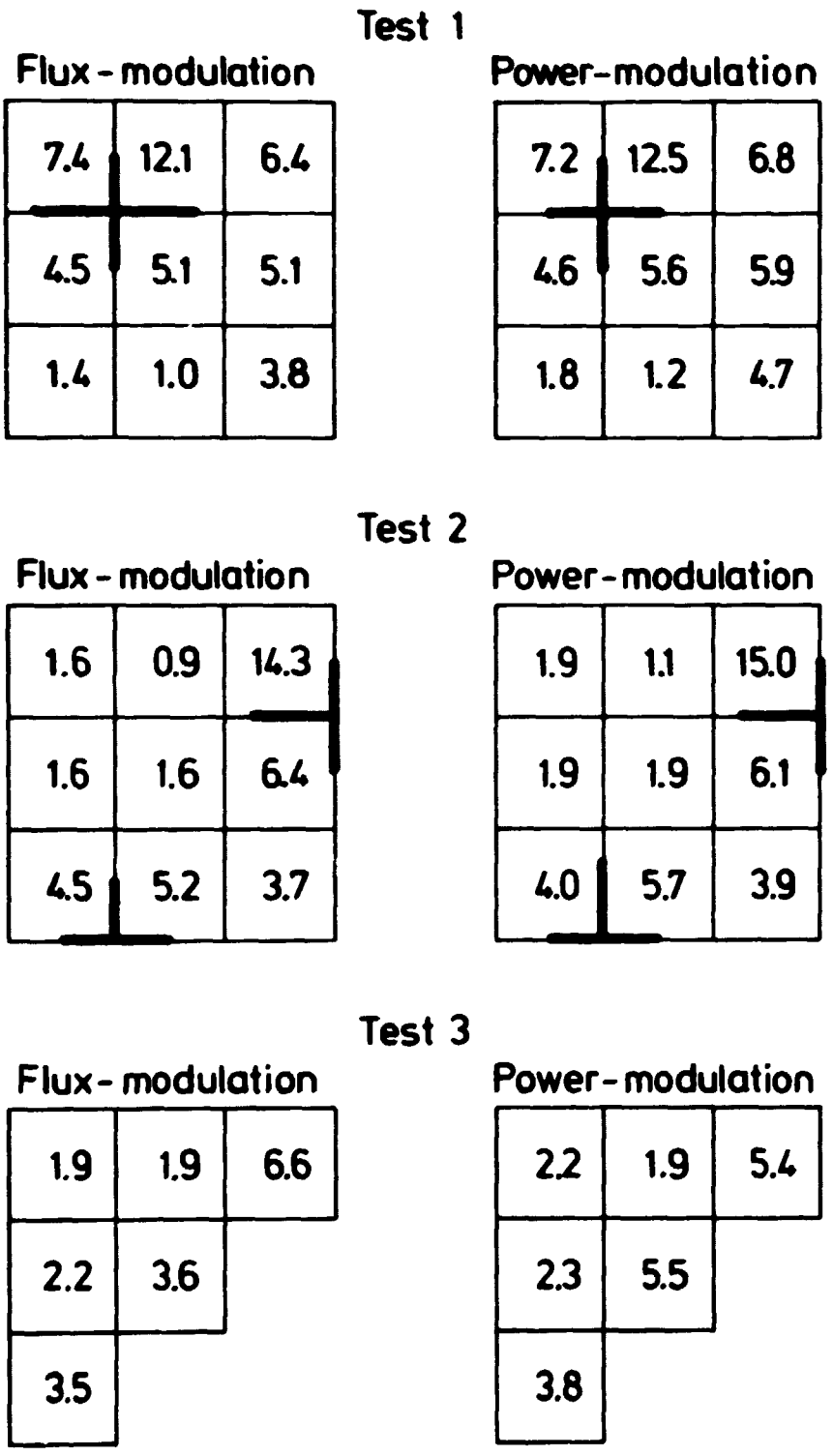

Fig. 6.7. Maximum errors in the local pin power determination using HHM based on flux-volumen weighted homogenized cross sections. (Error in % of average assembly power).

Test 1

10.9	17.6	6.6
13.6	13.0	14.1
5.6	6.3	3.4

Test 2

4.7	7.1	21.8
5.9	12.3	23.7
14.7	17.1	16.7

Test 3

5.1	6.0	6.2
6.2	8.9	
6.7		

Fig. 6.8. Maximum errors in the local pin power determination using HHM based on flux-volumen weighted cross sections. Only the average values of the net neutron currents from the overall solution are considered. (Error in % of average assembly power).

Test 1

18.3	39.0	14.2
68.8	65.5	19.0
4.6	5.5	17.1

Test 2

7.3	8.8	96.6
4.9	5.4	69.7
70.5	65.3	12.5

Test 3

16.8	15.7	41.6
16.3	26.3	
42.6		

Fig. 6.9. Maximum errors in the local pin power determination using HHM. The homogenized flux solutions are approximated using a fourth-order polynomial with 21 coefficients. (Error in % of average assembly power).

Test 1

10.9 18.4	17.6 22.3	6.6 11.3
13.6 23.9	13.0 20.8	14.1 20.5
5.6 11.2	6.3 9.8	3.3 9.2

Test 2

4.6 9.9	7.1 9.7	21.7 30.2
5.9 11.5	12.3 17.2	23.7 32.6
14.7 24.9	17.1 25.6	16.7 23.5

Test 3

5.0 10.1	6.0 10.5	6.2 14.6
6.2 10.2	8.9 20.4	
6.7 15.4		

"CDB"
Polynomial approximation

Fig. 6.10. Maximum errors in the local pin power determination using HHM based on generalized equivalence homogenization. The homogenized flux solutions are calculated using either "CDB" or a polynomial approximation. Only average values of the net neutron currents are considered. (Error in % of average assembly power).

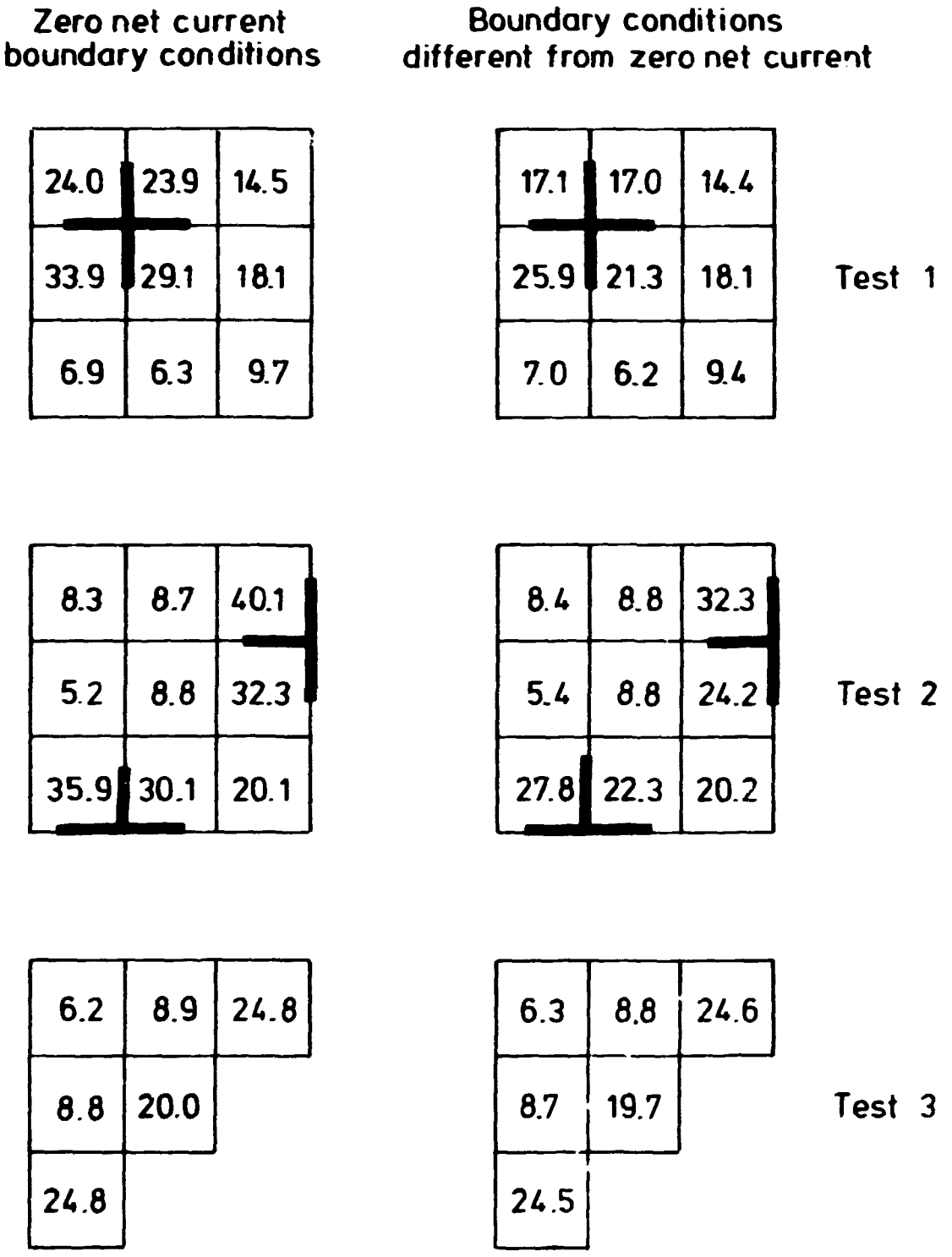

Fig. 6.11. Maximum errors in the local pin power prediction. The homogenized solutions are determined applying an interpolation procedure.

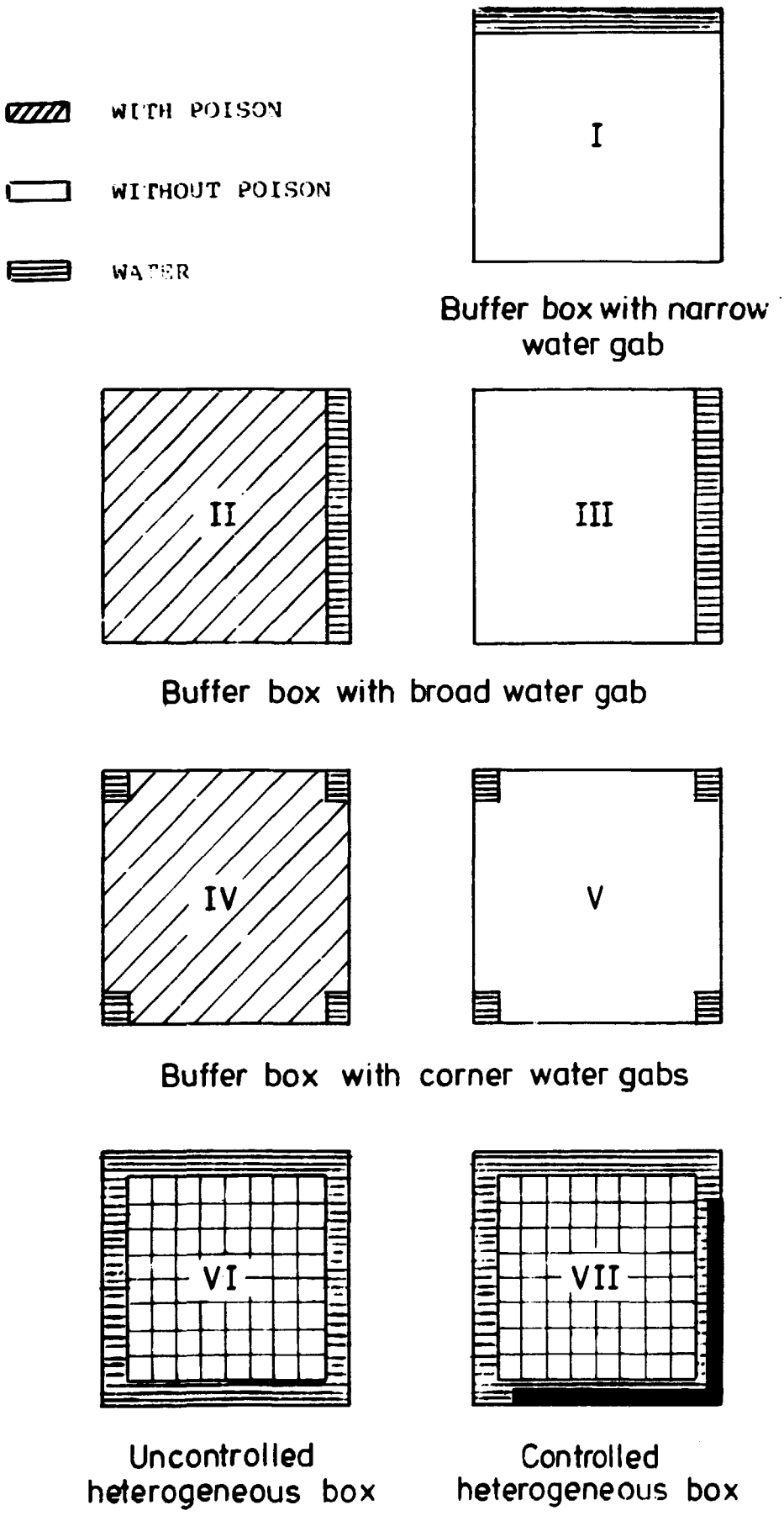

Fig. 7.1. The seven node-types in Test One.

The heterogeneous reference solution

0.56	0.57	0.72
0.91	0.91	0.99
1.61	1.57	1.16

keff=1.0000

The homogeneous solution

0.67	0.68	0.64
0.98	1.01	0.90
1.52	1.51	1.08

keff=1.0046

Fig. 7.2. The average assembly pin powers. (Normalized to unity).

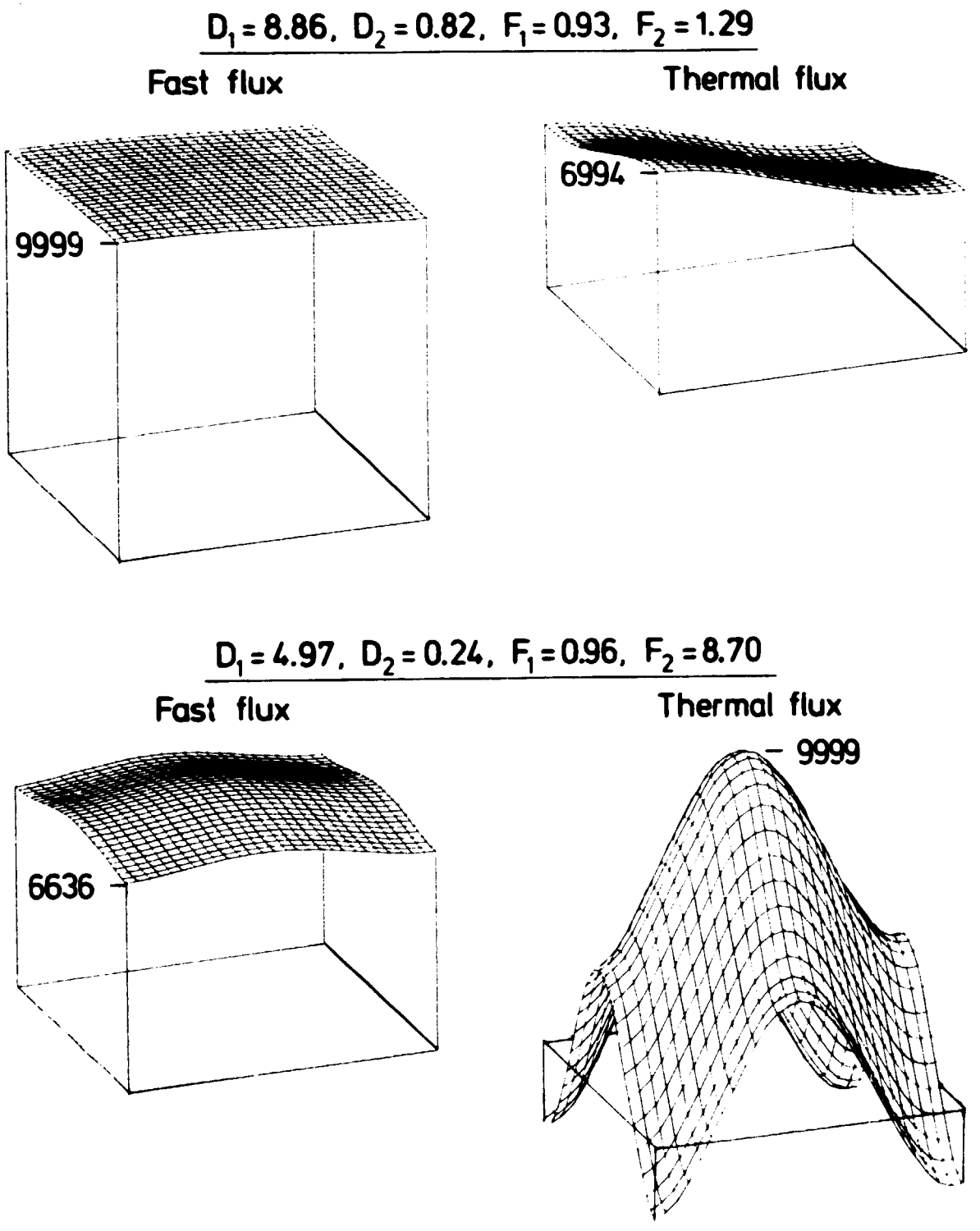

Fig. 8.1. Equivalence flux solutions to Test 2/II.

Sales distributors:
Jul. Gjellerup, Sølvgade 87,
DK-1307 Copenhagen K, Denmark

Available on exchange from:
Risø Library, Risø National Laboratory,
P.O.Box 49, DK-4000 Roskilde, Denmark

ISBN 87-550-0904-2
ISSN 0106-2840